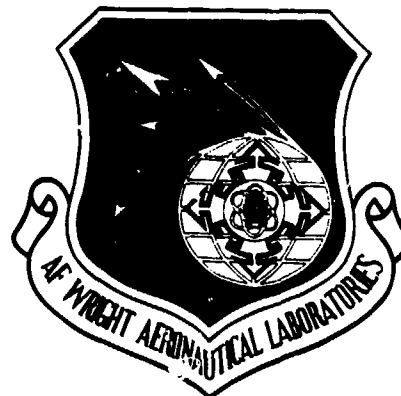


12

AFWAL-TR-82-4186

ACCELERATED CORROSION TESTING



M. Khobaib, Ph.D.

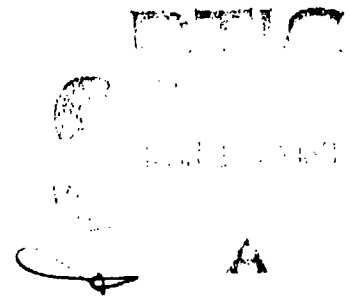
Research Applications Division
Systems Research Laboratories, Inc.
2800 Indian Ripple Road
Dayton, OH 45440-3696

December 1982

Final Report for Period 1 June 1979 - 31 May 1982

Approved for public release; distribution unlimited.

MATERIALS LABORATORY
AIR FORCE WRIGHT AERONAUTICAL LABORATORIES
AIR FORCE SYSTEMS COMMAND
WRIGHT-PATTERSON AIR FORCE BASE, OH 45433



83 03 15 00 8

AD A1 25639

DTIC FILE COPY

NOTICE

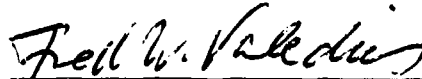
When Government drawings, specifications, or other data are used for any purpose other than in connection with a definitely related Government procurement operation, the United States Government thereby incurs no responsibility nor any obligation whatsoever; and the fact that the government may have formulated, furnished, or in any way supplied the said drawings, specifications, or other data, is not to be regarded by implication or otherwise as in any manner licensing the holder or any other person or corporation, or conveying any rights or permission to manufacture use, or sell any patented invention that may in any way be related thereto.

This report has been reviewed by the Office of Public Affairs (ASD/PA) and is releasable to the National Technical Information Service (NTIS). At NTIS, it will be available to the general public, including foreign nations.

This technical report has been reviewed and is approved for publication.



THEODORE NICHOLAS, Acting Chief
Metals Behavior Branch
Metals and Ceramics Division



FRED W. VAHLDIK
Project Engineer
Metals Behavior Branch

FOR THE COMMANDER



DONALD M. FORNEY, JR., Acting Chief
Metals and Ceramics Division
Materials Laboratory

"If your address has changed, if you wish to be removed from our mailing list, or if the addressee is no longer employed by your organization please notify MLLN, W-PAFB, OH 45433 to help us maintain a current mailing list".

Copies of this report should not be returned unless return is required by security considerations, contractual obligations, or notice on a specific document.

UNCLASSIFIED

SECURITY CLASSIFICATION OF THIS PAGE (When Data Entered)

REPORT DOCUMENTATION PAGE		READ INSTRUCTIONS BEFORE COMPLETING FORM
1. REPORT NUMBER AFWAL-TR-82-4186	2. GOVT ACCESSION NO. A125 639	3. RECIPIENT'S CATALOG NUMBER
4. TITLE (and Subtitle) ACCELERATED CORROSION TESTING		5. TYPE OF REPORT & PERIOD COVERED Final Report 1 June 1979 - 31 May 1982
		6. PERFORMING ORG. REPORT NUMBER 6507 Final
7. AUTHOR(s) M. Khobaib, Ph.D.		8. CONTRACT OR GRANT NUMBER(s) F33615-79-C-5109
9. PERFORMING ORGANIZATION NAME AND ADDRESS		10. PROGRAM ELEMENT, PROJECT, TASK AREA & WORK UNIT NUMBERS 2416 241803 24180307
11. CONTROLLING OFFICE NAME AND ADDRESS Materials Laboratory (AFWAL/MLLN) AFSC Air Force Wright Aeronautical Laboratories Wright-Patterson Air Force Base, OH 45433		12. REPORT DATE December 1982
		13. NUMBER OF PAGES 147
14. MONITORING AGENCY NAME & ADDRESS (if different from Controlling Office)		15. SECURITY CLASS. (of this report) unclassified
		15a. DECLASSIFICATION/DOWNGRADING SCHEDULE
16. DISTRIBUTION STATEMENT (of this Report) Approved for public release; distribution unlimited.		
17. DISTRIBUTION STATEMENT (of the abstract entered in Block 20, if different from Report)		
18. SUPPLEMENTARY NOTES		
19. KEY WORDS (Continue on reverse side if necessary and identify by block number) Accelerated corrosion testing, realistic environments, crack growth, localized environmental enhancement, rising-load testing, low-cycle corrosion fatigue.		
20. ABSTRACT (Continue on reverse side if necessary and identify by block number) Available methods for accelerated testing of corrosion behavior yield results which are not sufficiently accurate or reliable for predicting the service life of aircraft components and materials which degrade or fail due to environmental attack. Research has been conducted in controlled atmospheres on the localized environmental enhancement of crack-growth rates of aerospace alloys in order to provide the basis for development of realistic accelerated corrosion tests. Slow-strain-rate, corrosion-fatigue, and rising-load experiments have been		

DD FORM 1 JAN 73 1473

EDITION OF 1 NOV 65 IS OBSOLETE

UNCLASSIFIED

SECURITY CLASSIFICATION OF THIS PAGE (When Data Entered)

UNCLASSIFIED

SECURITY CLASSIFICATION OF THIS PAGE(When Data Entered)

20. Abstract Continued

conducted on high-strength 4340 steel and 7075-T6 aluminum alloy using accelerating pollutants such as sulfur dioxide, nitrogen dioxide, surface salt, and ambient to 100%-relative-humidity (RH) air in a specially designed atmospheric chamber.

The results indicate that a realistic environmental enhancement of crack-growth rates can be employed to develop accelerated tests which can be related to actual in-service degradation. For materials with high stress-corrosion susceptibility, the threshold for crack growth (K_{ISCC}) was estimated to be 45-46 $\text{MPa}\sqrt{\text{m}}$ for 4340 steel at a 1440-MPa yield-strength level, as compared to 49-52 $\text{MPa}\sqrt{\text{m}}$ as determined by means of rising-load tests and 44-46 $\text{MPa}\sqrt{\text{m}}$ by fracture analysis in 1000 ppm SO_2 at 80% RH. Similarly, the K_{ISCC} for high-strength Al 7075-T6 was estimated to be 13-14 $\text{MPa}\sqrt{\text{m}}$ by extrapolation of corrosion-fatigue test data as compared to 14-15 $\text{MPa}\sqrt{\text{m}}$ as determined by rising-load tests and 12 $\text{MPa}\sqrt{\text{m}}$ as approximated by fracture analysis in 100 ppm NO_2 + 80% RH + 5% surface salt. Thus, a rapid and reproducible method for K_{ISCC} determination appears feasible.

UNCLASSIFIED

SECURITY CLASSIFICATION OF THIS PAGE(When Data Entered)

PREFACE

This report was prepared by Dr. M. Khobaib with the assistance of Mr. Earnest Keppler, Ms. Frieda Thornton, and Ms. Laura Quackenbush. Work was performed under Contract F33615-79-C-5109 by the Research Applications Division of Systems Research Laboratories, Inc., 2800 Indian Ripple Road, Dayton, OH, 45440. The contract was administered under the direction of the Air Force Wright Aeronautical Laboratories, Materials Laboratory (AFWAL/MLLN), Wright-Patterson Air Force Base, OH, with Dr. C. T. Lynch and Mr. F. W. Vahldiek acting as the Government Project Monitors.

Studies were conducted during the period 1 June 1979 through 31 May 1982 at the Systems Research Laboratories, Inc., Corrosion Facility.

The author would like to acknowledge the editorial assistance of Mrs. Marian Whitaker in the preparation of this report.



A

TABLE OF CONTENTS

<u>Section</u>	<u>Page</u>
1 INTRODUCTION	1
2 TECHNICAL BACKGROUND	5
Crack-Growth-Rate Measurement	5
Slow-Strain-Rate-Test	16
Rising-Load Tests	17
General Corrosion	27
Salt Spray	30
Alternate Immersion	31
Other Accelerated-Corrosion Testing Techniques	32
Environmental Chamber for Realistic-Test-Condition Simulation	32
Remarks	35
3 EXPERIMENTAL INVESTIGATIONS	36
Program Overview	36
Phase I	36
Phase II	42
Experimental Results	49
Phases III and IV - Rising-Load KISCC Test and Crack-Growth Test	49
Corrosion-Fatigue Test in Controlled Environment	55
General Corrosion	79
4 CONCLUSIONS	84
5 RECOMMENDATIONS	85
REFERENCES	86
APPENDIX A - SLOW-STRAIN-RATE TESTING IN CONTROLLED ATMOSPHERES	100
APPENDIX B - ACCELERATED ATMOSPHERIC-CORROSION TESTING	128

LIST OF ILLUSTRATIONS

<u>Figure</u>		<u>Page</u>
1	Schematic Diagram of Applied Stress and Time to Failure.	6
2	Schematic Representation of the Influence of Stress Intensity upon Stress-Corrosion-Cracking Velocity.	8
3	Schematic Representation of the Influence of Stress Intensity upon the Growth Rate of Corrosion-Fatigue Cracks.	9
4	Types of Fatigue-Crack-Growth Behavior.	11
5	WOL Specimen Modified for Use as a Stress-Corrosion-Susceptibility Test Specimen (from Ref. 17).	18
6	Slow-Loading-Rate K_{ISCC} Test (from Ref. 17).	19
7	Schematic of Rising-Load K_{ISCC} Test (from Ref. 17).	20
8	Effect of Environment Upon Load-Displacement Behavior (from Ref. 17).	21
9	Effect of Loading Rate Upon Apparent K_{ISCC} (from Ref. 17).	23
10	Effect of Loading Rate Upon Apparent K_{ISCC} in H_2S (from Ref. 17).	24
11	Effect of Environment upon Static-Load Crack-Growth Rate (from Ref. 17).	26
12	Environmental-System Flow Diagram.	33
13	Compact-Tension Plane-Strain Fracture-Toughness Specimen.	38
14	WOL Plane-Strain Fracture-Toughness Specimen.	40
15	Tensile Specimen.	41
16	Close-up Photograph Showing Detailed Setup of Plexiglas Environmental Chamber.	43
17	Line Diagram of Stainless-Steel Chamber with Controls.	44
18	Gastec-Tube Calibration Curve.	46
19	Close-up View of SSR Machine.	50
20	Load-Train Components of SSR Machine.	51

LIST OF ILLUSTRATIONS (Continued)

<u>Figure</u>		<u>Page</u>
21	Schematic Diagram of Step Loading in Rising-Load Test.	53
22	Plot of da/dN vs ΔK in 80% RH + 100 ppm SO_2 .	56
23	Crack-Growth-Rate Data Obtained for 4340 Steel (1440 MPa) Tested in 1000 ppm SO_2 + 80% RH Environment.	57
24	Plot of da/dN vs ΔK in 90% RH + 1000 ppm SO_2 at $R = 0.6$ and $F = 0.1$ Hz.	58
25	Plot of da/dN vs ΔK in 90% RH + 1000 ppm SO_2 at $R = 0.6$ and $F = 0.25$ Hz.	59
26	Plot of da/dN vs ΔK in 90% RH + 1000 ppm SO_2 at $R = 0.6$ and $F = 1.0$ Hz.	60
27	Plot of da/dN vs ΔK Showing K_{ISCC} Extrapolation at Different Frequencies.	62
28	Plot of da/dN vs ΔK in 90% RH + 1000 ppm SO_2 at $R = 0.8$ and $F = 0.1$ Hz.	63
29	Plot of da/dN vs ΔK in 100 ppm NO_2 + 80% RH.	64
30	Plot of da/dN vs ΔK in 100 ppm NO_2 + 80% RH + 5% NaCl at $R = 0.6$ and $F = 0.1$ Hz (a) for 7075-T6 Specimen STA48, (b) for 7075-T6 Specimen STA45.	65
31	Plot of da/dN vs ΔK in 100 ppm NO_2 + 80% RH + 5% NaCl at $R = 0.8$ and $F = 0.1$ Hz (a) for 7075-T6 Specimen STA46, (b) for 7075-T6 Specimen STA47.	67
32	Fracture Surface of Al 7075-T6 Specimen STA45, tested in 100 ppm NO_2 + 80% RH + 5% NaCl at $R = 0.6$ and $F = 0.1$ Hz.	68
33	(a) Fracture Surface of Al 7075-T6 Specimen STA46 Tested in 100 ppm NO_2 + 80% RH + 5% NaCl at $R = 0.8$ and $F = 0.1$ Hz, (b) Higher Magnification of (a).	71
34	Fracture Surface Showing Severe Secondary Cracking and Brittle Mode of Failure.	72
35	Fracture Surface of Specimen Tested in 100 ppm NO_2 + 80% RH + 5% NaCl at $R = 0.8$ and $F = 0.1$ Hz at a K level of ~ 14 ksi/in.	73

LIST OF ILLUSTRATIONS (Concluded)

<u>Figure</u>		<u>Page</u>
36	Plot of da/dN -vs- ΔK for 4340 Steel Tested in 100 ppm NO_2 + 80% RH.	75
37	Fractograph Taken from 4340 Steel Specimen Tested in 10 ppm NO_2 + 80% RH.	76
38	Plot of da/dN -vs- ΔK for 4340 Steel Tested in 80% RH + 5% NaCl.	77
39	Plot of da/dN -vs- ΔK for 4340 Steel (10 ST) Tested in 100 ppm NO_2 + 80% RH + 5% NaCl.	78
40	Plot of a -vs- N for 4340 Steel Tested in 100 ppm NO_2 + 80% RH + 5% NaCl.	80
41	Plot of a -vs- N for 4340 Steel Tested in 10 ppm NO_2 + 80% RH + 5% NaCl.	81
42	Plot of da/dN -vs- ΔK for 4340 Steel (BST) Tested in 100 ppm NO_2 + 80% RH + 5% NaCl.	82
43	Plot of da/dN -vs- ΔK for 4340 Steel (9ST) Tested in 10 ppm NO_2 + 80% RH + 5% NaCl.	83

LIST OF TABLES

<u>Table</u>		<u>Page</u>
1	Comparison of Data Scattering for 4340 Steel in Stress-Corrosion Cracking and in Corrosion Fatigue.	14
2	Summary of Some Stress-Corrosion Threshold Data (from Ref. 17).	25
3	Rising-Load Results.	54

Section 1

INTRODUCTION

Over the past several years a considerable number of studies have been conducted within the Air Force and at the National Bureau of Standards regarding the total cost of corrosion prevention and control for aircraft. The inescapable conclusion is that total corrosion costs in terms of life-cycle management and maintenance of aircraft represent an intolerable burden to the Air Force in maintaining force effectiveness at a reasonable cost to the taxpayer. In a 1978 NBS report¹ the total corrosion cost was calculated to be 70 billion dollars nationally. For the Air Force the direct cost of corrosion maintenance in the field and at the depot level has been estimated to be 750 million dollars, and the total corrosion cost including facilities is estimated to be in excess of one billion dollars. During the 1975 and 1977 AFOSR-AFML Corrosion Workshops, improved accelerated tests were cited as being a major area of need requiring further research.^{2,3} One of the major problems in effectively reducing aircraft-corrosion maintenance costs has been the inability of the research community to develop realistic corrosion tests which give meaningful results in a reasonable length of time. There are no accurate methods for accelerated testing for corrosion which yield reliable results for predicting the service life of aircraft components and materials which degrade or fail due to environmental attack. Current alternatives involve the use of gross tests such as salt-water immersion which yield relative corrosivity values that have no quantitative relation to service life or outdoor atmospheric exposure tests which require experiments of three to five years or longer and are specific to one local environment.

It is extremely difficult to discuss accelerated corrosion testing in a general sense because the type of test will depend upon the type of corrosion and its cause and operating mechanisms. Stress-corrosion cracking, corrosion fatigue, and atmospheric weathering have become a major problem of the aircraft industry. Because conventional corrosion testing requires a long testing time, is expensive, and does not

accurately simulate realistic environments, the first step toward achieving the cost-reduction goal in the area of corrosion is to develop realistic accelerated testing methods which are applicable to aerospace materials in service environments and which, therefore, meet Air Force needs.

This report describes a comprehensive experimental and analytical research program whose primary objective was the determination of the feasibility of developing an accelerated-corrosion testing technique for high-strength aerospace materials. The accelerated-corrosion testing technique in this study is generally understood to be a testing method which will reduce the routine testing time from months to days and will be sufficiently realistic to predict long-range corrosion behavior (such as stress-corrosion cracking, corrosion fatigue, and atmospheric weathering) of materials in service environments. It would have been an insurmountable task to study the quantitative details of the effect of a realistic environment upon the corrosion process. At the same time it was almost impossible to simulate accurately a service environment in the laboratory; even a serious attempt to achieve close simulation would have been prohibitively expensive. Fortunately, most of the ingredients present in the environment have negligible effects upon the corrosion process. Hence, the main aggressive components of an industrial atmosphere--such as SO_2 , NO_2 , and surface salt in the presence of air at several humidity levels--were used to simulate the environment. Concentration of the gas and the level of humidity were monitored and controlled within a specially designed environmental chamber.

The state-of-the-art in accelerated-corrosion testing methods as described in the ASTM Book of Standards and approved by the National Association of Corrosion Engineers involve the aforementioned use of gross tests such as salt fog and alternate salt-immersion tests with their lack of quantitative values for corrosivity or relative corrosivity with respect to service experience. Atmospheric outdoor tests where panels are exposed to various environments require a time scale which precludes rapid

materials-selection decisions or paint-protection-measures evaluations. These tests are specific to limited environments and seldom take into account stress factors which may accelerate the localized corrosion and enhance crack growth leading to premature failure. Cyclic loading is, of course, also precluded. Establishing realistic test environments requires, at a minimum, a reasonable selection of atmospheric environmental variables coupled with stress factors which aerospace components are expected to experience. The selection of appropriate air-quality standards is difficult and should be based upon knowledge of ambient-air pollutant levels and experimental work to determine the relative importance of these pollutants. The effects of SO_2 and NO_2 for high-strength steels and aluminum alloys must be related to the interaction of these gases with water vapor, surface salt, and airborne particulates and to casual factors.

The first set of tests involved slow-strain-rate measurements to determine the susceptibility of a material to stress-corrosion cracking.¹⁻⁷ In this study several corrosion testing methods such as slow strain rate, rising load, and corrosion fatigue were investigated for their adaptability as universal accelerated corrosion tests. The slow-strain-rate testing technique is used to determine the susceptibility of a material to stress-corrosion cracking (SCC).⁴⁻¹⁴ Over the past decade this technique has found wide-spread application due to the reproducibility of the data and relatively short period of testing time involved. The technique has been used mainly to optimize the simulated environment which results in accelerated crack growth and failure by SCC.¹⁵

McIntyre, et al.,¹⁶ introduced the idea of exploring the rising-load method as an accelerated test to determine the threshold stress intensity for SCC (K_{ISCC}). In fact, they demonstrated that the testing time could be reduced from many hours to even a few minutes in some cases. This method is currently being used quite extensively for rapid determination of approximate values of K_{ISCC} .^{17,18}

Static SCC tests rank poorly in reproducibility due to the wide scatter in the data, apart from the long testing time involved. The counterpart dynamic crack-growth experiments, i.e., the low-cycle corrosion-fatigue tests, have no such drawbacks; and these tests can be tailored to generate information which is similar to that obtained from static SCC tests. Several investigators¹⁹⁻²¹ have attempted to predict SCC behavior from corrosion-fatigue tests. The present study deals extensively with the feasibility of determining K_{ISCC} through an accelerated testing technique for 4340 steels and Al 7075-T6 in simulated industrial environments.

General-corrosion field-exposure tests were conducted to obtain data for correlation with that obtained from laboratory tests conducted in a simulated environment, as well as to provide justification for the use of simulated environments for other tests.

Section 2

TECHNICAL BACKGROUND

A state-of-the art survey was conducted on techniques showing potential as accelerated-corrosion tests. The survey was limited in scope to (1) localized corrosion including stress corrosion cracking (SCC) and corrosion fatigue (CF) and (2) general corrosion. These failure modes were selected because general corrosion and crack growth due to SCC and CF are major causes of corrosion damage to Air Force vehicles. As a first step the pertinent information available in the literature relative to this investigation was reviewed, some of which will be discussed here.

CRACK-GROWTH-RATE MEASUREMENT

Since structural failure results from some type of environmentally assisted crack initiation and propagation, crack-growth behavior should be investigated under controlled environmental conditions in order to develop quantitative models which can be extrapolated to predict material behavior in field environments. This section will discuss crack-growth behavior and the techniques commonly used for accelerated-corrosion testing.

Environmentally enhanced cracking is a difficult corrosion problem to test accurately in the laboratory. Traditionally, static weight-loaded tests are conducted over periods of 200 to 1000 hr to determine the SCC behavior. The data are then extrapolated to structures which must have a useful lifetime of many thousands of hours.

Generally, the time to failure is plotted as a function of applied stress (Fig. 1), and an attempt is often made to define a "threshold" stress below which no SCC will occur. In many cases, however, crack initiation is the controlling factor in these tests, and the data are often widely scattered and irreproducible. In order to avoid the inherent lack of reproducibility, several experimental techniques²² have been

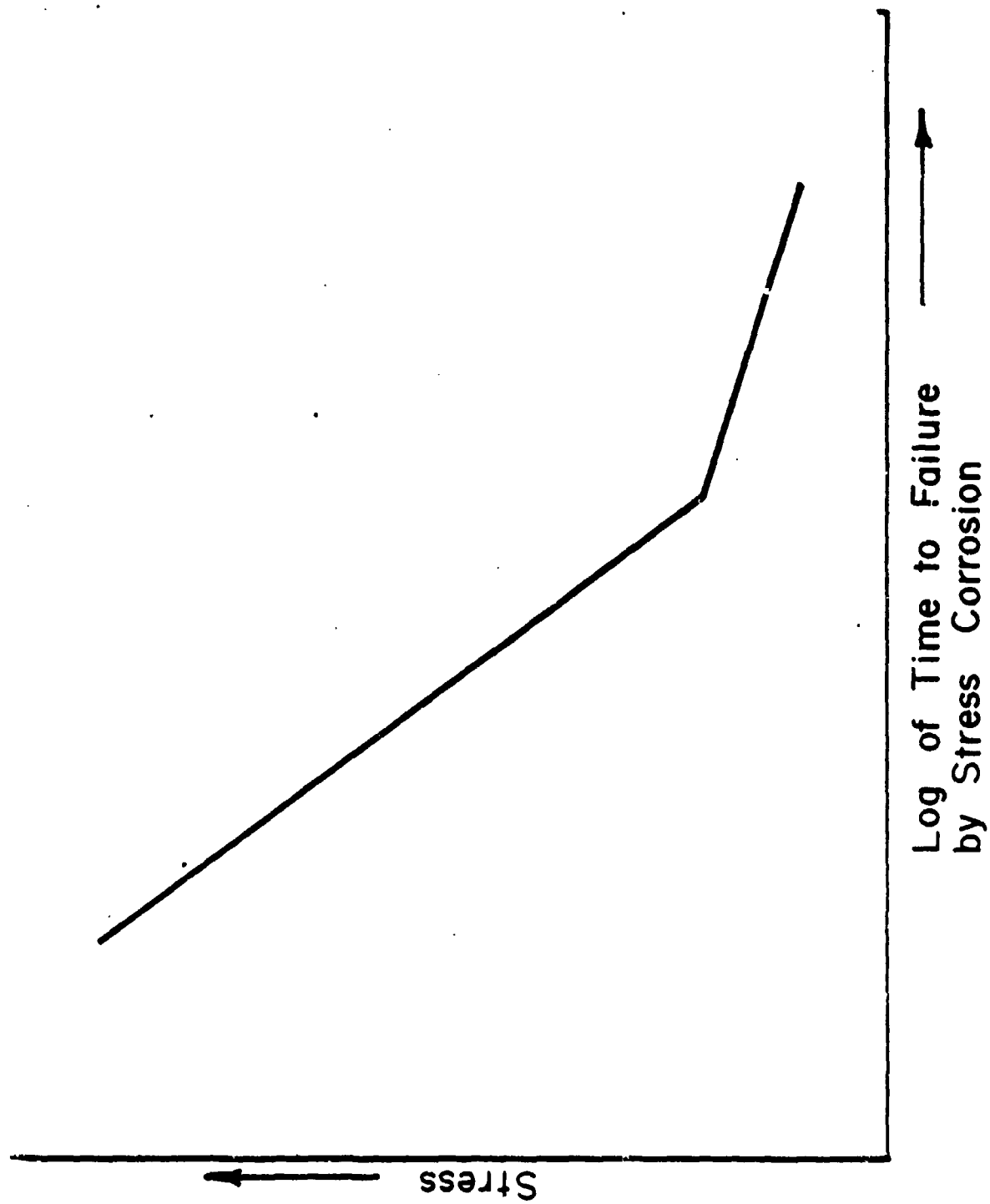


Figure 1. Schematic Diagram of Applied Stress and Time to Failure.

suggested as alternatives to the standard static SCC test. Experiments utilizing fracture-mechanics^{22, 23} principles have been developed to monitor crack-growth rates as a function of stress concentration where a stress-intensity factor is defined as

$$K = \sigma\sqrt{a}$$

σ = applied stress

a = crack length

The schematic representation of such crack-growth data yields a curve having three distinct regions²⁴ as shown in Fig. 2. The crack-growth rate in Regions I and III of this curve is strongly stress-intensity dependent, while in Region II where a plateau is exhibited, the crack-growth rate is virtually independent of stress intensity. Often Regions I or III are not observed. For example, Region I is often absent in titanium alloys tested in neutral aqueous-halide solutions.²⁵ In the same environment, most commercial high-strength aluminum alloys and magnesium alloys exhibit Regions I and II but not Region III.^{26, 27} For many high-strength aluminum alloys, it has been impossible to establish a threshold stress intensity (K_{ISCC}) below which stress-corrosion cracks will not propagate.^{26, 27} K_{ISCC} is a useful parameter for engineering-design purposes, but its routine determination is a long drawn-out procedure because the crack must be propagated very slowly in order to define Region I.

As in the case of SCC, the use of fracture-mechanics techniques has also been applied, and similar three-region behavior is obtained on the ΔK -vs- da/dN curve for corrosion fatigue. For example, Fig. 3 is a plot of crack velocity (da/dN) as a function of ΔK for three cases.

The crack-growth rate in Region I at low ΔK values is extremely stress-intensity dependent, and the da/dN -vs- ΔK curve becomes almost parallel to the crack-growth-rate axis. The corresponding stress intensity appears to be an environment-dependent threshold which is denoted by ΔK_{ICF} ,

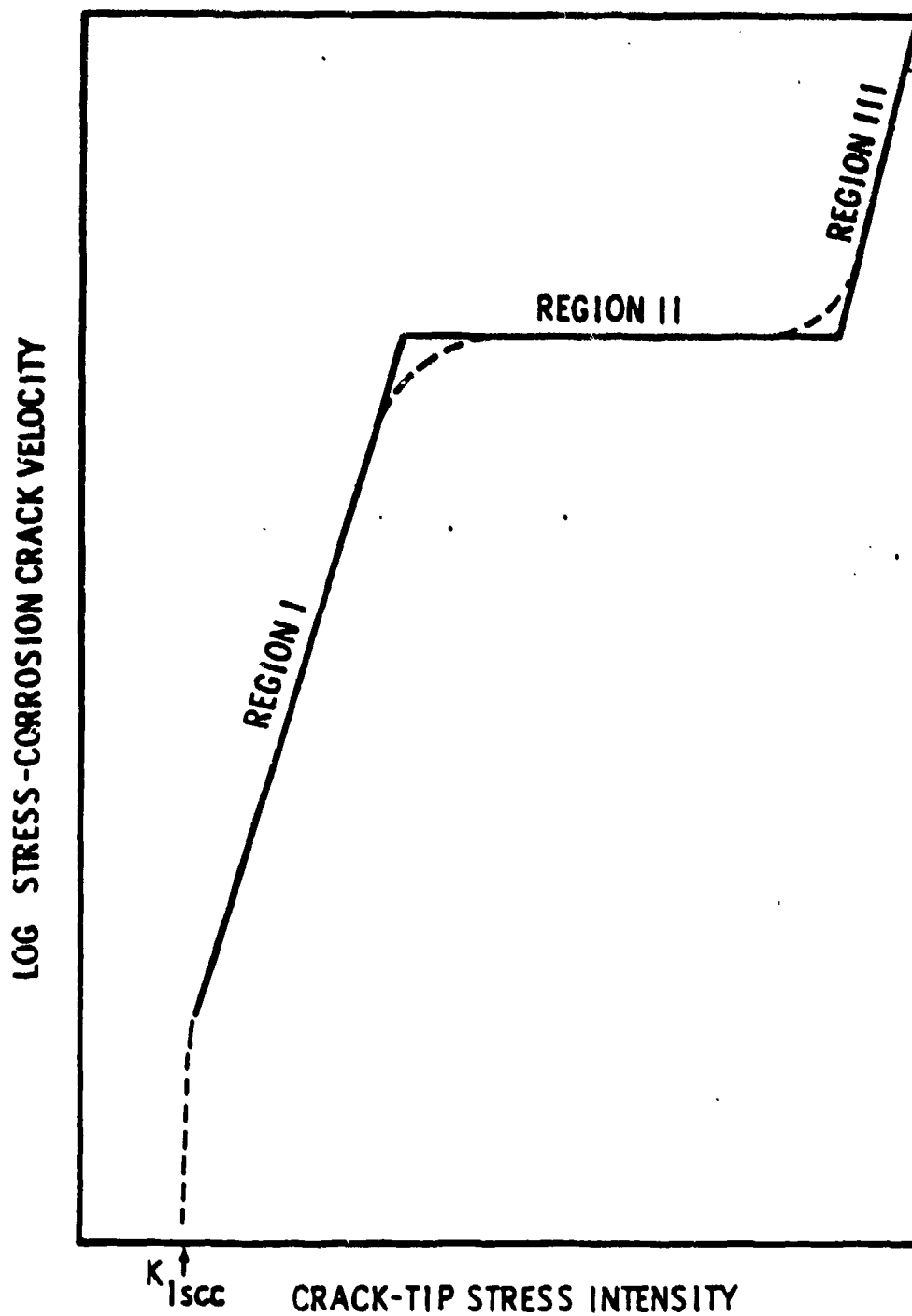


Figure 2. Schematic Representation of the Influence of Stress Intensity upon Stress-Corrosion-Cracking Velocity.

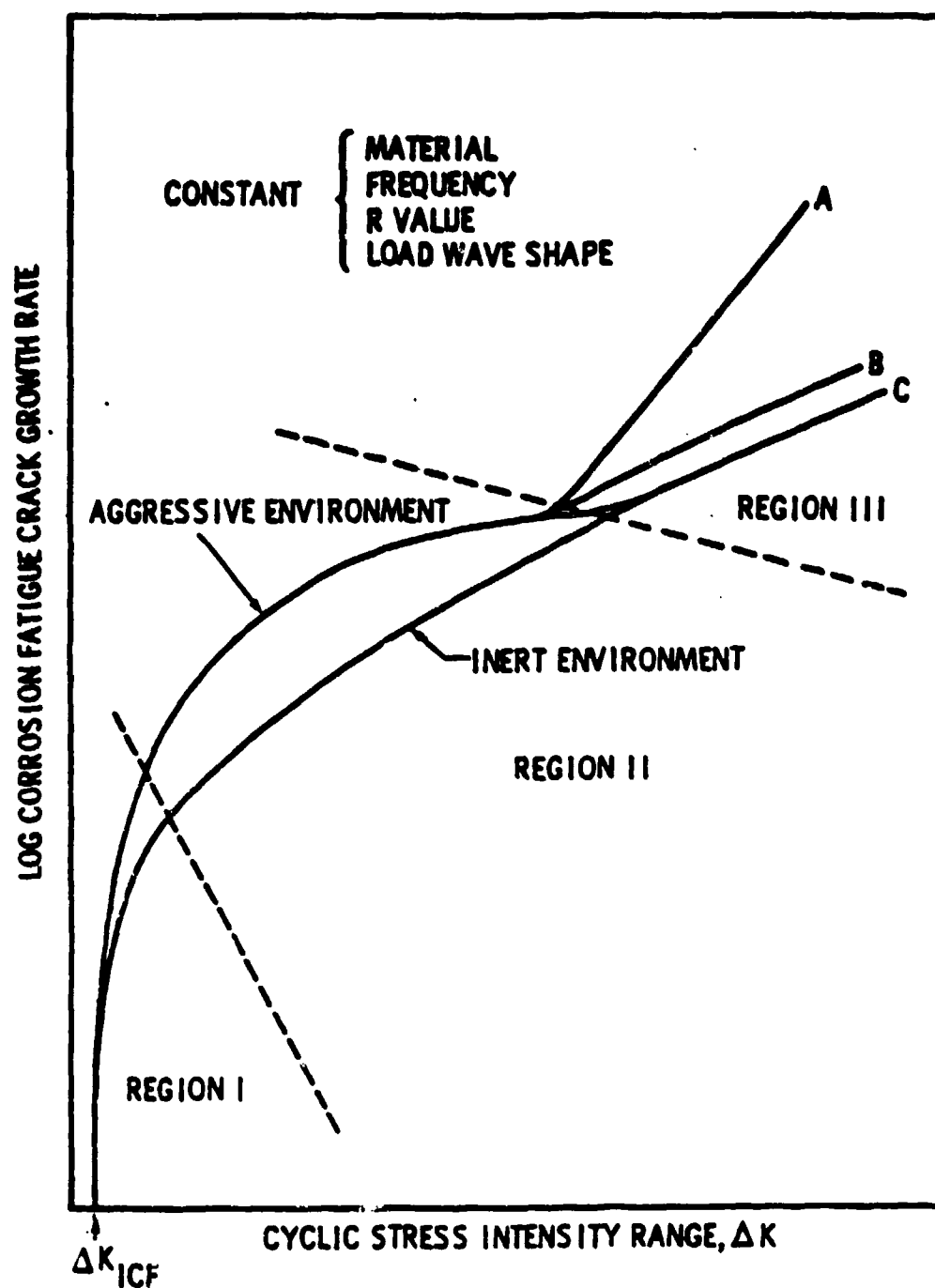


Figure 3. Schematic Representation of the Influence of Stress Intensity upon the Growth Rate of Corrosion-Fatigue Cracks.

in analogy to K_{ISCC} .²⁸ In Region II the corrosion-fatigue crack-growth rate often depends strongly upon the environment, but its stress dependence is considerably reduced. Indeed, in some instances (e.g., a titanium alloy exposed to sea water),²⁹ a plateau in Region II has been reported. Inert environments such as dry argon or vacuum produce fatigue-crack-growth rates in Region II which are always stress dependent. In this region, the functional relationship between the crack-growth rate and the crack-tip stress-intensity range ΔK can often be approximated by a fourth-power law³⁰

$$da/dN = \text{const } (\Delta K)^4$$

On the basis of data gathered over the past 20 years, the steady-rate response of fatigue-crack growth to environments may be grouped into three basic types and will be discussed in relation to K_{ISCC} as in Fig. 4. Type-A behavior is typified by the Al-water system.³¹ Environmental effects result from the interaction of fatigue and environmental attack. Type-B behavior is represented by the hydrogenated system.^{32,33} Environmental crack growth can be directly related to sustained-load crack growth, with no interaction effects.³⁴⁻⁴¹ Type-C represents the behavior of most alloy-environment systems. Above K_{ISCC} , the behavior tends toward Type A, with the associated interaction effects. The transition between Type B and C behavior is not always sharply defined. While these data (stress corrosion and corrosion fatigue) are highly useful, it should be realized that they are dependent upon many variables, e.g., mechanical, environmental, metallurgical, and geometrical. Some of these variables are listed below.

Mechanical Variables

- Maximum-stress or stress-intensity factor
- Cyclic-stress or stress-intensity-factor range
- Stress ratio or load ratio, R
- Cyclic frequency

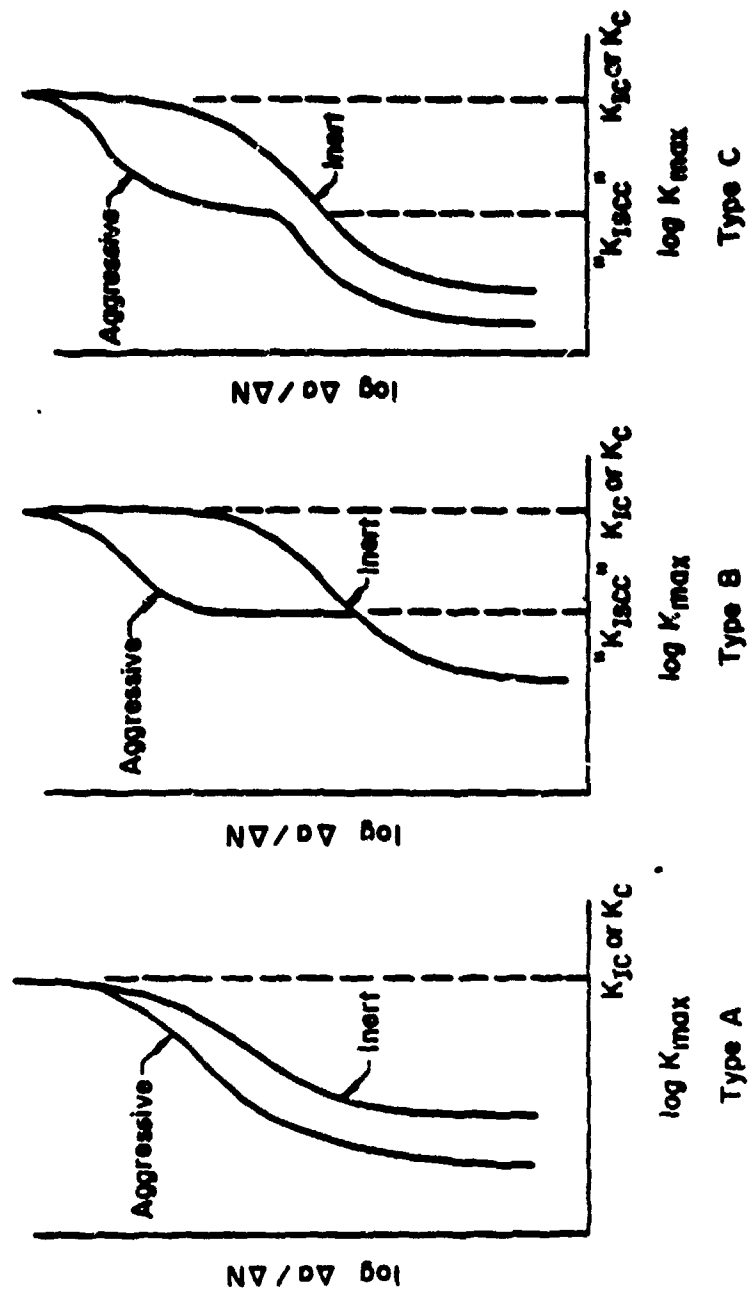


Figure 4. Types of Fatigue-Crack-Growth Behavior.

Mechanical Variables Cont'd

- Cyclic waveform
- Load interaction in variable-amplitude loading
- Residual stress

Environmental Variables

- Types of environment
- Concentration of damaging species in the environments
- Temperature
- Pressure
- Electrochemical potential
- pH
- Electrolyte viscosity
- Velocity of the environment

Metallurgical Variables

- Alloy composition
- Distribution of alloying elements and impurities
- Microstructure and crystal structure
- Orientation of grain and grain boundaries

Geometrical Variables

- Crack geometry
- Crack size in relation to component dimensions
- Component geometry adjoining crack
- Stress concentration associated with design

Some of these variables interact, e.g., some loading variables may interact with the environment (many of the observed effects of irreproducibility can be traced directly to environmental interactions).⁴²⁻⁴⁶ The large number of variables make the reduction of laboratory-obtained data to practice a highly complex problem. Only very careful control of these parameters along with practical experience will yield successful predictability.

Lynch, et al.,⁴⁷⁻⁴⁹ in an attempt to develop an inhibitor for crack inhibition of high-strength steels for aerospace applications, found corrosion-fatigue crack-growth experiments to be far better than static stress-corrosion tests with respect to reproducibility. The static SCC tests rank poorly in reproducibility due to wide scatter in the data. For example, for 4340 steels tested in 0.1M NaCl solution, Lynch⁴⁸ found the crack-growth-rate data at the plateau portion ranging from 0.21 to 0.42 in./hr to be much more widely scattered than the data obtained from corrosion-fatigue tests of 2.4 to 3.4×10^{-4} in./cycle for the same material in the same environment.

Detailed data as presented in Table 1 have been retabulated from Lynch's work.⁴⁷ Good reproducibility was found for Al-alloys also when the crack-growth data were obtained from corrosion-fatigue tests;⁴⁹ the static test results, on the other hand, showed considerable scatter.

Russian investigators⁵⁰ have used corrosion-fatigue experiments as an alternative to SCC tests in predicting stress-corrosion cracking of casing steels in 3% NaCl solution. Japanese investigators⁵¹ have also used the corrosion-fatigue technique as an accelerated screening test for intergranular corrosion failures.

Because of wide scatter in the data and the long testing time required for a static stress-corrosion test, the search for an alternative test has continued. Currently suggestions¹⁹⁻²¹ are being made for predicting stress-corrosion-cracking behavior from crack-growth studies in corrosion fatigue. However, a very careful approach is needed in this direction. As mentioned earlier, corrosion-fatigue experiments, in general, are very complex due to the numerous independent parameters. The crack-growth rate in a corrosion-fatigue experiment is affected by frequency, stress ratio, mean stress, waveform, and nature of the aggressiveness of the environment; in addition, the geometry of the specimen itself could complicate the situation. But the environment and the geometry

TABLE 1
COMPARISON OF DATA SCATTERING FOR 4340 STEEL IN
STRESS-CORROSION CRACKING AND CORROSION FATIGUE

Environment: 0.1M NaCl Aqueous Solution

Crack-Growth Rate, Plateau			
Stress-Corrosion Cracking		Corrosion Fatigue	
Specimen	Rate (in./hr)	Specimen	Rate (in./cycle)
AT1	0.24	AT5	2.4×10^{-4}
AT7	0.21	AT6	2.4×10^{-4}
AT8	0.25	BL4	3.4×10^{-4}
AT9	0.22		
BL3	0.38		
BL8	0.42		

of the specimen could be made common for the two conditions--stress corrosion and corrosion fatigue--and the stress range could be manipulated somewhat to obtain the data required for correlation.

Gallagher and Wei¹⁹ suggested a linear hypothesis to predict the crack-growth rate in corrosion fatigue from static stress corrosion results. Based upon this Parkins and Greenwall⁵² found a good correlation between their corrosion-fatigue and stress-corrosion-cracking results (based upon their superposition model) for Mg alloys in carbonate solution. The model¹⁹ presents a very simple relation

$$da/dN|_c = da/dN|_{\text{environment}} + da/dN|_r$$

where $da/dN|_c$ is the corrosion-fatigue crack-growth rate, $da/dN|_{\text{environment}}$ is the environment attributed to crack-growth rate, and $da/dN|_r$ is the cycle-dependent fatigue-crack-growth rate measured in an inert atmosphere.

Wei and Landes⁵³ modified the environmental component, and Gallagher¹⁹ later introduced a frequency term to generalize the simple linear-summation model described earlier. Reasonable correlations have been obtained with several systems⁵⁴ above K_{ISCC} under very specific conditions. The main drawback of the model seems to be the absence of any interaction term, which could be difficult to handle; additional experimental work is definitely required in this direction.

After extensive investigation of crack-growth phenomena and fracture analysis of iron, aluminum, and titanium, Schwalbe⁵⁵⁻⁵⁷ suggested that crack propagation under both monotonic and cyclic loading conditions may be governed by essentially the same micromechanism and may be described by similar fracture laws. Although no direct correlation was suggested, there is good evidence of some possible extrapolations of crack-growth rates under monotonic loading conditions from the cyclic-load situation using the normalized da/dN -vs- ΔK curve.

Unfortunately, most of the tests in these investigations were conducted in an inert atmosphere or in laboratory air and did not extend to more-realistic and severe environmental situations. The environmental enhancement of crack growth is expected to be more dominant in aggressive environments. The stress-corrosion contribution in corrosion-fatigue experiments could be maximized by manipulating the stress ratio R and frequency which will provide a better opportunity for extrapolation of K_{ISCC} from such a test.

SLOW-STRAIN-RATE TEST

Many of the disadvantages of the traditional forms of SCC susceptibility testing are eliminated by testing smooth specimens at a constant strain rate rather than under conditions of constant load or constant strain.⁵⁸ The constant-strain-rate test is a form of simple tensile testing in which a smooth specimen is pulled in tension in the environment of interest at a constant strain rate until failure occurs. The constant-slow-strain-rate test^{4-14, 59-66} for stress-corrosion cracking has been extensively applied in the corrosion-research community during the last few years. This technique developed by Parkins^{8,9} provides a rapid and positive laboratory method for determining the SCC susceptibility of a material in a specific environment in which other tests do not detect SCC.

For a comparison of the severity of the SCC of materials in a fixed environment or of the aggressiveness of an environment, the commonly used parameters are time to failure, reduction of specimen area, and elongation of the specimen. However, only metallographic examination of the fractured surface can provide definite identification of the presence of SCC. The number of secondary stress-corrosion cracks and the length of the cracks are other parameters often used for quantitative comparison.

It seems probable that other SCC parameters such as threshold stress, incubation time, and crack-growth rate may also be obtained by the slow-strain-rate test which would greatly enhance the usefulness of this technique.

The constant-slow-strain rate test should be developed as an effective accelerated testing technique initially for SCC-susceptibility detection and later, in a modified form, for rapid determination of K_{ISCC} .

RISING-LOAD TESTS

Currently two methods⁶⁷⁻⁶⁸ are used for determining the K_{ISCC} value of a material: 1) the constant-load cantilever-beam test and 2) the constant-displacement or "bolt-loaded" compact-specimen test. The required test time for obtaining meaningful K_{ISCC} data often ranges from hundreds to thousands of hours. However, the testing time may be shortened by using, if feasible, 1) an approximation of K_{ISCC} from corrosion-fatigue test data obtained by crack-growth-rate tests and 2) the rising-load K_{ISCC} test described below.

The rising-load K_{ISCC} test was initially proposed in 1972 by McInyre, et al.;¹⁶ K_{ISCC} values were determined for a series of high-strength steels (200-400 ksi yield strength) exposed to sea water, hydrogen gas, and hydrogen-sulfide gas environments. These tests showed that the time required for K_{ISCC} determination can be reduced from many hours to even a few minutes in some cases. In 1975 Clark, et al.,¹⁷ reported the results of their work at Westinghouse Research to further evaluate the technique and establish its limitations. In Clark's report, K_{ISCC} data obtained from the long-time "dead-bolt" test and from the rising-load test were evaluated and compared. In Figs. 5 and 6 the specimens used in these tests are shown. For the rising-load K_{ISCC} test, the testing procedure is essentially the same as for the K_{IC} test described in ASTM E399-72 for plane-strain fracture-toughness measurements,⁶⁹ except that a slower loading rate is used (20-5,000 lb/min. vs 4,500-22,500 lb/min) and the specimen is exposed to the environment while being loaded. Figure 7 is a schematic of the rising-load K_{ISCC} test, and Fig. 8 demonstrates the effect of environment upon load-displacement behavior.

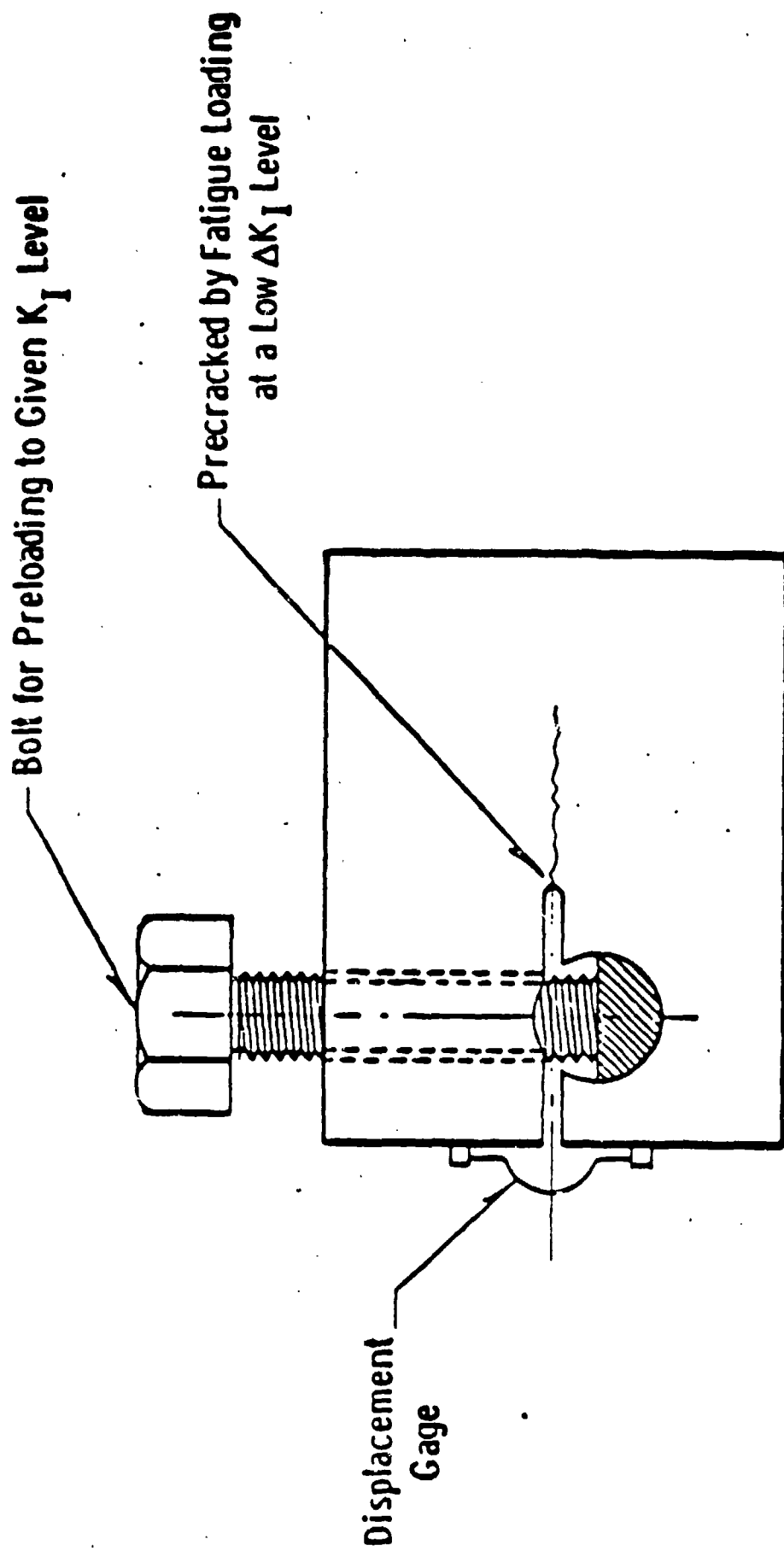


Figure 5. WOL Specimen Modified for Use as a Stress-Corrosion-Susceptibility Test Specimen (from ref. 17).

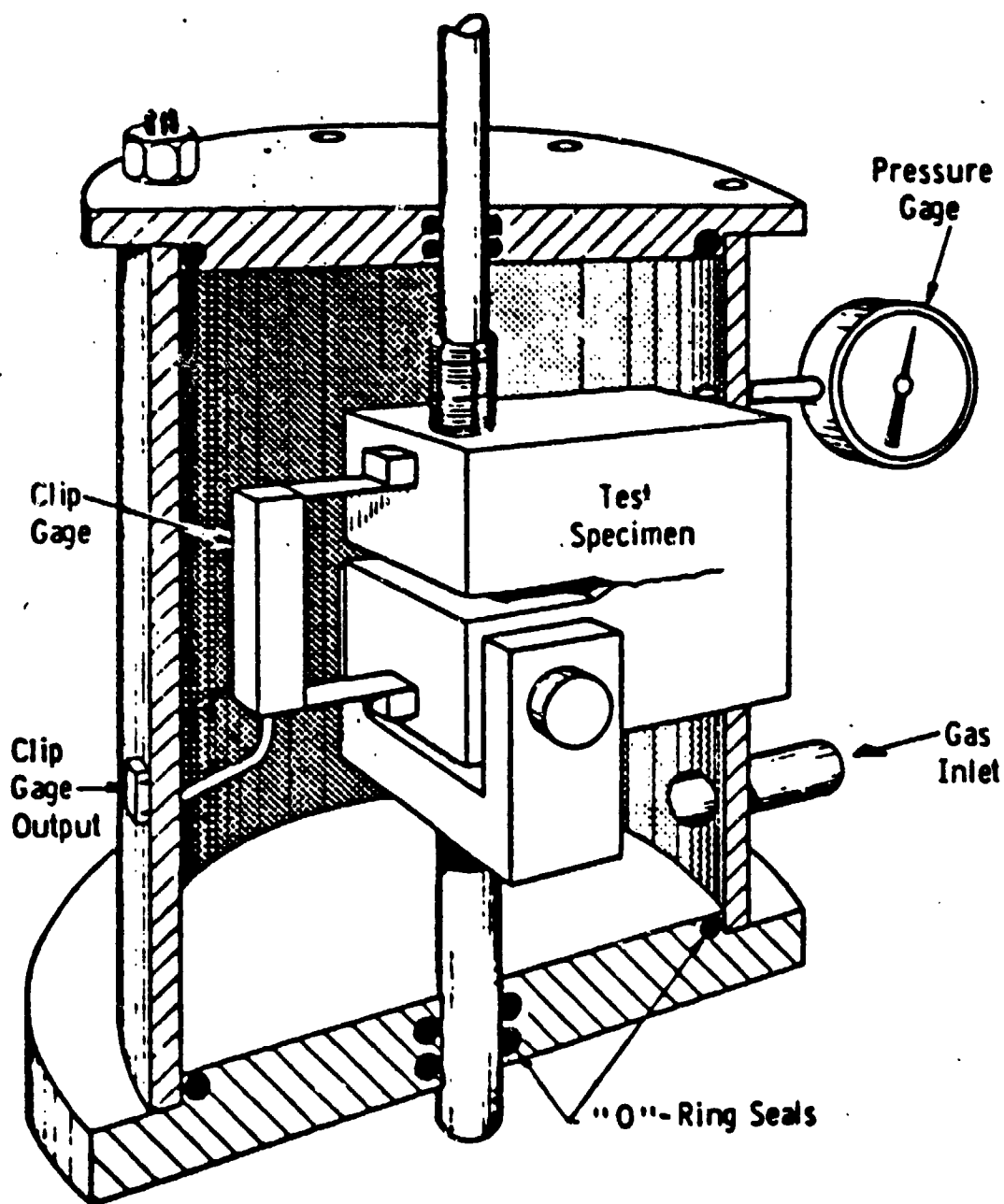


Figure 6. Slow-Loading-Rate K_{ISCC} Test (from Ref. 17).

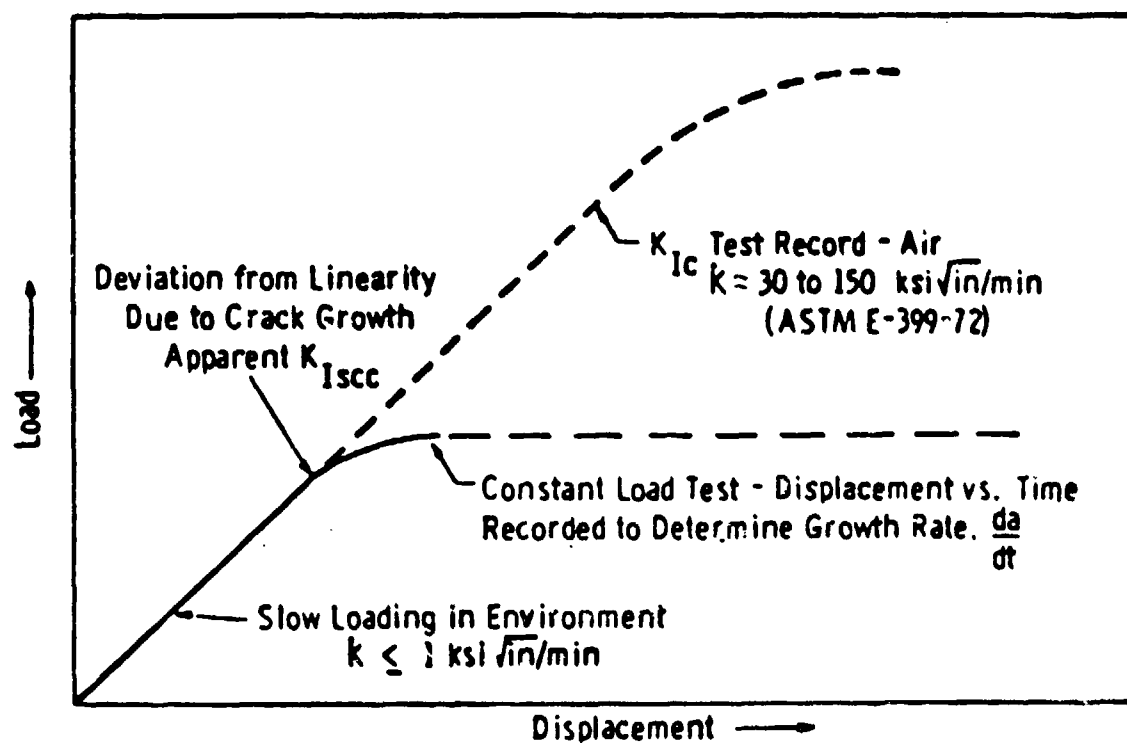


Figure 7. Schematic of Rising-Load K_{ISCC} Test (from Ref. 17).

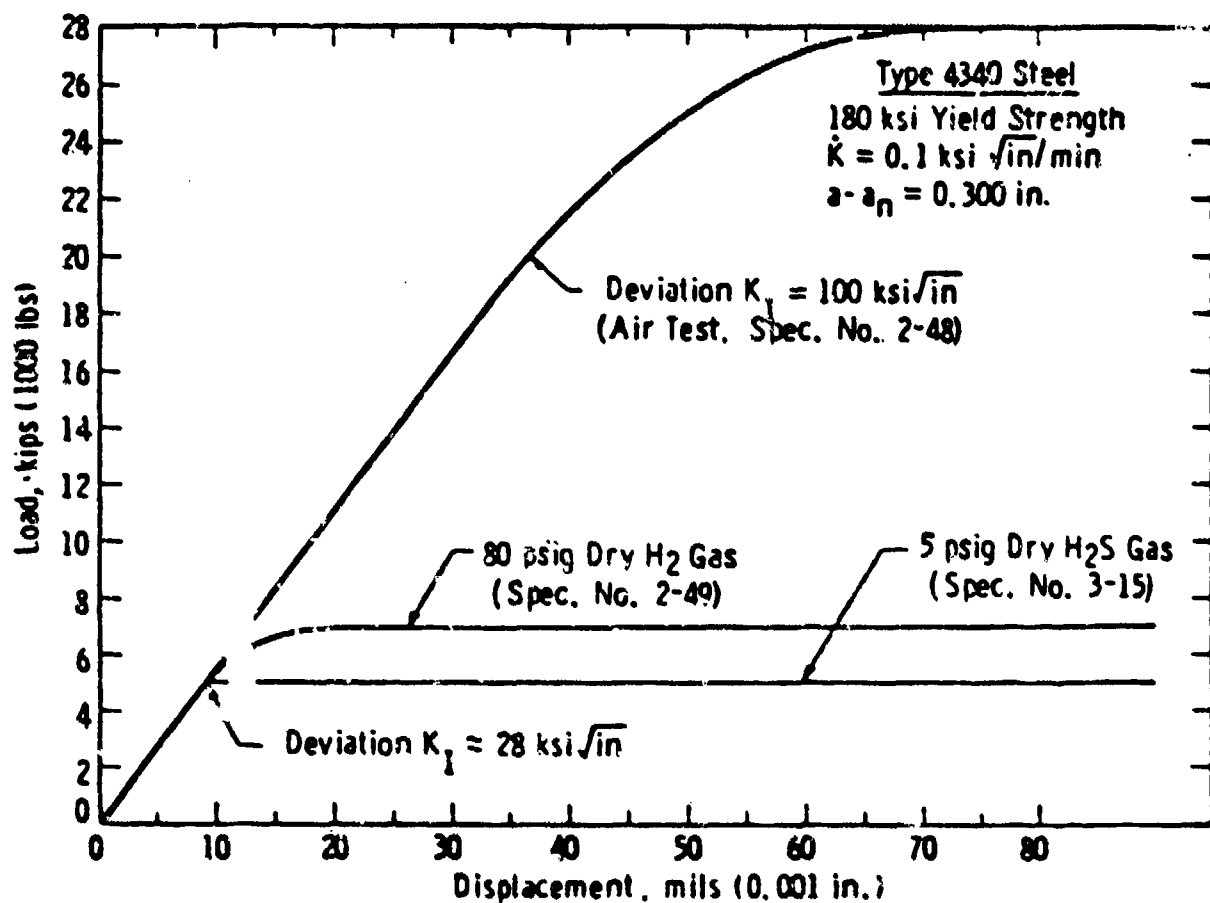


Figure 8. Effect of Environment Upon Load-Displacement Behavior (from Ref. 17).

The effect of the rising-load rate, K , upon the apparent K_{ISCC} is dependent upon the specific material-environment combination which is clearly shown in Figs. 9 and 10. However, the apparent K_{ISCC} approaches the K_{ISCC} obtained from the long-time test data as the loading rate decreases. Table 2 is a further comparison of K_{ISCC} data obtained by the two test methods.

The main advantage of the rising-load test for K_{ISCC} is rapid data collection. Because of the absence of a significant prior-history effect upon the apparent K_{ISCC} , the test time may be further reduced by preliminary rapid loading of the test specimen to about 80% of the K_{ISCC} if the long-time K_{ISCC} can be estimated. Slow-rising-load rates can then be applied to the test specimen in order to obtain the long-time K_{ISCC} . For example, if the long-time K_{ISCC} is assumed to be $\sim 80 \text{ ksi}\sqrt{\text{in.}}$, the test specimen can first be rapidly loaded to $60 \text{ ksi}\sqrt{\text{in.}}$ at a rate of $K = 10 \text{ ksi}\sqrt{\text{in.}}/\text{min.}$ and then at a low rate such as $K = 0.1 \text{ ksi}\sqrt{\text{in.}}/\text{min.}$ for assessing the long-time test K_{ISCC} value. Naturally, the loading-rate reduction will not be required if the long-time K_{ISCC} is only slightly dependent upon loading rate. Another advantage of the rising-load K_{ISCC} test is that a single specimen can be used to generate several data points. An apparent K_{ISCC} -vs-loading-rate curve such as that presented in Fig. 9 may be obtained using only one specimen. Finally, crack-growth rate may also be obtained by measuring the crack-extension rate while maintaining the load at a constant value. Likewise, a complete crack-growth-rate-vs-stress-intensity curve can also be obtained with a single specimen by maintaining the load at different K values as shown in Fig. 11.

Two limitations with the rising-load test were reported by Clark: 1) an incubation period of several days or more may exist in certain material-environment systems and 2) the test must be conducted at a loading rate which is sufficiently slow to allow the detection of crack growth before the load increases a significant amount beyond the onset of crack initiation. The faster the rate of crack growth associated with a given material-environment system, the less effect the loading rate will have

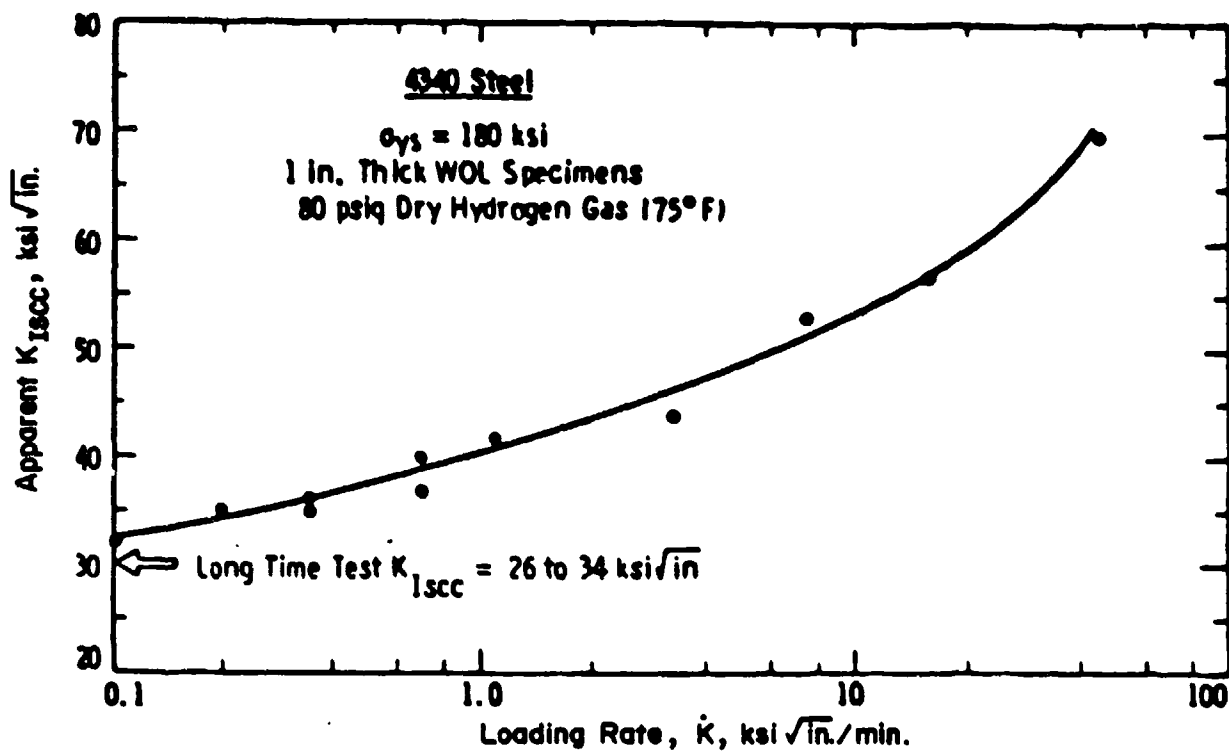


Figure 9. Effect of Loading Rate Upon Apparent K_{ISCC} (from Ref. 17).

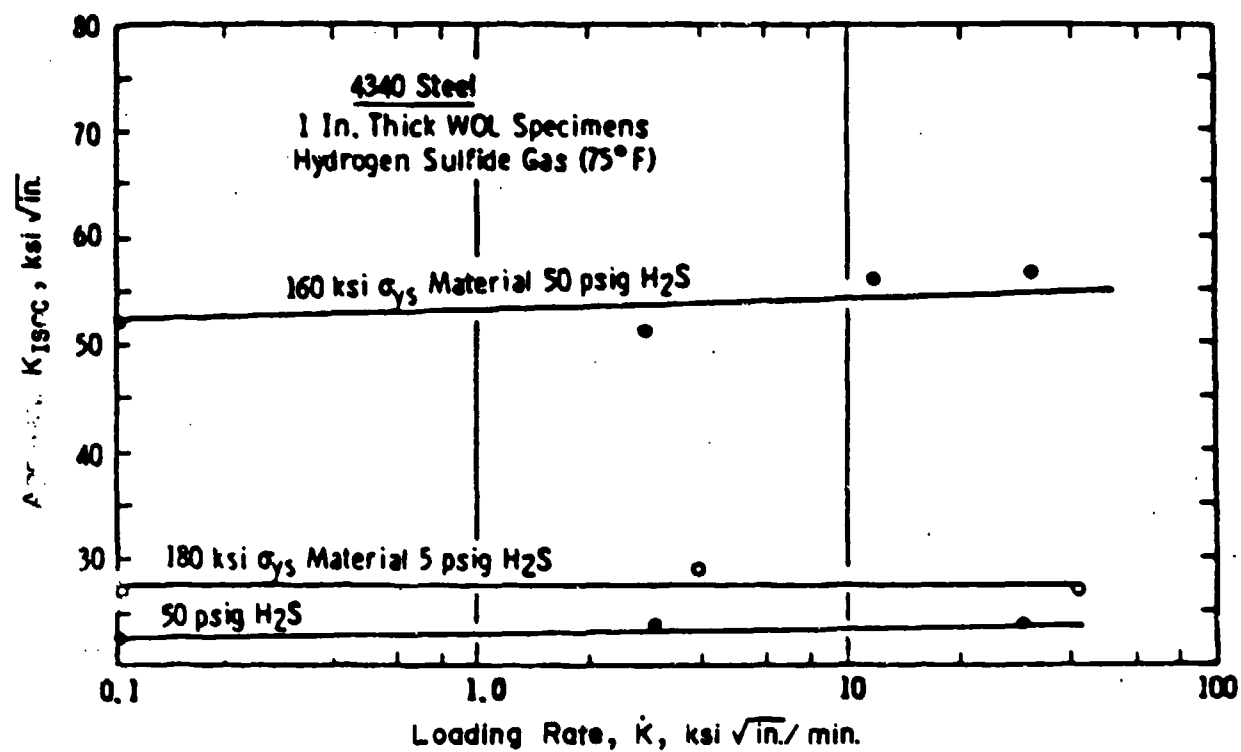


Figure 10. Effect of Loading Rate Upon Apparent K_{ISCC} in H_2S (from Ref. 17).

TABLE 2

SUMMARY OF SOME STRESS-CORROSION THRESHOLD DATA (from Ref. 17)

Environment	$K_{I,0.01}$, ksi $\sqrt{\text{in.}}$, (long time bolt loaded tests)	Apparent $K_{I,0.01}$, ksi $\sqrt{\text{in.}}$, (rising load tests)
180-KSI YIELD-STRENGTH TYPE 4340 STEEL*		
54% RH ^b air	no growth to $K_I = 105$	100
Synthetic seawater	37	no growth to 60
H ₂ gas, 80 psig	30	32
H ₂ S gas, 5 psig	26	27
H ₂ S gas, 18 psig	...	24
H ₂ S gas, 50 psig	27	23
H ₂ S gas plus 5 volume % air	...	26
160-KSI YIELD-STRENGTH TYPE 4340 STEEL		
Synthetic seawater	87	...
H ₂ gas, 80 psig	59	60
H ₂ S gas, 5 psig	...	88
H ₂ S gas, 18 psig	...	69
H ₂ S gas, 50 psig	60	54

* $\dot{K} \approx 0.1 \text{ ksi}\sqrt{\text{min}}$ ^b RH = relative humidity.

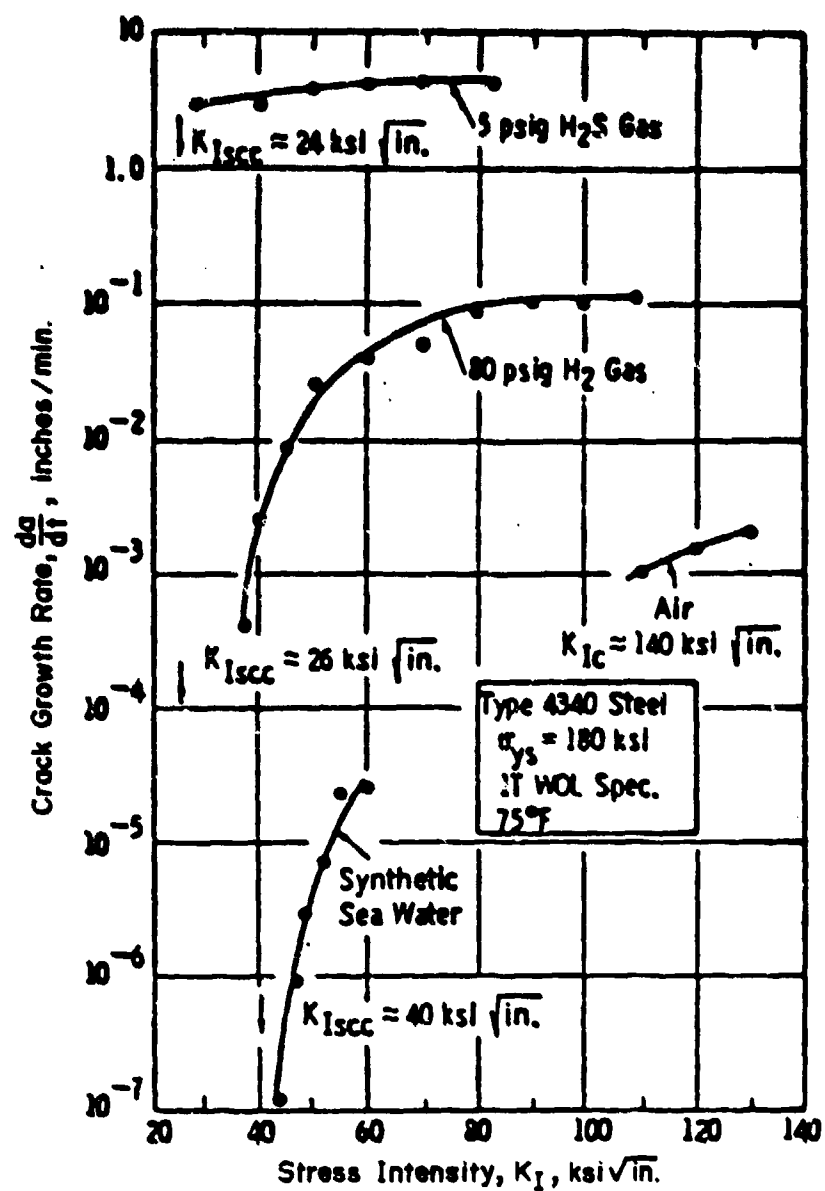


Figure 11. Effect of Environment upon Static-Load Crack-Growth Rate (from Ref. 17).

upon the apparent K_{ISCC} measured. Therefore, the rising-load technique is best suited for a material-environment system having a short SCC induction time but fast crack-growth rate.

It is clear that the rising-load test may be used as a valuable method for rapid evaluation of K_{ISCC} , although care should be taken to overcome certain limitations imposed by the technique. This technique was utilized to generate K_{ISCC} data in the gaseous environments used in this investigation.

GENERAL CORROSION

An accelerated-general-corrosion test for aircraft materials, especially for the aircraft skin materials, would be essentially the same as that for accelerated atmospheric corrosion because most military aircraft remain on the ground at various Air Force bases most of the time. The need for accelerated laboratory testing procedures for predicting atmospheric weathering has been widely discussed and reported.⁷⁰ Atmospheric corrosion studies have been conducted over a period of more than 30 years,⁷¹ however, these studies mainly concern the corrosion behavior of materials in broadly classified atmospheres such as industrial, marine, urban, and rural. The main purpose of these studies has been the development of weathering-resistant alloys⁷² rather than the investigation of environmental effects.

Capp⁷³ is said to be the first to publish a procedure for carrying out an accelerated test intended to simulate atmospheric exposure. Vernor⁷⁴⁻⁷⁷ described the importance of the critical-humidity concept in atmospheric corrosion. From this point on, much work was done in an attempt to improve the correlation between accelerated test results and atmospheric exposure data. The techniques utilized have involved the use of humidity cabinets,⁷⁸ cyclic or alternate dry-condensation conditions in a cabinet,⁷⁹⁻⁸² and spray and fogs.⁸³⁻⁸⁴ It was found³⁵ that the data obtained in accelerated laboratory testing of metals in the presence of SO_2 gas

and high-humidity conditions can be correlated to some degree with actual corrosion behavior in an industrial environment.^{1-2, 86-89} However, no reliable and predictive equation relating environmental factors and corrosion rates has been established based upon these results.

A recent work by LeGault, et al.,⁹⁰⁻⁹² on prediction of the atmospheric corrosion of steel in industrial and marine environments is of interest. They developed a correlation between the time periods during which a specimen is exposed in the laboratory and in the field based upon oxide reduction time, e.g., one day of lab exposure is equal to one month of field exposure. Whether this relationship exists in other metal-environment systems has not been investigated thoroughly and deserves further exploration.

In this work it appears that it was not possible to develop good correlation between environmental factors and corrosion rates of metals. LeGault⁹¹ attempted to utilize Pourbaix's concept⁹³ of measuring open-circuit potential instead of weight loss; however, he was unable to arrive at any useful "time-equivalency" relationship such as the one he had obtained using the oxide-reduction-time measurement. This could be due to the fact that Pourbaix's technique is effective only in specific metal-environment systems.

In the last decade, as a result of advances made in gaseous-pollutant monitoring and sampling instruments, it has become known that the urban atmosphere consists of several corrosive components such as SO_2 , NO_2 , O_3 , hydrocarbons, nitrates, other salts, and particulates. Thus, it is feasible to investigate the correlation between atmospheric corrosive agents and the atmospheric corrosion of metals. Several early studies⁹⁴⁻¹⁰⁰ showed the effects of SO_2 content and relative humidity in the atmosphere upon the corrosion of Zn and Fe. However, until recently, very few attempts have been made to simulate realistic weathering conditions in the laboratory and to correlate these with atmospheric corrosion obtained from outdoor exposure.

Mansfield¹⁰¹ conducted an extensive investigation on atmospheric weathering for the purpose of predicting metal corrosion in the urban atmosphere. This study was supported by the work of Haynie¹⁰²⁻¹⁰⁶ at the EPA who designed a special chamber to simulate atmospheric weathering in an attempt to predict atmospheric corrosion from laboratory test results. These attempts resulted in a predictive equation which requires further consideration.

More recently, Pourbaix¹⁰⁷ conducted some experimental work on the corrosion behavior of weathering steels in Western Europe. He simulated outdoor exposure in the laboratory by alternately immersing steel specimens in salt solutions and polluted atmospheres. In this way he found that the weight loss of these steels consistently follows the general rate law of $\Delta W = kt^N$, where ΔW and t are weight loss and test duration of the specimens and k and N are experimentally determined constants. The values of k and N are different for the same steel exposed in different simulated atmospheric environments. His observations are interesting, but the predictability of his equations remains to be seen.

The most efficient method for developing accelerated-corrosion tests appears to involve statistically designed experiments in an environmental chamber with provisions for simulating day and night situations as well as environmental conditions. Corrosion-coupon exposure and aggressive gases such as SO_2 , NO_2 , and O_3 as well as particulates of known concentrations should be introduced into the chamber and their effects determined by weight-loss measurements or oxide-reduction time on the test coupons. These results should then be compared with outdoor exposure data. The acceleration effect can be achieved by the introduction of higher-concentration gases and the manipulation of temperature and humidity. Statistical design and regression analysis can be used as mathematical tools to formulate a model for correlating laboratory and outdoor exposure results.

SALT SPRAY

The salt-spray test involves exposure of standard specimens to a fine spray or mist of a solution of sodium chloride at a specified temperature for a specified period of time. The fog particles settle on the surfaces of the test specimen and thereby constantly replenish the film of solution on the surface. The quality of the metal can then be assessed through measurement of the extent and nature of corrosion of the metal surface after a specified exposure. Salt spray has been extensively used in the metal industry as an acceptance test. Initially the purpose of the test was the assessment of the quality of a protective coating such as galvanized steel in ASTM B117.¹⁰⁸ Currently the salt test is being applied to all metallic parts--bare or coated. The basic test requires a salt solution in the range of 3-5% which is generally used to simulate marine-atmosphere exposure. Numerous variations of salt concentration, cabinet design, test duration, pH, and emersion time have been employed.¹⁰⁹⁻¹¹⁸ In order to accelerate the corrosion process, many variations in the chemistry of the solution¹¹⁹ other than salt composition have been used.¹²⁰⁻¹²² Salt spray has been extensively used in some cases for exfoliation tests,¹²³ even though this test is very time consuming--requiring six months to one year or longer. However, recently some modified accelerated-salt-spray tests have been developed mainly as exfoliation tests.¹²⁴⁻¹²⁵ The main application of the salt-spray test is in quality control or evaluation of the relative corrosion resistance of materials in a high-humidity marine environment. This test cannot be used to predict long-range corrosion behavior or corrosion characteristics in urban or industrial atmospheric environments.

The salt-spray test does not appear to have a potential as a good accelerated-corrosion test for aerospace materials in realistic environments. It could not be shown that the results of salt-spray tests (using a very specific type of salt at specific concentrations, etc.--factors which must be specifically developed) could be correlated with the service performance of aerospace materials; hence, it was not pursued for accelerated testing.

ALTERNATE IMMERSION

The alternate-immersion test simulates the effects of the rise and fall of tidal and other waters and the movements of corrosive liquids in chemical plants. It also provides a relatively rapid test for the corrosive effect of aqueous solution upon metals and alloys. The test is most commonly used as a means of comparing the corrosion resistance of materials in a wide variety of corrosive media. It is also used as a control test for checking the quality of successive lots of certain alloys in commercial production. Although common test procedures have been described in the literature¹²⁶⁻¹²⁸ and at one time a tentative procedure was formulated by ASTM committee B-4,¹²⁹ this procedure is no longer recommended as an ASTM standard method. One reason for discontinuation of this test might be the complexity involved in testing and in simulating service environments in the laboratory.

Some unsatisfactory attempts have been made to correlate the corrosion test results obtained from alternate-immersion testing with those obtained from atmospheric tests. For example, Rawdon¹³⁰ has shown for Al alloys that some general conclusion can be drawn from alternate-immersion tests in the laboratory and from atmospheric field tests; however, he made no attempt at a quantitative correlation between laboratory and field tests. In addition, Jacob, et al.,¹³¹ in a recent report on stress-corrosion-cracking methods, concluded that alternate-immersion and salt-spray tests are more severe than industrial atmospheric tests. Since it lacks specificity with respect to environment, it is mainly used as an acceptance test, and no definite correlation has been made with routine, static stress-corrosion tests.

Alternate immersion might have potential as an accelerated corrosion testing method if the service environment were similar to the rise and fall of tidal waters. Of course, this is not the case for the actual service environment of aerospace materials. In specific cases,¹³²⁻¹³³ some degree of success has been achieved by formulating specific media for a specific system. However, a realistic environment is still not represented, and the test results are not reproducible. The selection of an aqueous

solution which would represent field conditions is a very difficult problem. which might be overcome after a great amount of effort and time has been expended. However, the effort to accomplish this and the uncertainty of the results do not appear to be worth the time and expense required.

ALTERNATE-POLARIZATION TEST

Recently, Rosenfeld, et al.,¹³⁴ used an alternating anodic and cathodic polarization technique for rapid detection of the tendency of steel alloys to undergo stress-corrosion cracking. They found the optimum condition to be initial anodic polarization of samples in 3% NaCl for 30 min. and subsequent cathodic polarization up to the appearance of cracking. This is an accelerated test for SCC susceptibility which is applicable to steels in NaCl solution regardless of the probable mechanism. This technique may also be applicable to other metal-electrolyte systems, and it appears worthy of further exploration.

OTHER ACCELERATED-CORROSION TESTING TECHNIQUES

Numerous less common accelerated testing techniques exist other than the crack-growth, constant-slow-strain-rate, rising-load K_{ISCC} , salt-spray, alternate-immersion, and other techniques described for general corrosion earlier in this report. Most of these were developed for specific purposes where all parameters were strictly defined. The majority of them, namely, the immersion-emersion¹³⁵ test, the Suzuki method,¹³⁶ and the Corrodokote technique,¹³⁷ are alternatives to the techniques previously described.

ENVIRONMENTAL CHAMBER FOR REALISTIC-TEST-CONDITION SIMULATION

Haynie,¹³⁸ in his material-testing work, developed an elaborate environmental chamber system. Figure 12 is a simplified flow diagram of the test system. Ambient air, after being filtered to remove particulates and gaseous pollutants, was cooled and dehumidified. The conditioned air then flowed into ducts for reconditioning to the desired

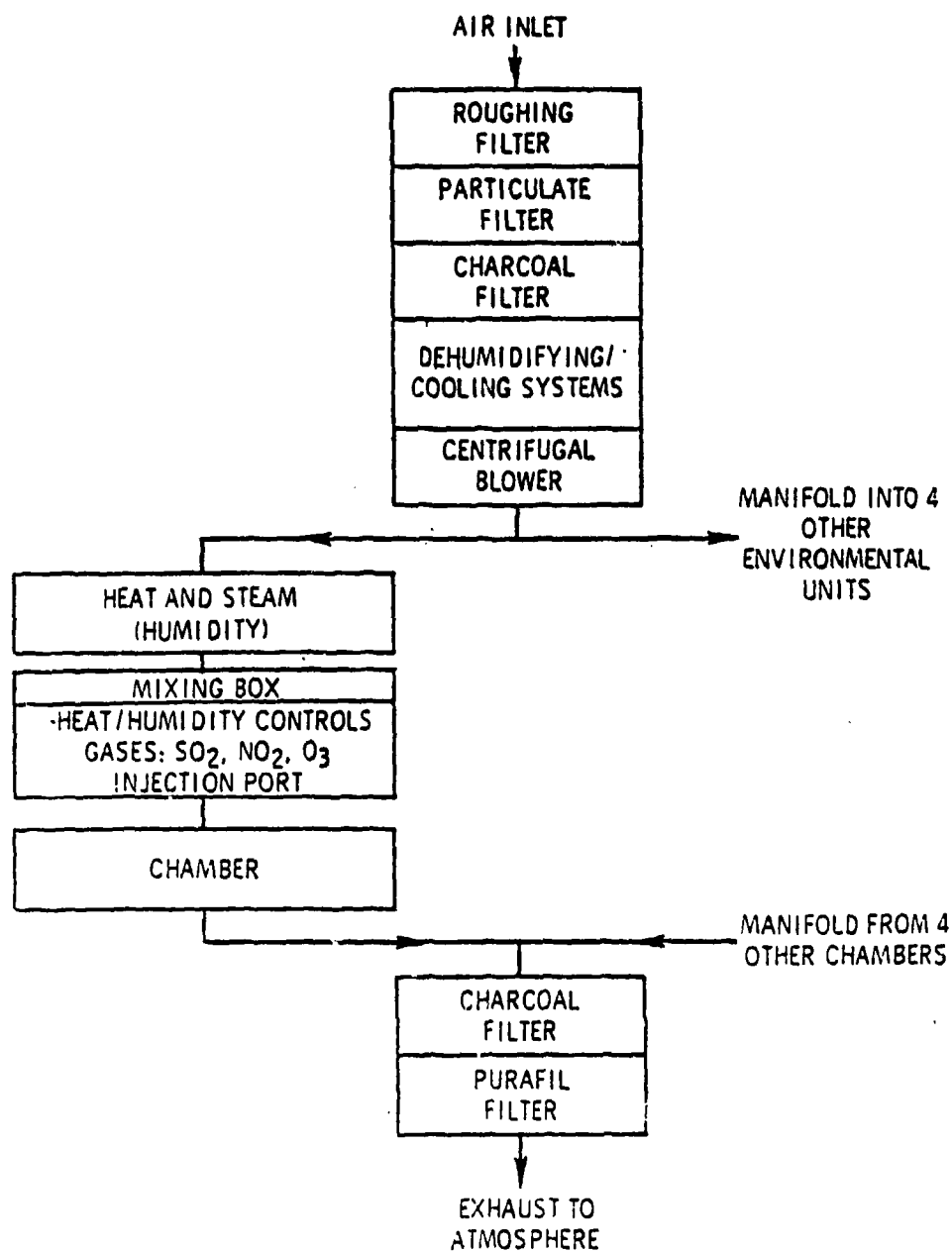


Figure 12. Environmental-System Flow Diagram.

temperature and relative humidity. From each duct the air entered a mixing box where SO_2 , NO_2 , and O_3 were added before the air reached the test chamber. Finally, the air left the chamber and was decontaminated and exhausted to the atmosphere.

The accelerated-corrosion effect upon the test specimens was generated by a day/night cycle provided by a built-in xenon lamp and chilling rack. The temperature and relative humidity of the air flowing to the chambers were maintained at desired levels. However, the temperature of the specimens varied continually during the day/night cycle, thus changing the local relative humidity. Moisture condensed on the specimens when the temperature was below the dew point. This mode of exposure allowed the surfaces of the test materials to adsorb the gaseous pollutants and to increase the pollutant concentration as in real environments. The cost of a series of chambers such as those described above and the associated pollutant-gas-dispensing and -monitoring devices would be quite high. However, a simplified version with certain modifications could be designed which would reduce cost somewhat.

Since most of the time aircraft are on the ground at various Air Force bases, it appears reasonable to investigate the effect of corrosion upon aerospace materials due to base ground environments. In other words, the effect of corrosion due to the polluted atmosphere at various bases upon aerospace materials should be investigated. Simulation of such a realistic service environment could be achieved by carrying out tests in an environmental chamber such as the one described. Certain modifications should be made such as incorporation of the chamber into the MTS test frame in order to permit dynamic measurements of such parameters as crack-growth rates and slow strain rates, in addition to coupon weight loss. It will be easier to correlate data thus obtained with environmental factors, to develop predictive equations, and to compare these data with field tests and service records simply because test environments are more realistic.

REMARKS

Corrosion-fatigue crack-growth measurement has been used generally for mechanical (fatigue) and environmental interaction of the material. The technique has great potential due to the good reproducibility of the test data. Recently it has been used as a screening test (accelerated-testing technique). With the information on a possible correlation to use between SCC and corrosion fatigue, this technique must be explored extensively in order to develop this correlation. The constant-slow-strain-rate test is the most widely used technique for determining the susceptibility of a material to SCC. In general, a smooth or notched tensile specimen is used for testing, but a compact-tension specimen may also be used. The introduction of a compact-tension fracture-toughness specimen into a constant slow-strain-rate test lends tremendous potential. The rising-load K_{ISCC} test is an extremely rapid method for evaluation of material. Much success has been achieved in predicting the development of a corrosive-rate equation using an environmental chamber and statistical methods. Further exploration is needed to verify the applicability of this test to commonly known aerospace materials. Several interesting investigations have been conducted in order to predict atmospheric weathering from simulated laboratory tests. Results are encouraging, but prediction attempts still fall short of the main goal. Further effort in this area hopefully will result in the formulation of a predictive model.

Section 3

EXPERIMENTAL INVESTIGATIONS

PROGRAM OVERVIEW

The investigation was carried out in four phases to permit a systematic approach to this complex problem. Phase I of the program mainly involved the selection of material, determination of the nature of environmental simulation, specimen preparation, preliminary crack-growth tests in the environmental chamber, and initiation of general-corrosion field tests. During Phase II design and fabrication of both the slow-strain-rate test machine and the environmental chamber were completed and the equipment put into operation. The crack-growth-rate experiments in simulated environments were also conducted in this phase. Rising-load tests on precracked compact-tension specimens and slow-strain-rate tests on smooth tensile specimens in a controlled environment were conducted during Phase III. The crack-growth-rate tests at specific stress ratios and frequencies were also carried out during this period. These tests were continued through Phase IV. In Phase IV rising-load, slow-strain-rate, corrosion-fatigue tests were continued in a controlled environment and general-corrosion field and laboratory exposure tests (in a controlled environment) were carried out. Fractographic analyses were performed in Phases II - IV. Crack-growth and other experimental data were analyzed in Phases III and IV. The results indicated that K_{ISCC} can be predicted from corrosion-fatigue tests, as described in detail in the section on crack growth.

PHASE I

Material Selection

Since the main objective of this program was the development of a realistic accelerated-corrosion test technique for aerospace structural materials, the alloys were selected from those used typically in aircraft such as

high-strength steels (AISI 4340, AF 1410, D6AC, etc) and high-strength aluminum alloys (Al 7075-T6, Al 7079-T6, Al 7061-T4, Al 2024-T3). Following a careful literature survey, AISI 4340 and Al 7075-T6 were primarily selected as being representative of the high-strength steels and Al alloys for this investigation.

Environment Simulation

Stress-corrosion cracking, corrosion fatigue, and general corrosion are more pronounced in an industrial atmosphere than in a rural atmosphere. It would have been enormously expensive to simulate the true industrial environment due to the large number of gases present in different concentrations. Fortunately, most of the ingredients present have negligible effects upon the corrosion process. Hence, the primary aggressive ingredients such as SO_2 , NO_2 , and surface salt along with relative humidity in varying concentrations were selected as the main constituents of the simulated environment. NO_2 in the presence of humidity is known to accelerate the corrosion process in both steel and aluminum alloys. The corrosion is expected to be more severe in the presence of surface salt; therefore, SO_2 and NO_2 in the range 10 - 1000 ppm, along with 5% surface salt and varying amounts of humidity (50-95%), were used for testing. The required combination of gases was obtained through a special setup, and the controlled environment was maintained in a specially designed environmental chamber, which will be described in detail later.

Specimen Preparation

Initially 45 compact-tension plane-strain fracture-toughness specimens of AISI 4340 steel with yield strength of \approx 180 ksi were fabricated per ASTM specifications. The specimen design is shown in Fig. 13. These specimens were mainly used to investigate the effect of humidity upon the low-cycle corrosion-fatigue behavior of high-strength 4340 steel. A batch of five more specimens of 4340 steel with a higher yield strength

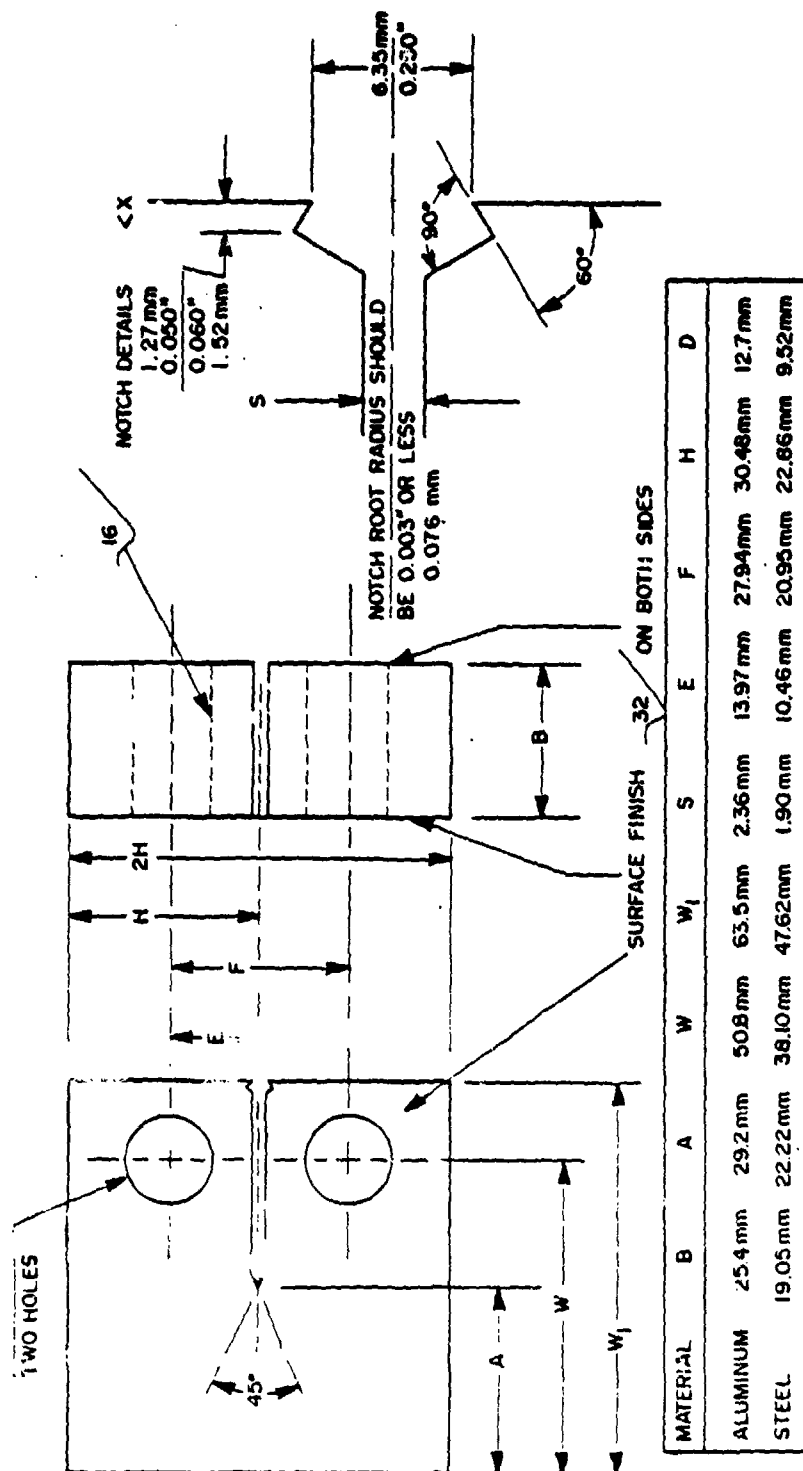


Figure 13. Compact-Tension Plane-Strain Fracture-Toughness Specimen.

of \approx 210 ksi were fabricated later. They were tested to determine the degree of embrittlement due to an aggressive gas such as SO_2 and relative humidity.

Another set of 30 wedge-open-loaded (WOL) plane-strain fracture-toughness specimens of 4340 steel with a heat of \approx 210 ksi was later fabricated to obtain a broader spectrum of crack-growth data. The design of the WOL specimen is shown in Fig. 14.

Compact-tension specimens of high-strength Al 7075-T6 in the short-transverse orientation were also fabricated, per ASTM specifications (see Fig. 13).

More than 30 tensile specimens each of 4340 steel and Al 7075-T6 to be stressed in the short-transverse orientation were fabricated for slow-strain-rate tests. The specimen design is shown in Fig. 15.

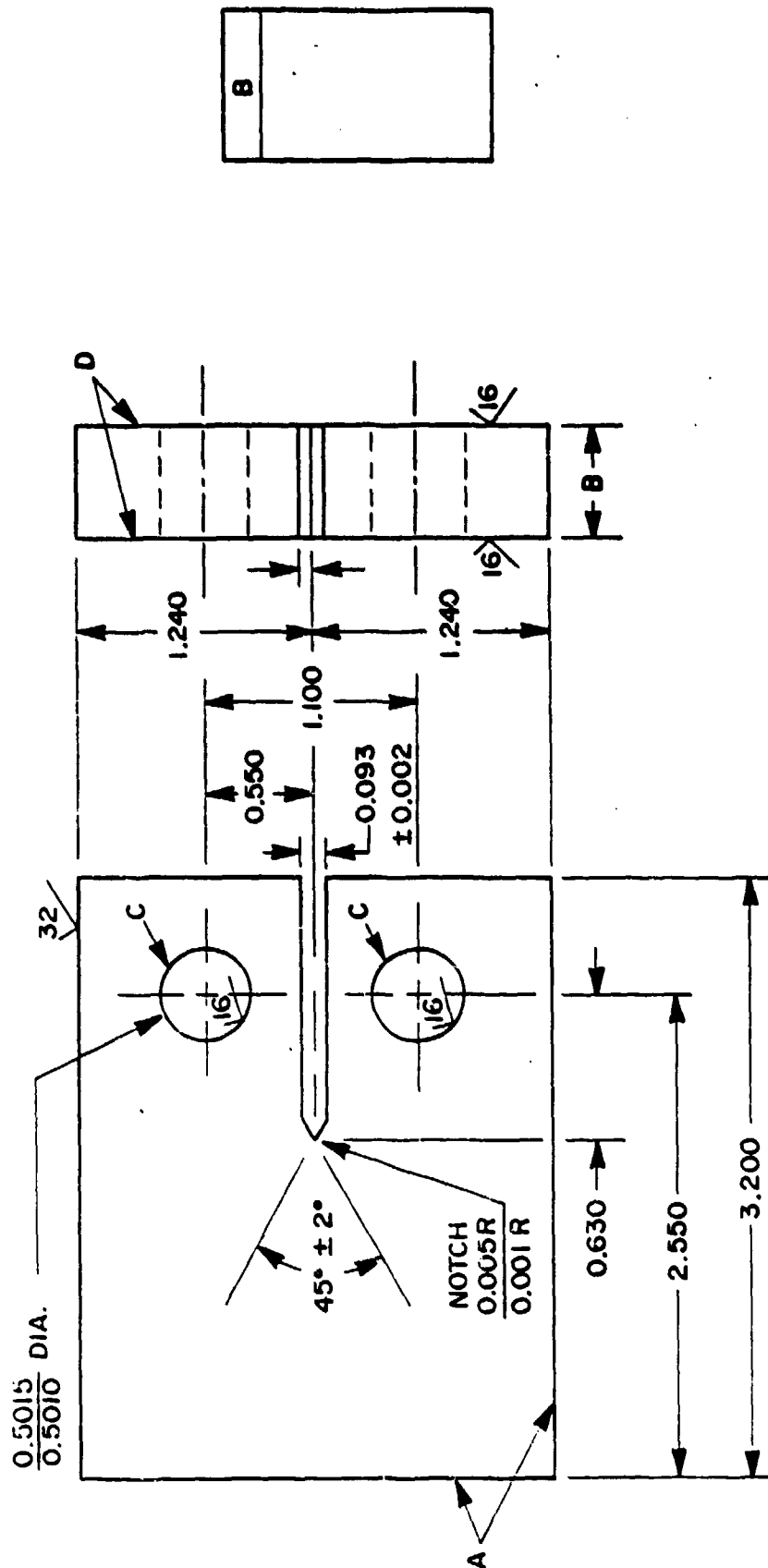
Crack-Growth Studies

The crack-growth experiments were initiated during this phase and will be described in detail in the Experimental Results Section.

General-Corrosion Outdoor-Field-Exposure Tests

Due to the lack of easy accessibility and adequate funding, only two sites were selected for the investigation of general corrosion. Wright-Patterson Air Force Base (WPAFB) was selected to represent the urban site, while Cape Kennedy represented the typical high-chloride sea-coast environment.

The outdoor-field-exposure panels (specimens) at the test site at WPAFB were set up on December 13, 1979. A total of 30 steel and 30 aluminum panels were placed on the test rack. All specimens were cleaned, weighed, and identified according to ASTM specifications prior to field exposure. The steel samples measured $5 \times 5 \frac{5}{8} \times 1/16$ in.



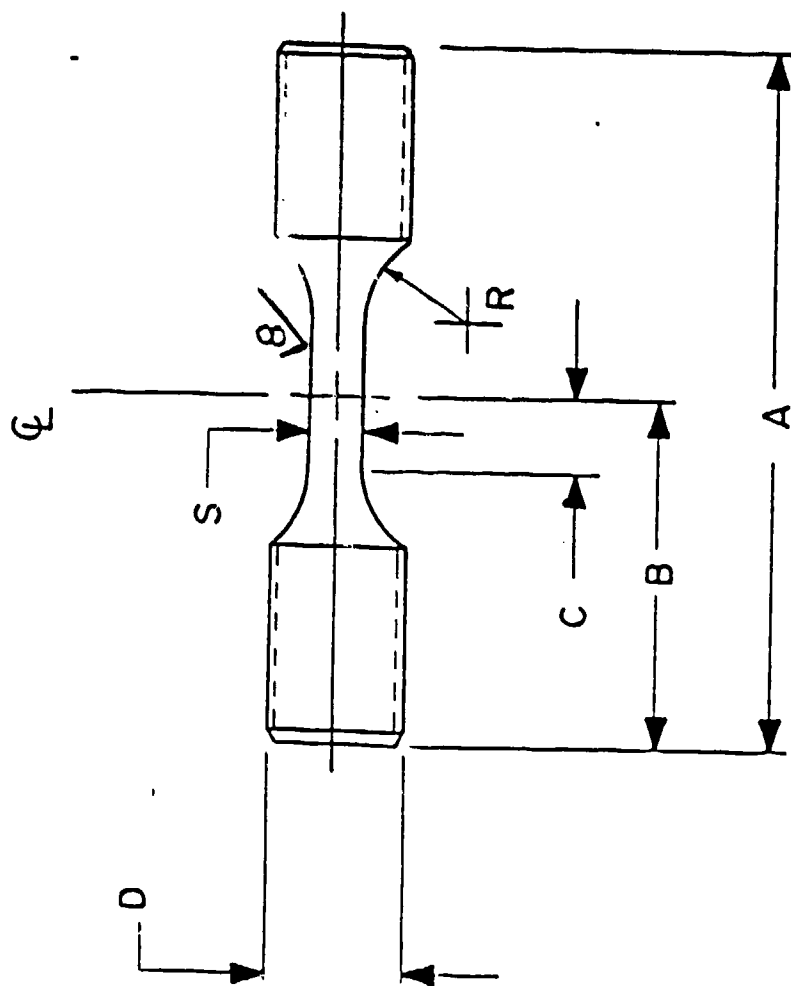
NOTES:

1. All dimensions are in inches.
2. Tolerances on dimensions are ± 0.004 ", unless given otherwise
3. A-surfaces to be perpendicular and parallel as applicable to within 0.002" TIR.
4. C-surfaces to be perpendicular and parallel as applicable to within 0.0005" TIR.
5. D-surfaces to be parallel within 0.002".
6. The intersection of the tips of the machined notch with D-surfaces shall be equally distant from the bottom and top edges of the specimen, to within 0.001".

MATERIAL:

TITLE: WEDGE-OPENING-LOADING (WOL),
W = 2.55", SPECIMEN

Figure 14. WOL Plane-Strain Fracture-Toughness Specimen.



NOTES:

1. Dimensions in inches.
2. RAD. and Gage Section to blend smoothly without undercut.
3. All diameters to be concentric within .001 TIR.

4. RAD. and uniform gage section to be finished using low stress grinding.
5. All surfaces 32/ unless otherwise indicated.

TENSILE SPECIMEN UNIFORM SECTION	
A	3.00"
B	1.50"
C	0.625"
D	0.500"
R	0.125" R
S	0.250"

MATERIAL: Aluminum

Figure 15. Tensile Specimen.

The samples at Cape Kennedy were set on test racks for exposure on November 13, 1979. A total of 35 steel and 30 aluminum panels are exposed at this site. The field-exposure data are not complete; hence no serious effort was made to develop a predictive model. Four batches of specimens (panels) have been removed to date--the first batch after nearly six months, the second after one year, the third after eighteen months, and the fourth after exposure for two years. Approximately one-half of the panels remain for additional exposure. Initial plans were to provide sufficient panels for a five-year field-exposure study. The corrosion data on the specimens removed after each six-month period have been reported previously in the interim reports.¹³⁹

PHASE II

Environmental Chamber

Initially a plastic (acrylic) environmental chamber was designed and fabricated for the purpose of conducting crack-growth tests in controlled humidity. The chamber has provisions for a gas inlet, a gas outlet, and controls for gas concentration and humidity levels. A BMA, Inc., wet- and dry-bulb humidity controller has also been installed on this chamber for controlling the relative humidity inside the chamber. This chamber was incorporated into the MTS machine for conducting corrosion-fatigue tests in controlled humidity. A close-up view of this chamber is shown in Fig. 16. This chamber has now been replaced by a stainless-steel environmental chamber, and the plastic chamber has been set up in the constant-slow-strain-rate machine.

While the stainless-steel chamber was being designed and fabricated, tests in controlled environment were conducted in the plastic chamber. The stainless-steel chamber¹⁴⁰ was designed for larger volume, more flexibility, and provisions of controls for aggressive gases and temperature. The complete setup is shown in Fig. 17.

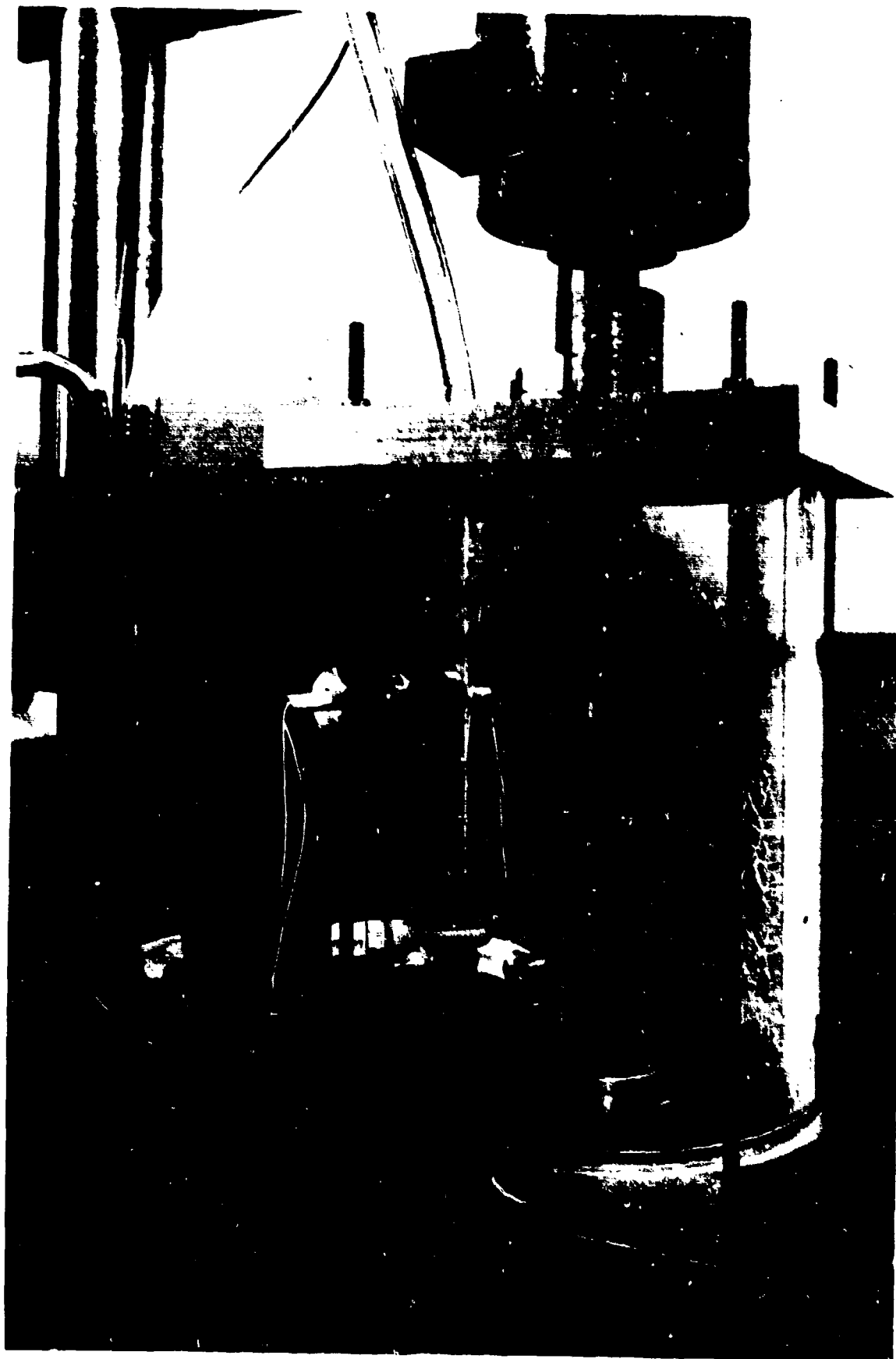


Figure 16. Close-up Photograph Showing Detailed Setup of Plastic Environmental Chamber.

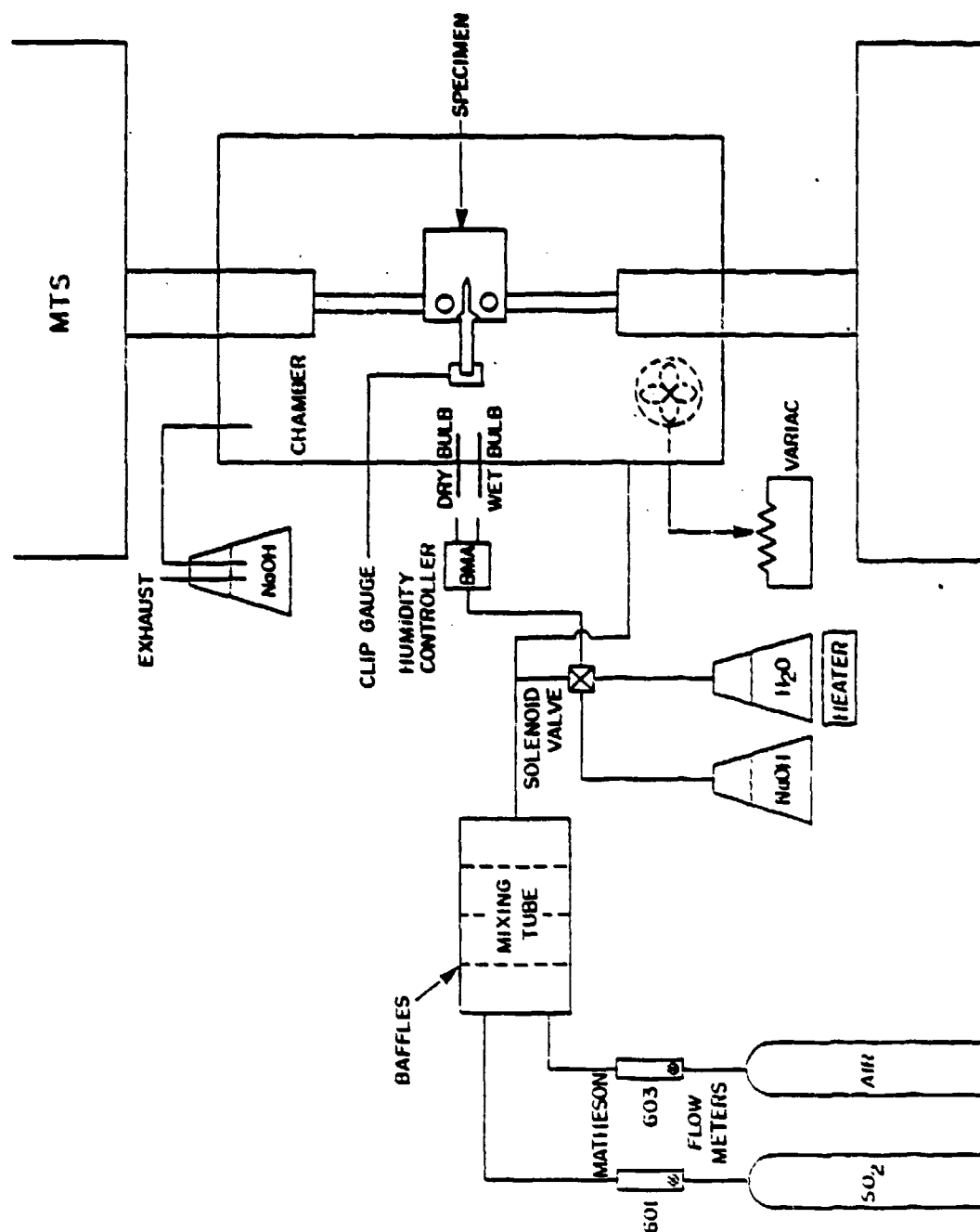


Figure 17. Line Diagram of Stainless-Steel Chamber with Controls.

Gastec-Tube Calibration

Environments such as a mixture of SO_2 , air, and relative humidity or a mixture of NO_2 , air, and relative humidity were simulated in the test chamber. The average crack-growth experiment generally required five days. Premixed gases of known concentration were introduced into the test chamber, and concentrations were maintained at the desired level by means of control devices. Samples of the mixed gases were drawn out during the test at different intervals for accurate analysis to insure the consistency of the gas mixture in the test chamber. A Bendix Gas Detector System was selected for routine checking of the SO_2 or NO_2 concentration in the test gas. The tube was calibrated to insure the accuracy of results. Three randomly selected SM SO_2 tubes with a measuring range of 100 - 1800 ppm were calibrated at four points using three different known concentrations of the SO_2 /air mixture. A standard wet-chemical titration method was used in determining the SO_2 concentration.

Figure 18 is a typical calibration curve obtained from the chemical analysis. The calibration curve indicates higher accuracy at low concentrations of SO_2 . This was encouraging because most of the crack-growth experiments were conducted at the lower end of the calibration curve. The general accuracy of the tubes was found to be well within 10% of the standard concentration which was adequate for routine gas-concentration control.

The calibration tube was frequently used to monitor the concentration of gases in the chamber. Generally one sample in the morning and one in the evening at an interval of six to eight hours was taken for analysis during tests in the environmental chamber.

Slow-Strain-Rate (SSR) Machine

The SSR machine is a type of tensile-test machine, its main feature being its ability to produce very slow strain rates on the order of 10^{-4} to 10^{-8} in./sec., usually not possible with commercial tensile machines.

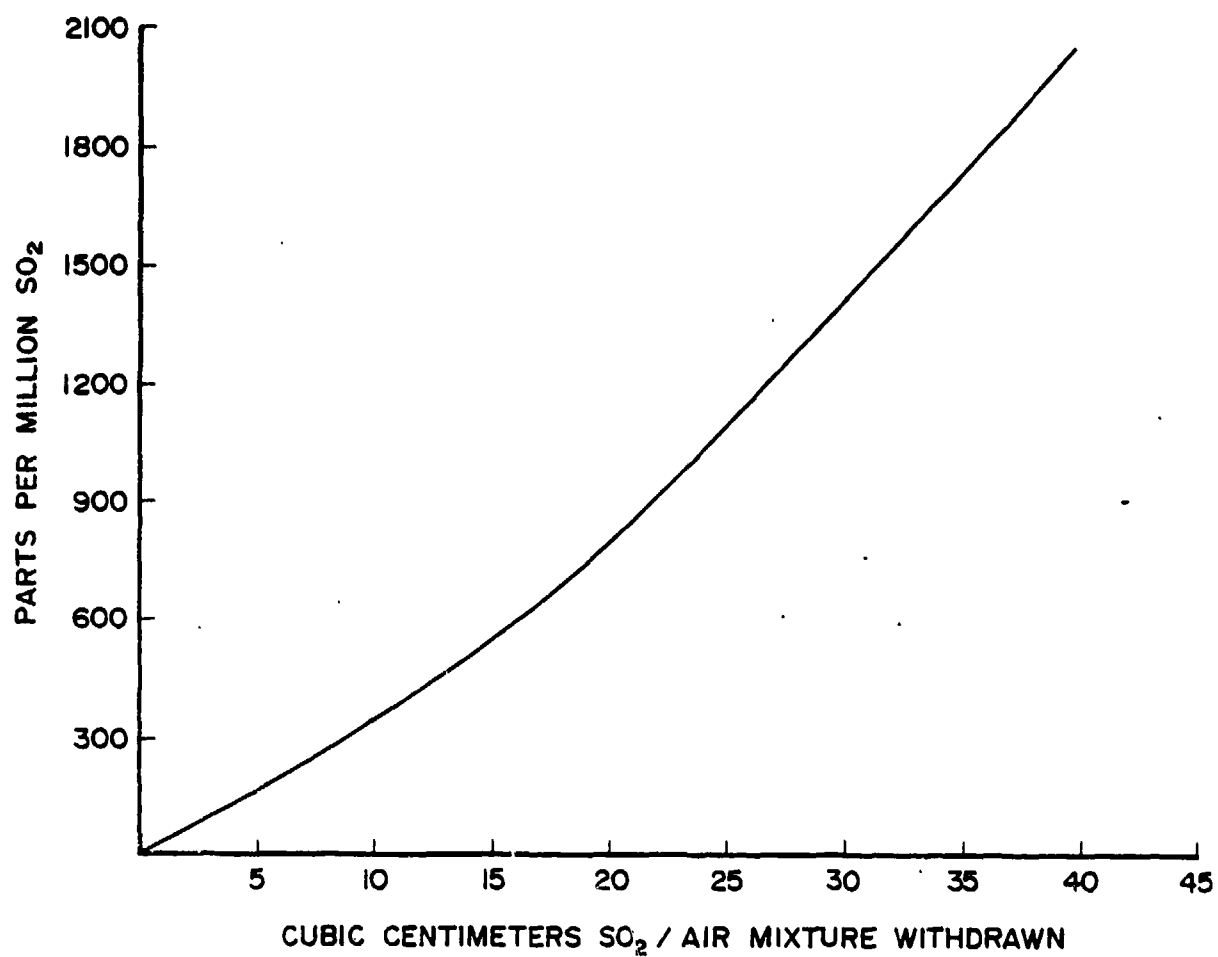


Figure 18. Gastec-Tube Calibration Curve.

This requirement differentiates it from a simple tensile-test machine, necessitating a special design. An SSR machine was designed and fabricated in our laboratory for this investigation. The performance of the machine was tested, and experimental tests were conducted. Details of the components of the machine are given below for purposes of familiarizing the reader with the operation of the machine. The main objective was to keep the design simple and inexpensive, yet allow maximum versatility in the testing.

Machine Properties

a) Strain Rate

The machine is designed to provide a slow strain rate in the range of 10^{-4} to 10^{-8} in./sec. The optimum strain rate for testing stress-corrosion-cracking susceptibility depends mainly upon the metal-environmental system. This wide range of strain rate covers most of the metal/environment systems encountered in practice.

b) Capacity

The capacity of the machine is governed by the ultimate strength of the material and the geometry of the specimen to be tested. Generally, the specimens used for stress-corrosion-cracking susceptibility are hour-glass-type specimens with a gage diameter of up to 0.625 cm. Based upon this assumption, a machine with a capacity of ~ 15000N should be adequate for most materials. Since it was planned to test high-strength steels and to conduct crack-propagation-rate tests with specimens having different geometries and requiring thicker sections, the machine was designed to have a capacity of 20,000 lbs. (88964N).

c) Major Components

The SSR machine is relatively simple because the main function of this device is to pull the specimen at a predetermined rate. The principal

components of the machine are the drive-train assembly which consists of a) a gearhead motor, b) a motor speed controller, c) a screw jack, and d) gearboxes--variable and fixed type, and the load cell, universal joints, and machine frame.

Gearboxes. The most important aspect of the SSR machine is provision of a wide strain-rate range (10^{-4} to 10^{-8} in./sec.). The total reduction needed in order to obtain a crosshead speed of 10^{-8} in./sec. is several decades. This necessitates the use of several gearboxes--obviously, at least two. In order to meet the requirement for flexibility in the selection of the desired strain rate over four orders of magnitude (10^{-4} to 10^{-8} in./sec.), a combination of variables and fixed gearboxes was used. The variable gearbox Apcor Model 2813, having ratios of 1, 2, 4...512, was obtained from Geartronic Corporation; while Boston Gear Model LW21, having a gear ratio of 135:1, was selected as the fixed gearbox. The gearboxes, motors, and screw jacks were coupled using timing belts and pulleys.

Screw jack. The screw jack is one of the most important components of the machine. A worm-gear screw jack was used to convert the rotary motion into vertical lift. The screw jack was obtained from Templeton Kinly Co. and has a rating of 6-in. stroke and 36 turns per inch of travel. This rating provides a simultaneous reduction in speed also. The 6-in. vertical travel of the screw is sufficient for most of the testing anticipated.

Universal joints. A universal joint is used to correct any small misalignment due to slight mismatch of the specimen fixture and pull-rod assembly. The universal joint is placed between the pull rod and the specimen holder.

Load cell. A load cell is the simplest load-indicating device in such a testing machine. A load cell--Model 3157-20K, low profile of 20,000 lb.--was obtained from Lebero-Associates, Inc., of Troy, Michigan, and obviously is sealed and temperature compensated.

Machine frame. A very rigid frame having four steel posts 2-in. in diam. and two top and bottom frames made of 2 1/2-in.-thick steel plate was designed and fabricated for the machine. The dimensions of the frame were also guided by the requirement of installation of an environmental chamber. The machine frame can be seen in Fig. 19. The load-train components are mounted to one side of the upper steel plate of the machine, as shown in Fig. 20.

d) Environmental Chamber

An environmental chamber was designed and fabricated for conducting slow-strain-rate tests in a controlled atmosphere. The environmental chamber, along with the gas-train assembly incorporated into the SSR machine, is shown in Fig. 16. The chamber is made from an 8-in.-diam., 3/8-in.-thick acrylic pipe and has provisions for gas inlet, gas outlet, and controls for gas-concentration and humidity levels. A BMA, Inc., wet- and dry-bulb humidity controller is used to control the relative humidity inside the chamber. The gas-train assembly is very similar to that described in a previous report.¹³⁹

EXPERIMENTAL RESULTS

Most of the details of the slow-strain-rate testing conducted during Phases III and IV are given in the paper included as Appendix A.

PHASES III AND IV - RISING-LOAD K_{ISCC} TEST AND CRACK-GROWTH TEST

Rising-Load K_{ISCC} Test

The apparent threshold for sustained-load stress-corrosion cracking, K_{ISCC} , in humid air and in different mixtures of humid air and SO_2 was estimated using the accelerated rising-load procedure.¹⁶ The testing technique utilized is essentially identical to the procedure used for K_{IC} fracture-toughness testing (ASTM Test for Plane-Strain Fracture Toughness of Metallic Materials E399-72), except that a slower rate of loading is

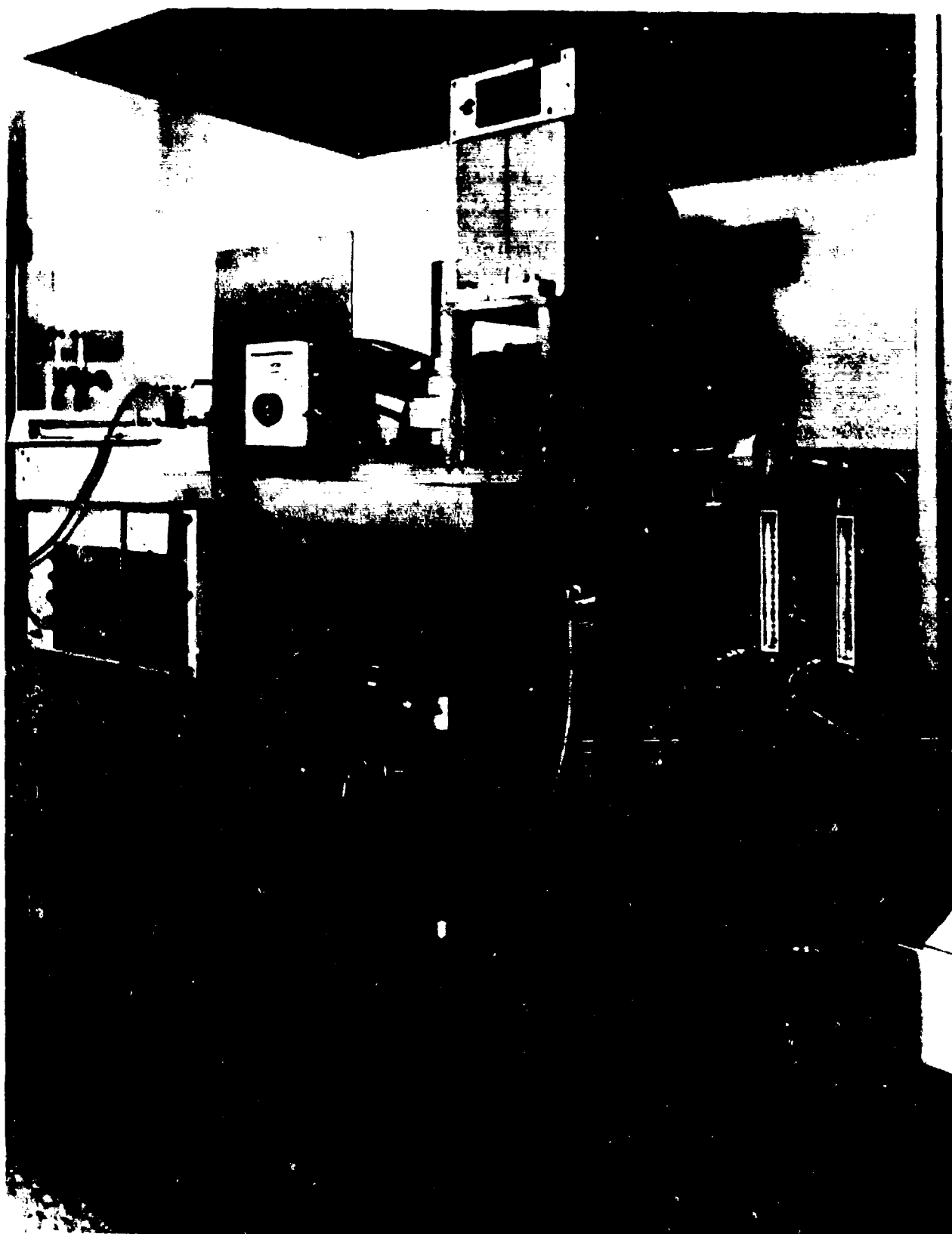


Figure 19. Close-up View of SSR Machine.



Figure 20. Load-Train Components of SSR Machine.

involved. Normally the specimen is exposed to the environment during loading. These tests were conducted with standard compact-tension 4340 steel specimens. The specimens were precracked to a crack length 0.0254 mm at stress intensities below $15 \text{ MPa}\sqrt{\text{m}}$ ($R = 0.1$ and $f = 0.1 \text{ Hz}$). The environmental chamber was used to maintain and control the constituents of the specific environment required for the test. One specimen was loaded in air, which produced the K_{IC} value. The others were loaded in mixtures of 1000 ppm SO_2 + 80% RH, 1000 ppm SO_2 + 100% RH, 100 ppm SO_2 + 80% RH + 5% surface salt, 100 ppm NO_2 + 80% RH, 100 ppm NO_2 + 80% RH + 5% surface salt, etc. at different loading rates corresponding to 0.2-0.06 $\text{MPa}\sqrt{\text{m}}/\text{sec}$. The K_{ISCC} values were estimated from the load-displacement record using a five percent secant offset procedure similar to that used for K_{IC} testing (ASTM method E399-72). Some of the results are listed in Table 1 of the paper included as Appendix A.

In the case of Al 7075-T6, the specimens were precracked to a length of 0.0254 mm at stress intensities below $7 \text{ MPa}\sqrt{\text{m}}$ ($R = 0.1$ and $f = 0.1 \text{ Hz}$). In this case the K_{ISCC} values were also estimated by an independent step-by-step loading practice. Initially the load was applied at 20 lb./min. up to 70% of the load level of the estimated K_{ISCC} value obtained from the previous rising-load test and was held for an extended period (24-50 hr.) to detect the onset of crack propagation (see the idealized case shown in Fig. 21). If no growth developed after a reasonable period (24-50 hr.), the load was incremented to a new level (80%) at a lower loading rate of 5 lb./min. for an additional hold period. The step loading was repeated until the onset of crack growth was clearly identified. The results are shown in Table 11 of the paper included as an Appendix A.

In some of the later tests, the slower loading rate (the lowest rate available in the machine) of 0.6 lb./min. was used to determine the influence of loading rate upon the approximation of K_{ISCC} . The results of some of the rising-load tests conducted on high-strength 4340 steel and 7075-T6 aluminum alloy in environments of a combination of NO_2 , RH, and surface salt are given in Table 3.

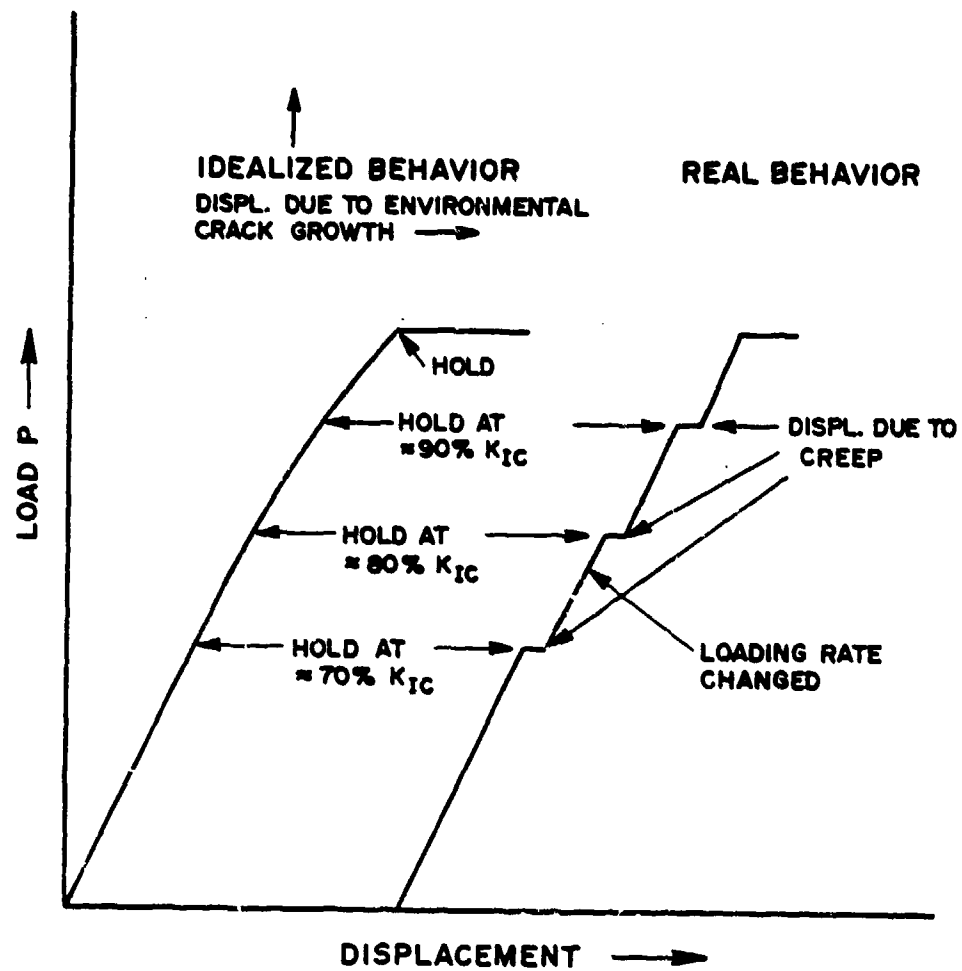


Figure 21. Schematic Diagram of Step Loading in Rising-Load Test.

Table 3

APPARENT K_{ISCC} VALUES OBTAINED BY RISING LOAD TESTS

SPECIMEN NO.	ENVIRONMENT	LOADING RATE lb/min	APPARENT K_{ISCC} ksi $\sqrt{in.}$
* STA 25	100 ppm NO ₂ + 80% RH	5	21.3
STA 22	100 ppm NO ₂ + 80% RH	5	21.8
STA 38	100 ppm NO ₂ + 80% RH	5	22.3
STA 2	100 ppm NO ₂ + 90% RH	5	21.66
STA 24	1000 ppm SO ₂ + 80% RH	5	21.4
STA 43	100 ppm SO ₂ + 80% RH + 5% NaCl	1	17.8
STA 44	100 ppm SO ₂ + 80% RH + 5% NaCl	1	17.3
** ST 23	100 ppm NO ₂ + 80% RH + 5% NaCl	0.606	21.96
STA 49	100 ppm NO ₂ + 80% RH + 5% NaCl	0.606	8.9
STA 41	100 ppm NO ₂ + 80% RH + 5% NaCl	1	13.2

*STA \equiv A1 7075-T6**ST \equiv 4340 Steel

CORROSION-FATIGUE TEST IN CONTROLLED ENVIRONMENT

A series of tests on high-strength steel 4340 and Al 7075-T6 has been conducted, whereas initially only the effect of various levels of humidity was investigated. These were followed up by tests where the environment was a mixture of 1000-10 ppm SO_2 and 80-90% RH, 100-ppm NO_2 + 80-95% RH, and 5% surface salt along with either mixture, i.e., SO_2 + RH or NO_2 + RH. In the case of both materials, the effect of R and frequency has also been studied. R was varied from 0.5 to 0.8, while most of the tests were conducted at a frequency of 0.1 Hz. A series of tests was also conducted at 0.25, 0.5, and 1 Hz. The concentration of SO_2 and NO_2 was lowered to 10-1 ppm, and some tests were conducted at a higher level of RH (i.e., 90-95%) also, along with SO_2 , NO_2 , and surface salt (as indicated earlier).

One of the most representative results of the crack-growth experiments in a mixture of 80% RH + 100 ppm SO_2 for a 4340 steel specimen is shown in Fig. 22. The da/dN -vs- ΔK data shown have been manipulated from the crack-length-vs-number-of cycles data. The da/dN -vs- ΔK behavior is typical of the crack-growth behavior already reported.¹⁴⁰ This figure shows a plateau intermediate region, followed by a maximum in the da/dN -vs- ΔK plot. This difference in the nature of the plot (or appearance of a plateau followed by a maximum) is expected when the level exceeds the K_{ISCC} value for the metal-environment system. The extrapolation from this slope change to the abscissa of the plot produces a K_{ISCC} value similar to that shown in Fig. 23. Accordingly, the K_{ISCC} value obtained from the extrapolation is $\sim 40 \text{ ksi} \sqrt{\text{in.}}$ obtained for this steel in an environment of 80% RH + 1000 ppm SO_2 . The increase in the value of K_{ISCC} could simply be due to the reduced level of SO_2 , which makes the environment less aggressive.

Figures 24-26 show the crack-growth behavior of high-strength 4340 steel tested in an atmosphere of 90% RH + 1000 ppm SO_2 . These tests were conducted at frequencies of 0.1, 0.25, and 1.0 Hz. The K_{ISCC} values have been extrapolated as shown in Figs. 24-26, and they vary from 27 to

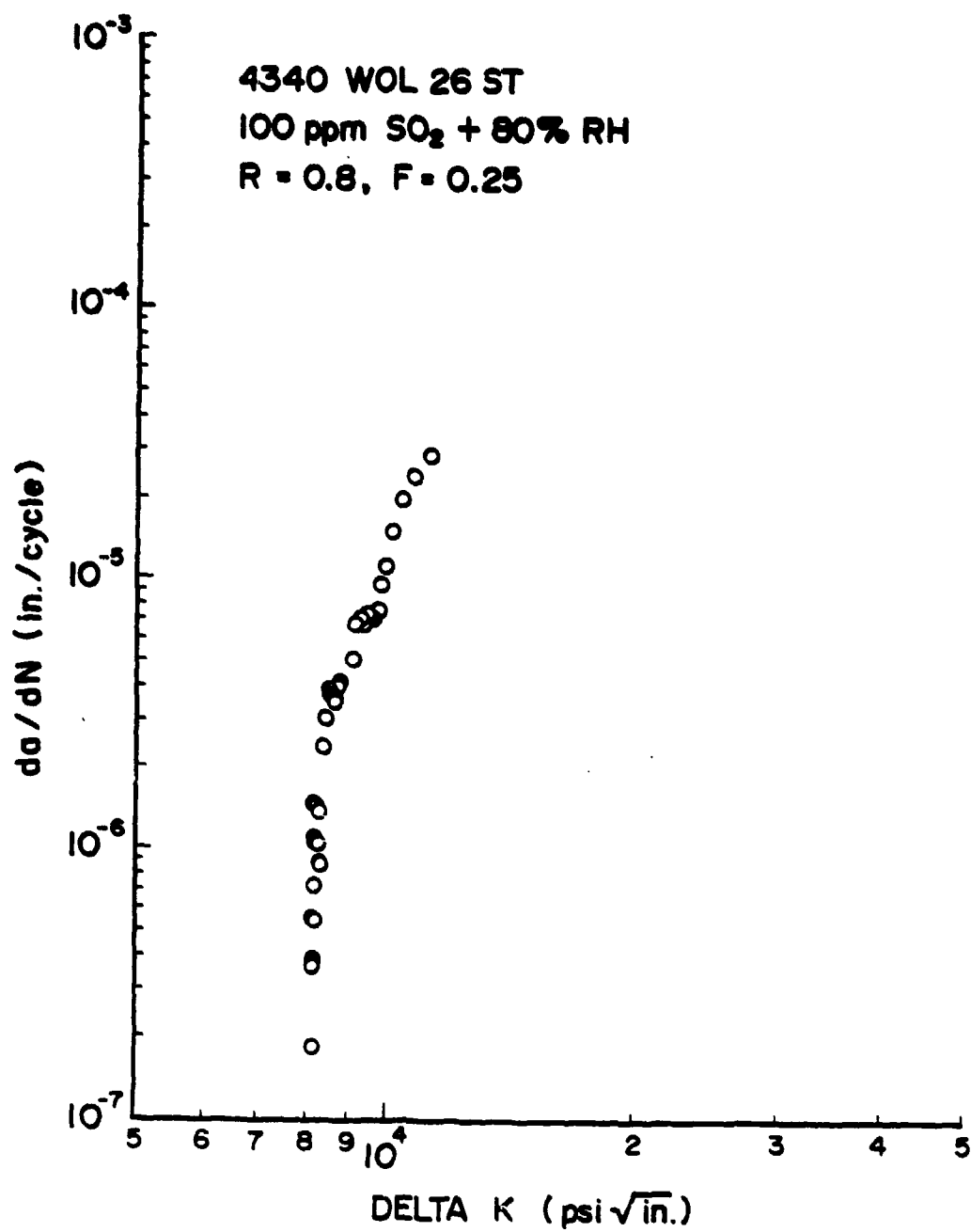


Figure 22. Plot of da/dN vs ΔK in 80% RH + 100 ppm SO₂.

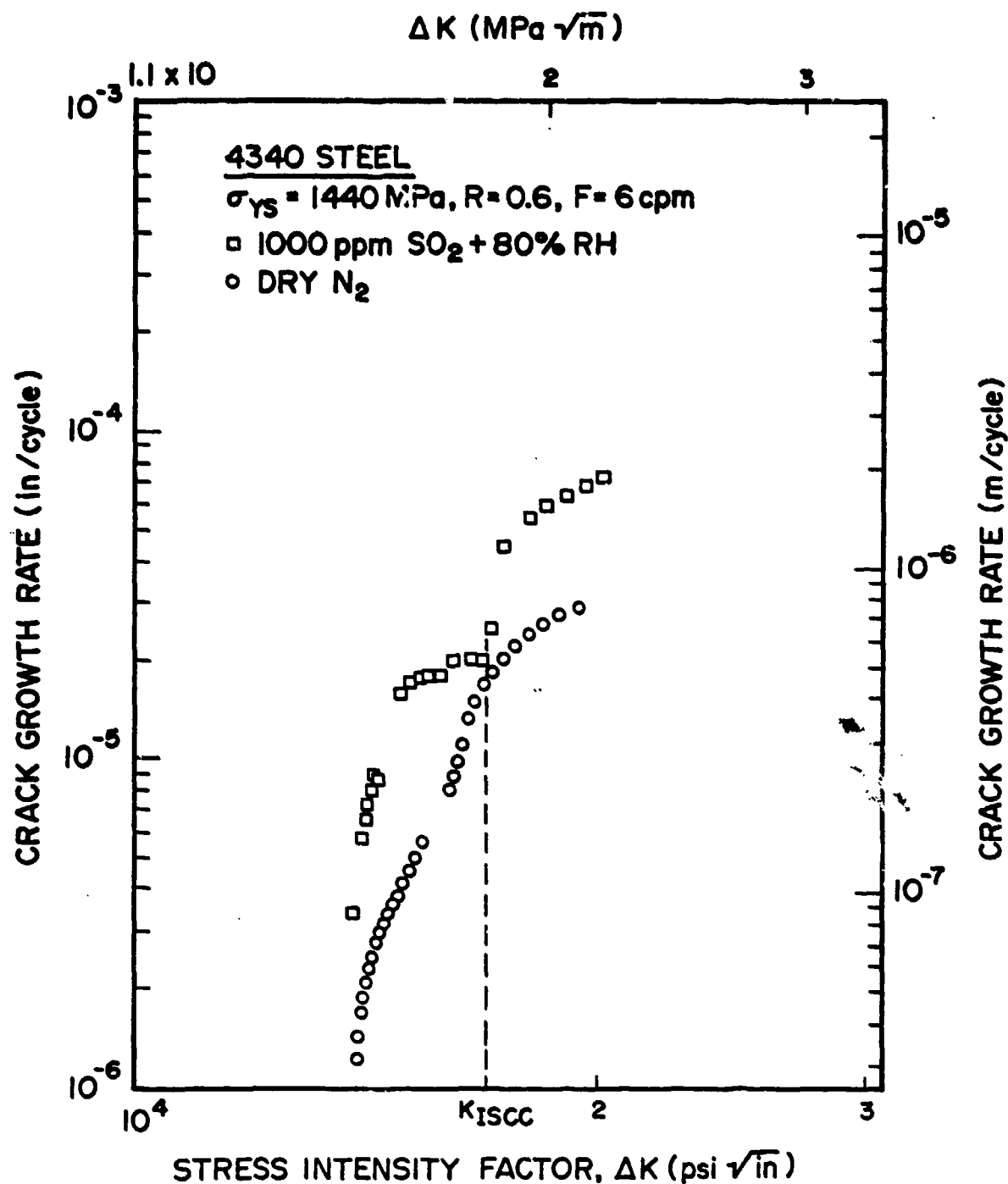
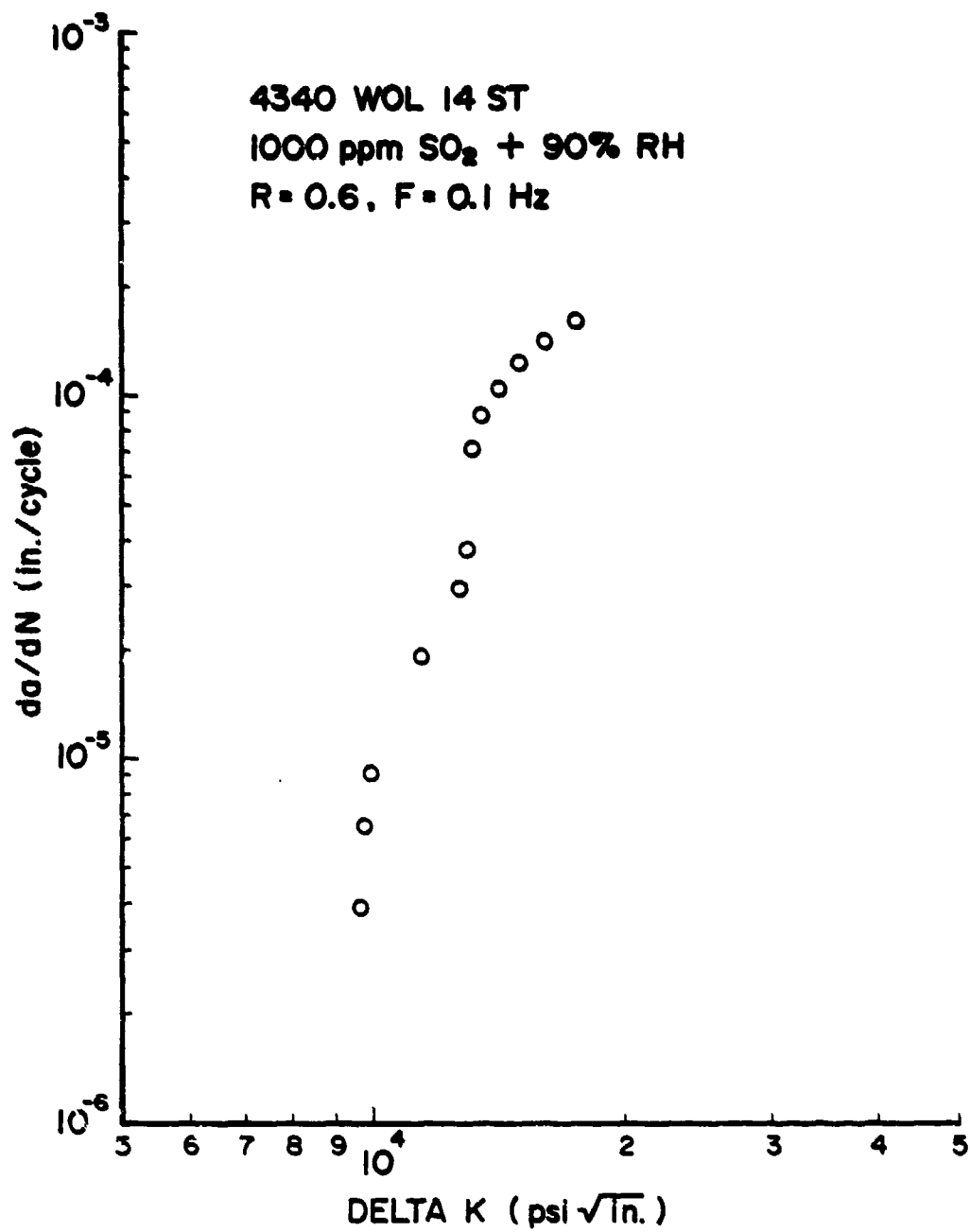
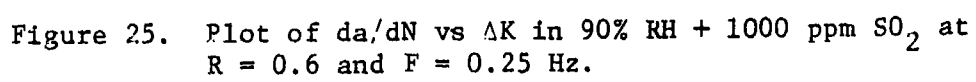


Figure 23. Crack-Growth-Rate Data Obtained for 4340 Steel (1440 MPa)
 Tested in 1000 ppm $\text{SO}_2 + 80\% \text{ RH}$ Environment.





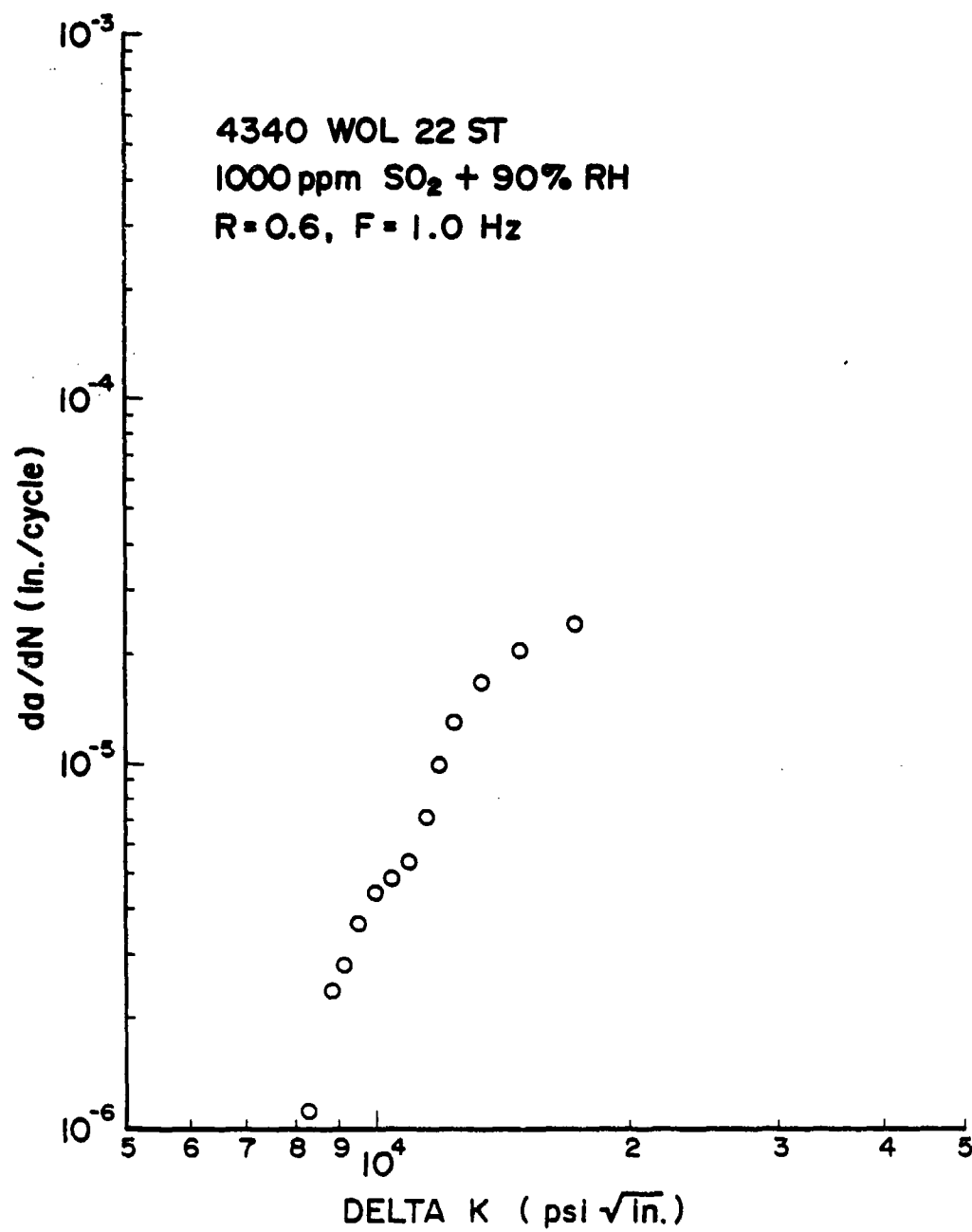


Figure 26. Plot of da/dN vs ΔK in 90% RH + 1000 ppm SO₂ at R = 0.6 and F = 1.0 Hz.

~ 30 ksi $\sqrt{\text{in.}}$. The crack-growth behavior at all these frequencies (0.1 - 1.0 Hz) has been plotted in Fig. 27 to permit a better extrapolation of the K_{ISCC} value, which gives a graphical average of the independent values. The values of K_{ISCC} extrapolated from the da/dN -vs- ΔK plots at different frequencies are within experimental error. More pronounced behavior was obtained when the R ratio was changed from 0.6 to 0.8. The extrapolated value of K_{ISCC} is shown in Fig. 28. The value of K_{ISCC} thus obtained is nearly 31 ksi $\sqrt{\text{in.}}$, which differs by only 3% from the extrapolated K_{ISCC} value obtained at a stress ratio of 0.6. These values are quite consistent.

The crack-growth behavior of Al 7075-T6 was also investigated in controlled environments in various combinations of SO_2 and RH. The test parameters were very similar to those employed for 4340 steel, except that lower loads were used due to the lower strength (nearly 28 ksi) of Al 7075-T6 as compared to 4340 steel (210 ksi). Most of the results, along with tests conducted on 4340 steel, are discussed in a previous report¹³⁹ and in Appendix B.

In a second set of experiments, tests were conducted both on high-strength 4340 steel and Al 7075-T6 where SO_2 was replaced by NO_2 . However, the maximum concentration of NO_2 used was only 100 ppm, and the lowest level investigated was 1 ppm NO_2 . In later experiments, 5% surface salt was introduced into the mixture of NO_2 and RH.

These tests were conducted at stress ratios of 0.6 ($R = 0.6$) and 0.8 ($R = 0.8$) and a frequency of 0.1 Hz. Crack-growth results for an Al 7075-T6 specimen tested in 100 ppm NO_2 and 80% RH at $R = 0.6$ and a frequency of 0.1 Hz are shown in Fig. 29. Figure 30 (a, b) is the da/dN -vs- ΔK plot for two Al 7075-T6 specimens tested in an environment of 100 ppm NO_2 + 80% RH and 5% surface salt at $R = 0.6$, while the da/dN -vs- ΔK plots for $R = 0.8$ are shown in Fig. 31 (a, b). The curves appear to be very similar, and a plateau region followed by a maximum in the da/dN -vs- ΔK curves is indicated. Similar behavior is obtained in an environment of 100 ppm NO_2 + 80% RH, but it is not so distinct as in the plots of Figs. 30 and 31.

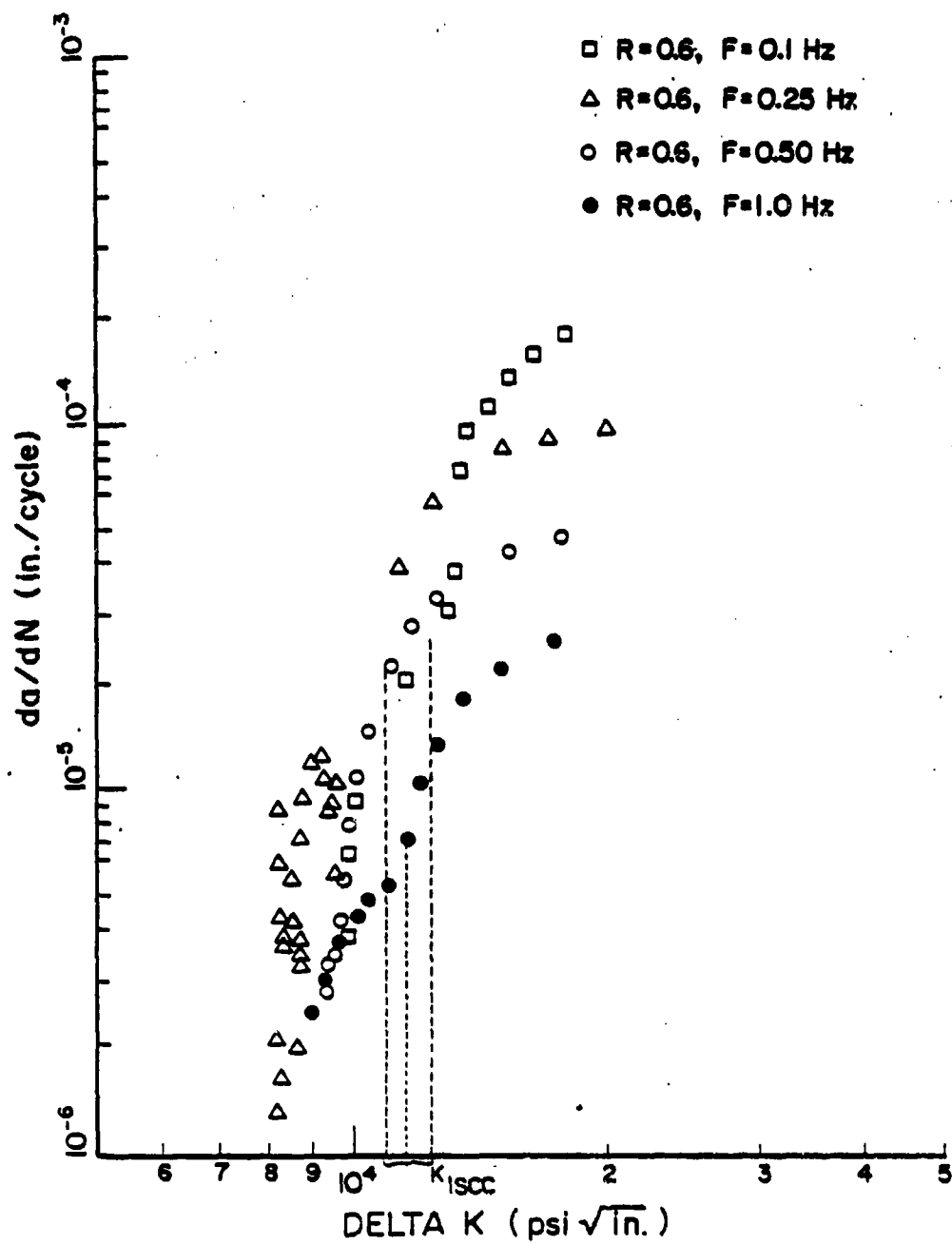


Figure 27. Plot of da/dN vs ΔK Showing K_{ISCC} Extrapolation at Different Frequencies.

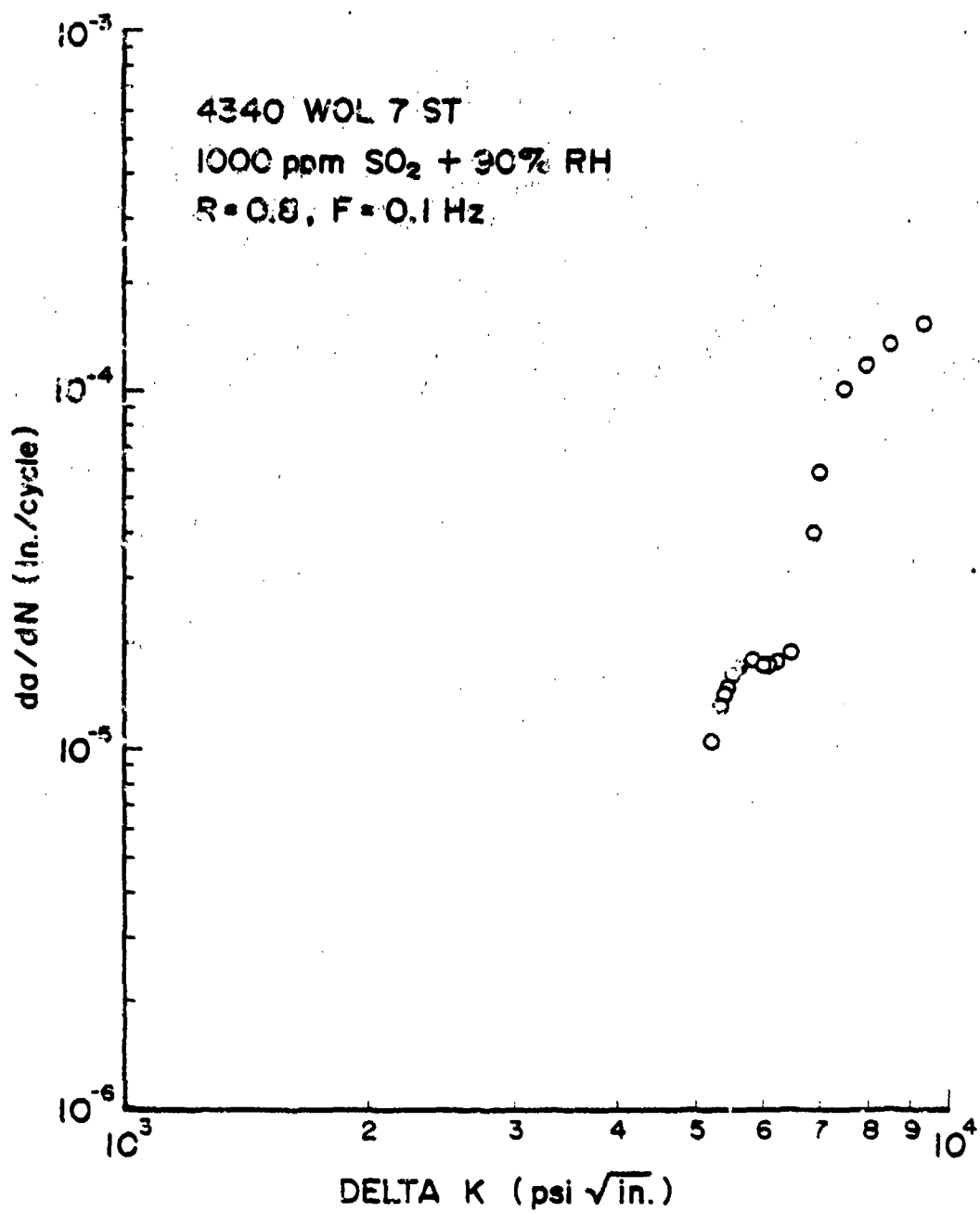


Figure 28. Plot of da/dN vs ΔK in 90% RH + 1000 ppm SO₂ at R = 0.8 and F = 0.1 Hz.

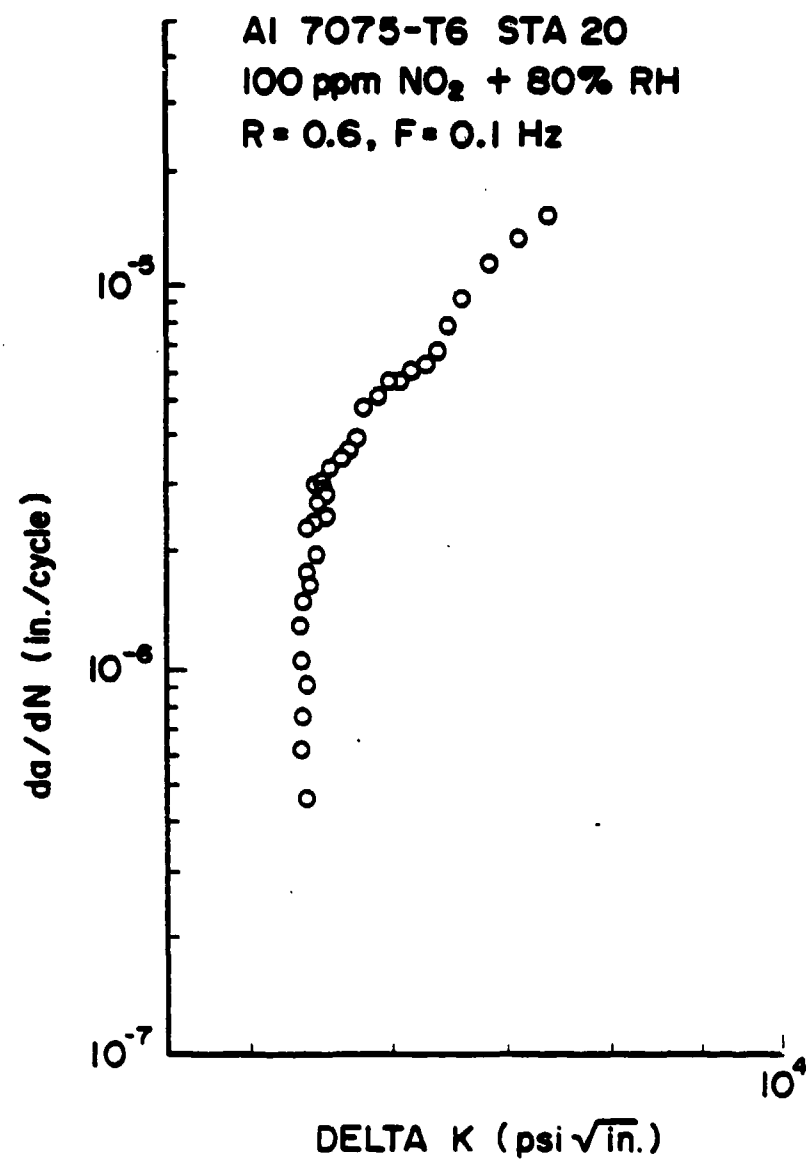


Figure 29. Plot of da/dN vs ΔK in 100 ppm NO₂ + 80% RH.

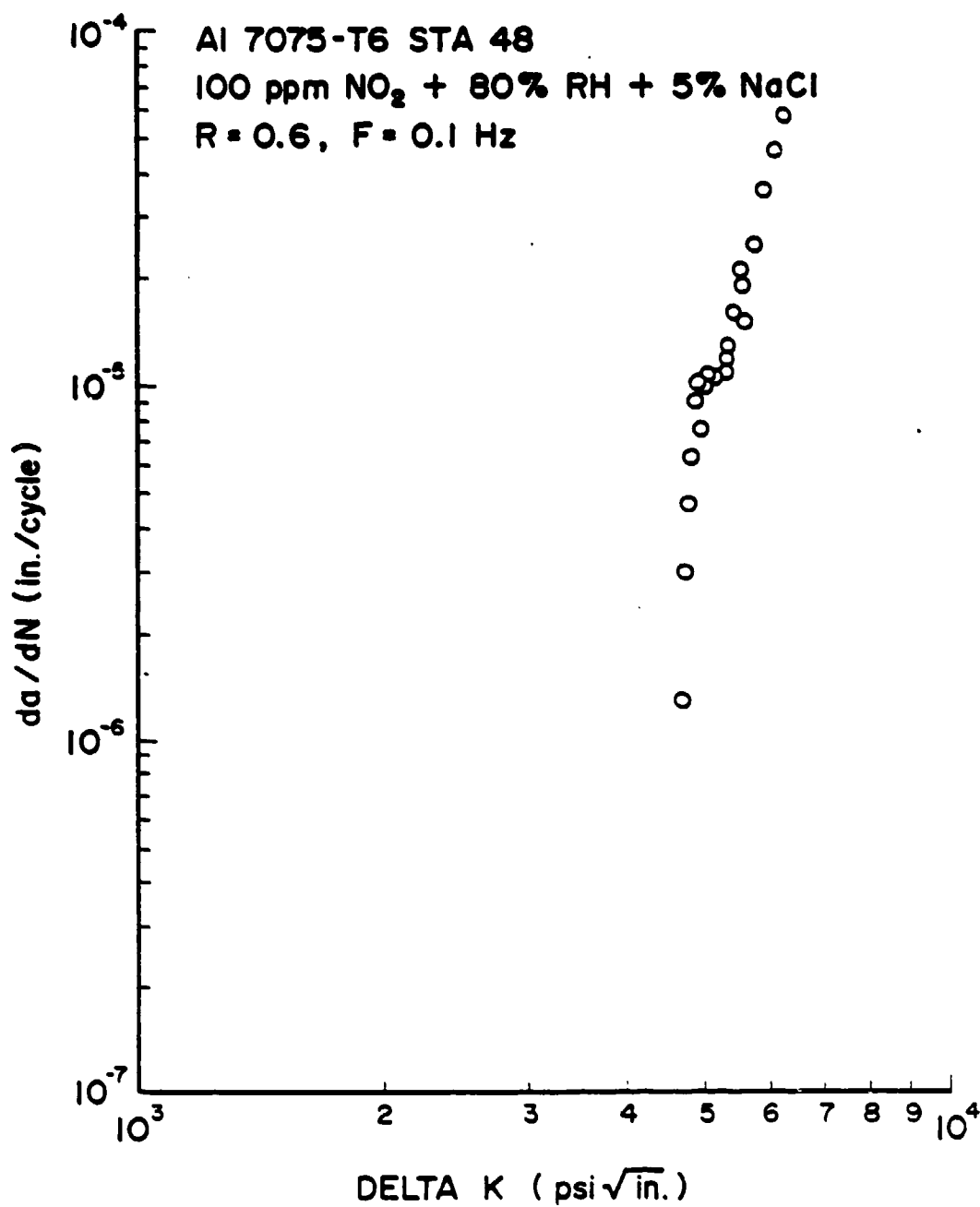


Figure 30. Plot of da/dN vs ΔK in 100 ppm NO₂ + 80% RH + 5% NaCl at R = 0.6 and F = 0.1 Hz (a) for 7075-T6 Specimen STA48.

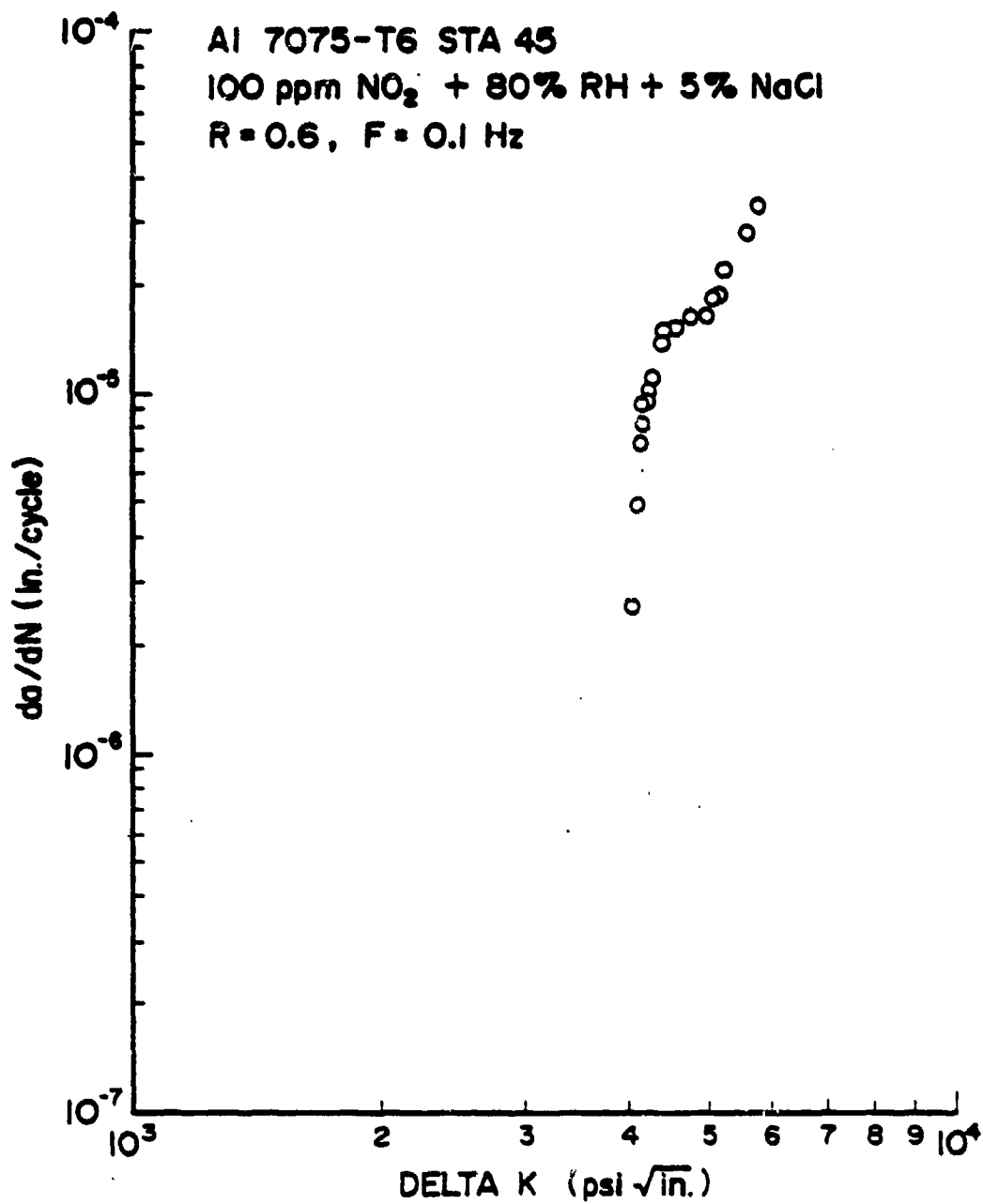
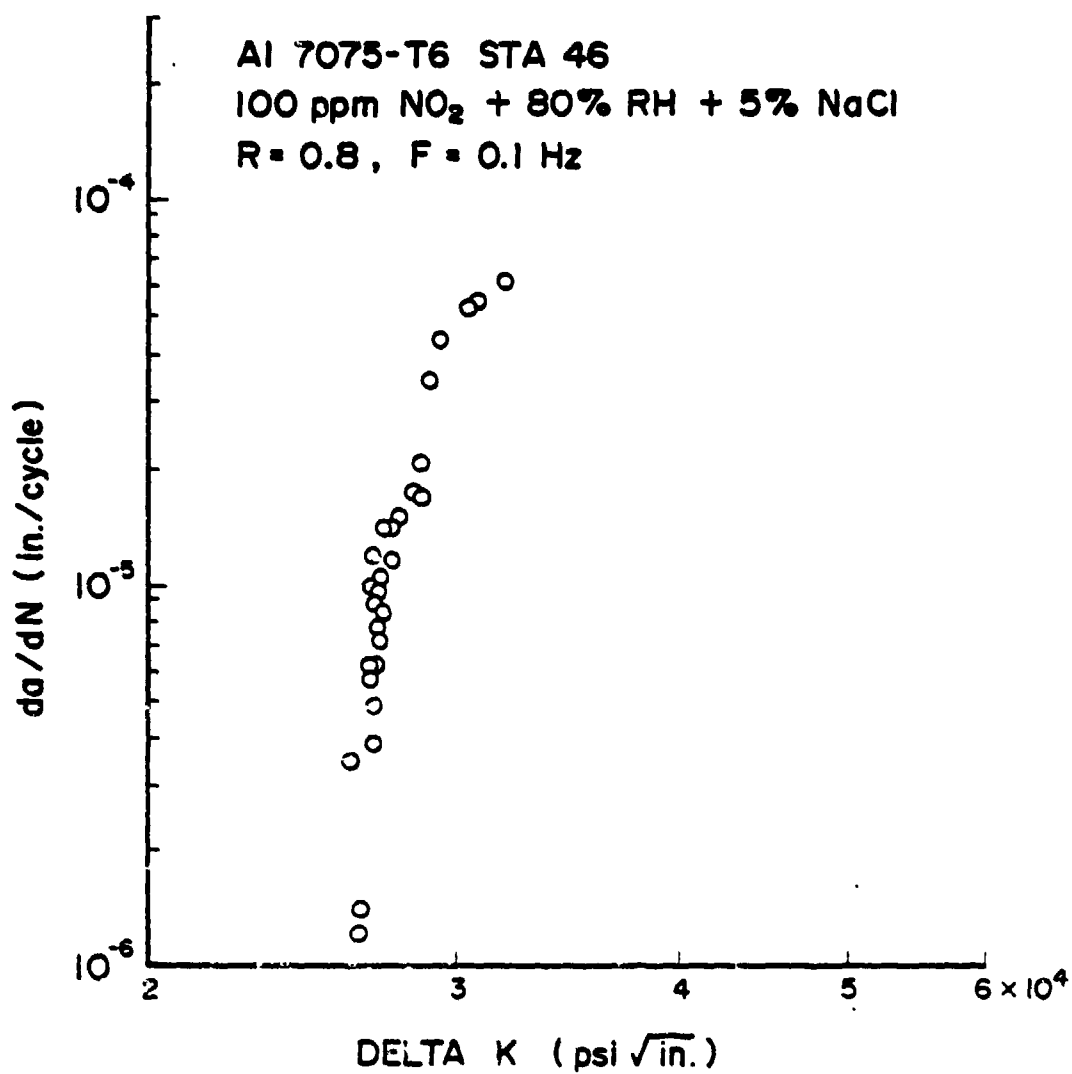


Figure 30. Plot of da/dN vs ΔK in 100 ppm NO₂ + 80% RH + 5% NaCl at R = 0.6 and F = 0.1 Hz (b) for 7075-T6 Specimen STA45.



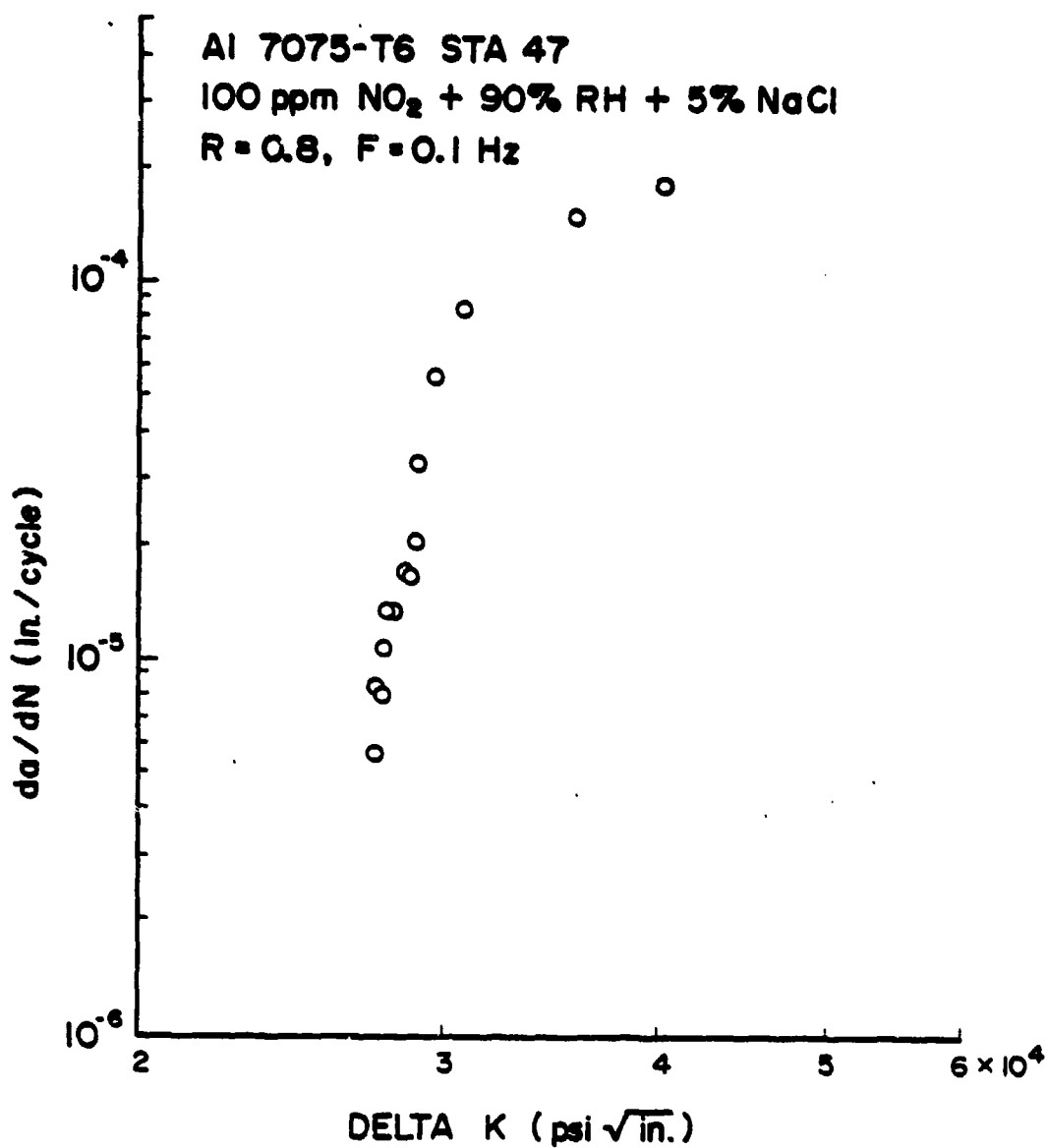


Figure 31. Plot of da/dN vs ΔK in 100 ppm NO₂ + 80% RH + 5% NaCl at $R = 0.8$ and $F = 0.1$ Hz (b) for 7075-T6 Specimen STA47.

obtained from tests in an environment of 100 ppm NO_2 + 80% RH and 5% surface salt. The values of K_{ISCC} obtained from extrapolation of Al 7075-T6 in an environment of 100 ppm NO_2 + 80% RH + 5% surface salt are between 13 and 14 $\text{ksi}\sqrt{\text{in}}$. These values are in good agreement with the value 12 $\text{ksi}\sqrt{\text{in}}$ obtained from rising-load tests as indicated in Table 3. Attempts were made to verify the accuracy of these estimates by fractographic observations. Some problem was encountered due to the reaction taking place on the surface, after specimen failure. In general, the chamber was flushed of all aggressive gases for 12-16 hr. after specimen failure before the fractured pieces were removed.

Figure 32 is one of the fractographs taken from the surface of Al 7075-T6, Specimen STA45 tested in 100 ppm NO_2 + 80% RH + 5% NaCl. Severe secondary cracking and brittle failure mode are indicated as well as limited ductility. This particular fractograph was taken at a K level of ~ 13 $\text{ksi}\sqrt{\text{in}}$.

Figure 33 (a, b) shows the surface features obtained from another specimen tested in the same environment and under similar conditions, except that a higher stress ratio of 0.8 (as compared to 0.6) was used. Figure 33(b) is a higher-magnification of Fig. 33(a) showing the stress cracking more clearly. Here also there is some evidence of void coalescence. This fractograph was taken at a K level of ~ 12 $\text{ksi}\sqrt{\text{in}}$. Another set of fractographs was taken at high K values. Figure 34 is a fractograph taken from the same specimen at a K value of ~ 16 $\text{ksi}\sqrt{\text{in}}$. The features are predominately brittle, and there is clear evidence of stress cracking. In general, the surfaces (fractograph) showed evidence of stress cracking at higher K values until fast fracture. Figure 35 is another fractograph taken from a different specimen tested in 100 ppm NO_2 + 80% RH + 5% surface salt. Although there is some evidence of quasi-cleavage, the fracture appears to be mainly brittle. This fractograph was taken at a stress-intensity level of ~ 14 $\text{ksi}\sqrt{\text{in}}$. The fracture features at higher K levels generally showed clear evidence of SCC. These fractographic analyses indicate a K_{ISCC} value of ~ 14 $\text{ksi}\sqrt{\text{in}}$ for Al 7075-T6 in an environment of 100 ppm NO_2 + 80% RH + 5% surface salt. The K_{ISCC} value for an extrapolation of



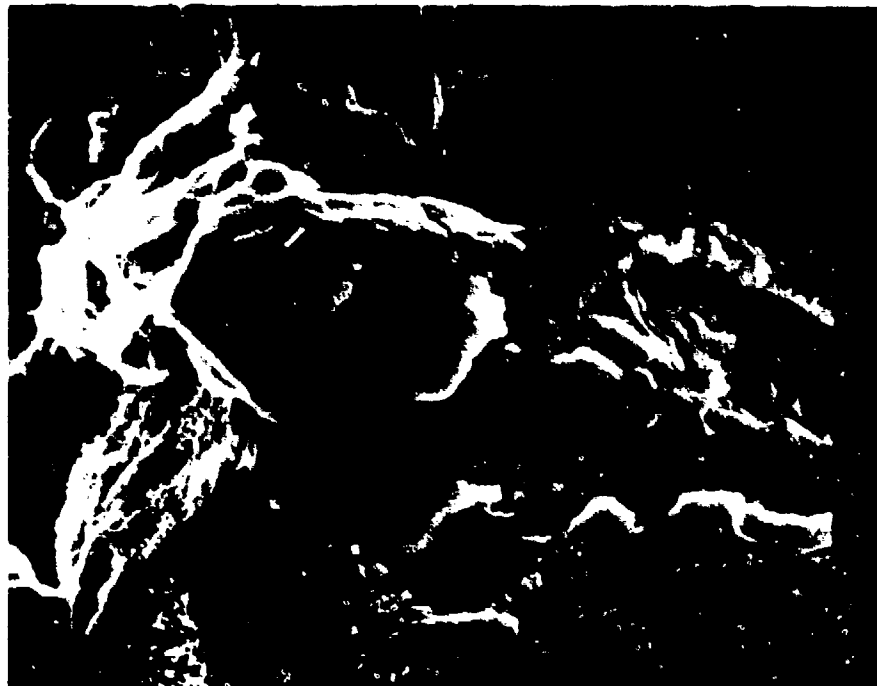
1600 x

Figure 32. Fracture Surface of Al 7075-T6 Specimen
STA45, Tested in 100 ppm NO₂ + 80% RH+5%
NaCl at R = 0.6 and F = 0.1 Hz.



400x

(a)



800x

(b)

Figure 33. (a) Fracture Surface of Al 7075-T6 Specimen STA46 Tested in 100 ppm NO_2 + 80% RH + 5% NaCl at $R = 0.8$ and $F = 0.1$ Hz.
(b) Higher Magnification of (a).



1600x

Figure 34. Fracture Surface Showing Severe Secondary Cracking and Brittle Mode of Failure.



450 X

Figure 35. Fracture Surface of Specimen Tested in
100 ppm NO_2 + 80% RH + 5% NaCl at $R = 0.8$
and $F = 0.1$ Hz at a K Level of $\sim 14 \text{ ksi}\sqrt{\text{in.}}$.

the da/dN -vs- ΔK curves obtained by means of corrosion-fatigue tests is also $\sim 14 \text{ ksi}\sqrt{\text{in.}}$. These two K values obtained through the use of two different techniques are in good agreement with the K_{ISCC} value calculated from rising-load tests. Hence, there is sufficient evidence to postulate the determination of the K_{ISCC} value from corrosion-fatigue tests (under controlled environment and test parameters).

The crack-growth behavior of high-strength 4340 steel in environments of mixture of NO_2 + RH and NO_2 + RH + surface salt was also investigated. Figure 36 is a da/dN -vs- ΔK plot for a 4340 steel specimen tested in 10 ppm NO_2 + 80% RH. The crack-growth behavior shows a near-plateau region followed by a maximum in the curve. An extrapolation of the K_{ISCC} value from this curve results in a value of $\sim 40 \text{ ksi}\sqrt{\text{in.}}$. Remember that this value is lower than the value ($\approx 44 \text{ ksi}\sqrt{\text{in.}}$) obtained for 4340 steel tested in an environment of 1000 ppm SO_2 + 80% RH. This suggests that NO_2 in the presence of RH is more damaging to 4340 steel (as far as the SCC property is concerned) than SO_2 in the presence of RH. The value of K_{ISCC} obtained here could not be verified by means of rising-load tests due to the lack of specimens as well as shortage of time. Attempts were made to analyze the fracture surface. Figure 37 is a representative fractograph from a specimen tested in 10 ppm NO_2 + 80% RH. There is clear evidence of severe secondary cracking; and the failure mode, in general, appears to be brittle. A quantitative determination of K_{ISCC} based upon the fracture surface was difficult due to the severe localized attack on the fractured surface (most of which may have occurred during the time when the chamber was flushed) after specimen failure.

Some problems were encountered when surface salt was introduced to only 80% RH air or a mixture of 100 ppm NO_2 and 5% surface salt. The results are shown in Figs. 38-39. The da/dN -vs- ΔK behavior does not follow the normal trend and exhibits some abnormality. This abnormality is mainly due to the discontinuous addition of 5% surface salt which was introduced at ~ 24 -hr. intervals. This assumption is supported by results of

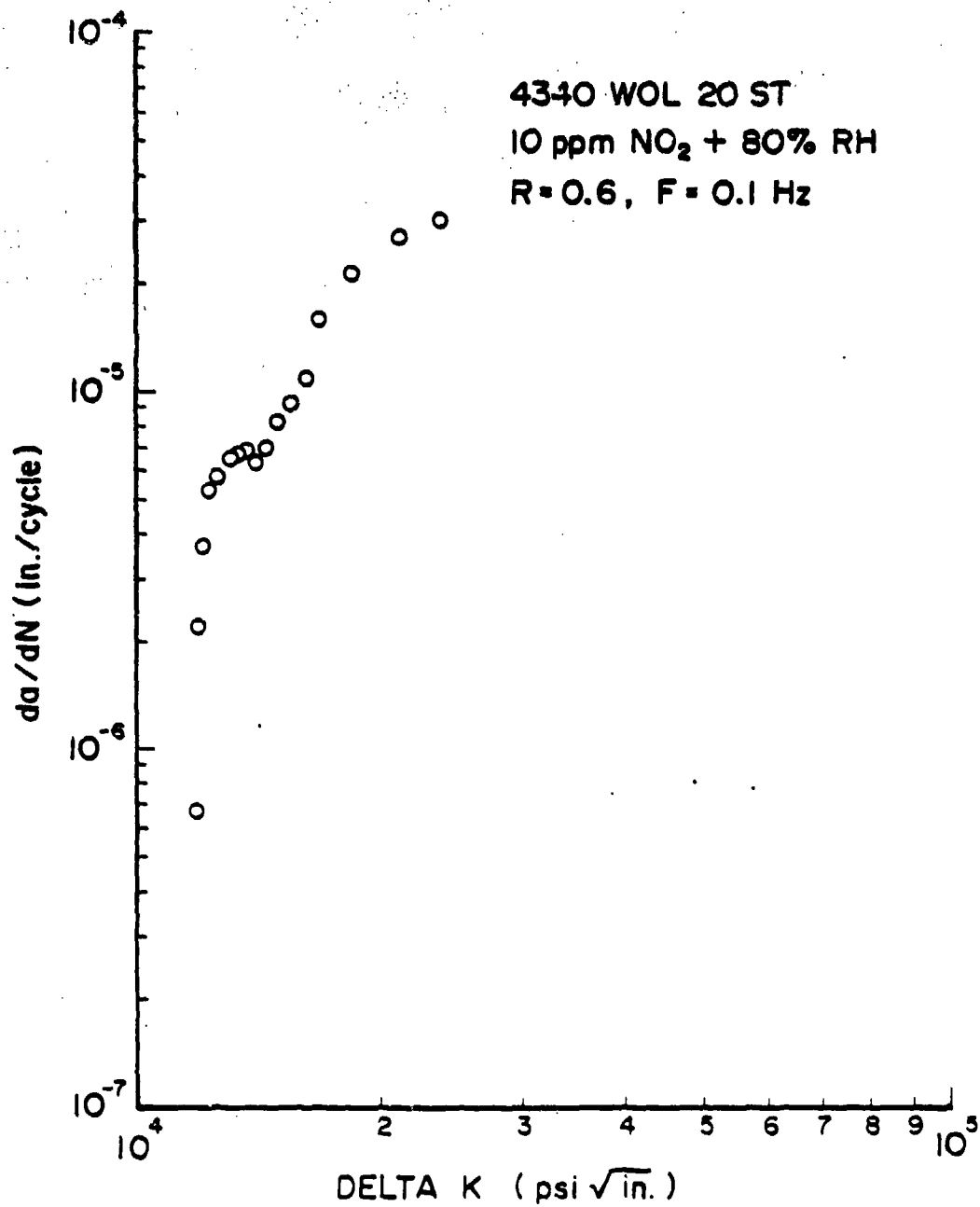


Figure 36. Plot of da/dN -vs- ΔK for 4340 Steel Tested in 100 ppm NO₂ + 80% RH.



400x

Figure 37. Fractograph Taken from 4340 Steel Specimen
Tested in 10 ppm NO₂ + 80% RH.

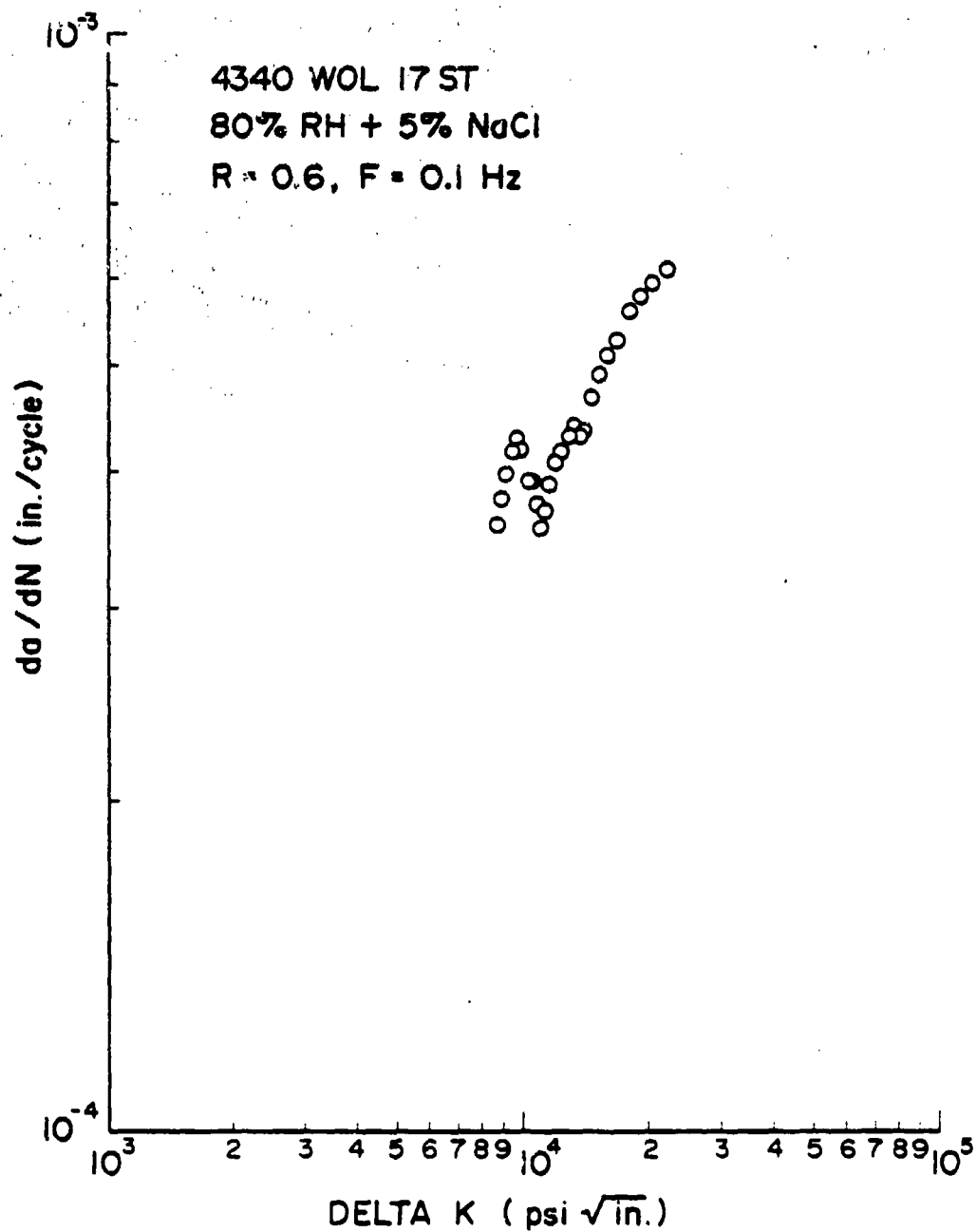


Figure 38. Plot of da/dN-vs- ΔK for 4340 Steel Tested in 80% RH + 5% NaCl.

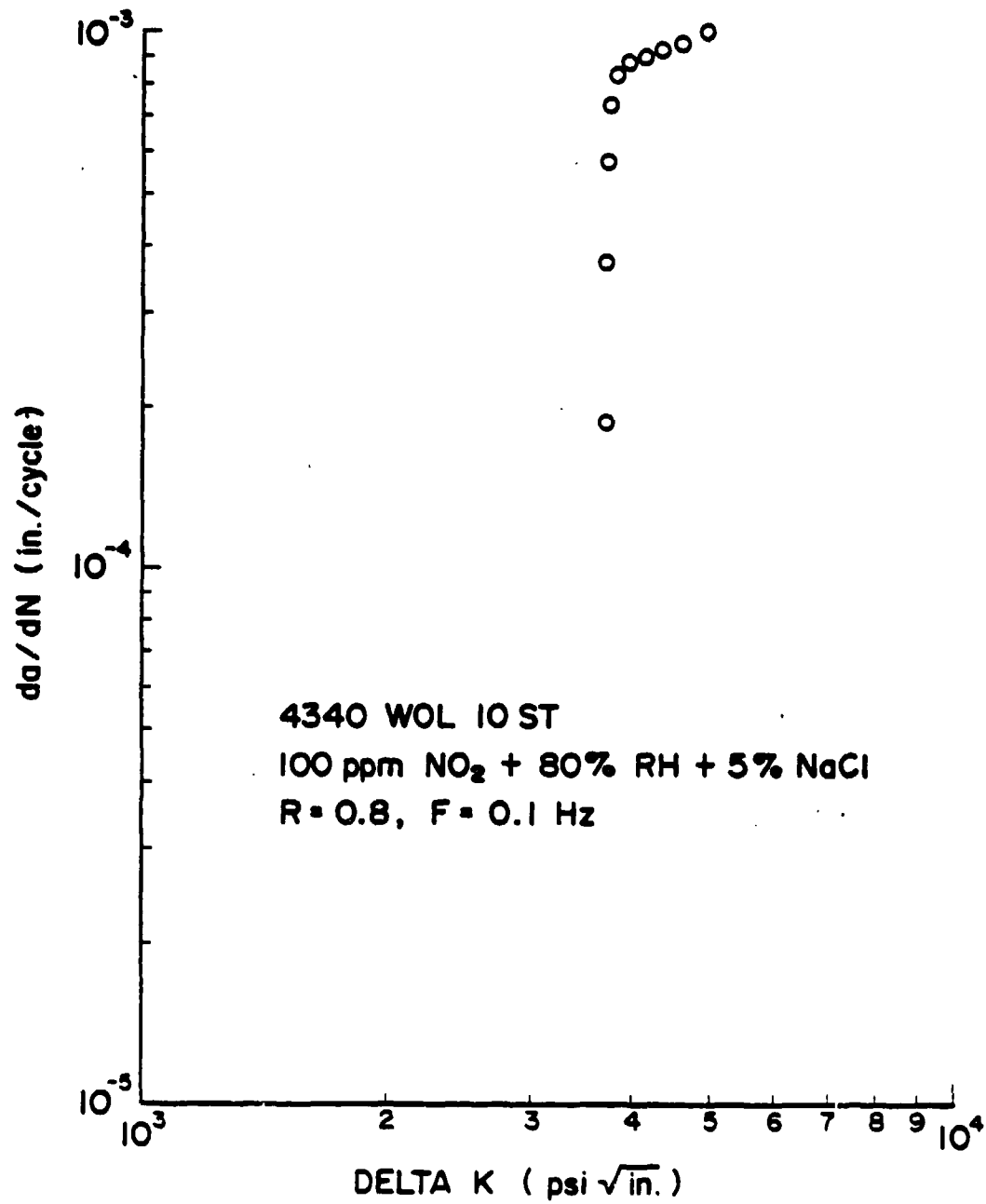


Figure 39. Plot of da/dN -vs- ΔK for 4340 Steel (10 ST) Tested in 100 ppm NO_2 + 80% RH + 5% NaCl.

a-vs-N plots obtained on specimens tested in such an environment. Figures 40-41 are a-vs-N plots showing discontinuity when salt was introduced into the environment. Figure 40 shows a sudden increase in crack length near 8000 cycles with the introduction of salt to the environment. A similar increase is evident at ~ 15000 and 22000 cycles, which eventually leads to specimen failure. A similar trend is evident from Fig. 41. The corresponding da/dN -vs- ΔK curves are shown in Figs. 42-43.

GENERAL CORROSION

Some tests were conducted in the laboratory in environments made up of various combinations of SO_2 , NO_2 , RH, and surface salts. The objective was to compare data from these tests with that obtained from field-exposure tests at Cape Kennedy and Wright-Patterson. Unfortunately, there is insufficient data to permit such correlation. One reason for this lack of data can be attributed partially to a problem which arose at the Cape Kennedy Site, rendering the data inconclusive. In one instance at this site all of the test coupons which had been subjected to exposure for nearly one and one-half years were removed from the rack and stacked in the field by a local corrosion engineer, without our knowledge. This constituted a devastating blow to our research efforts. Most of the data obtained on general corrosion have been reported in an interim report.¹³⁹

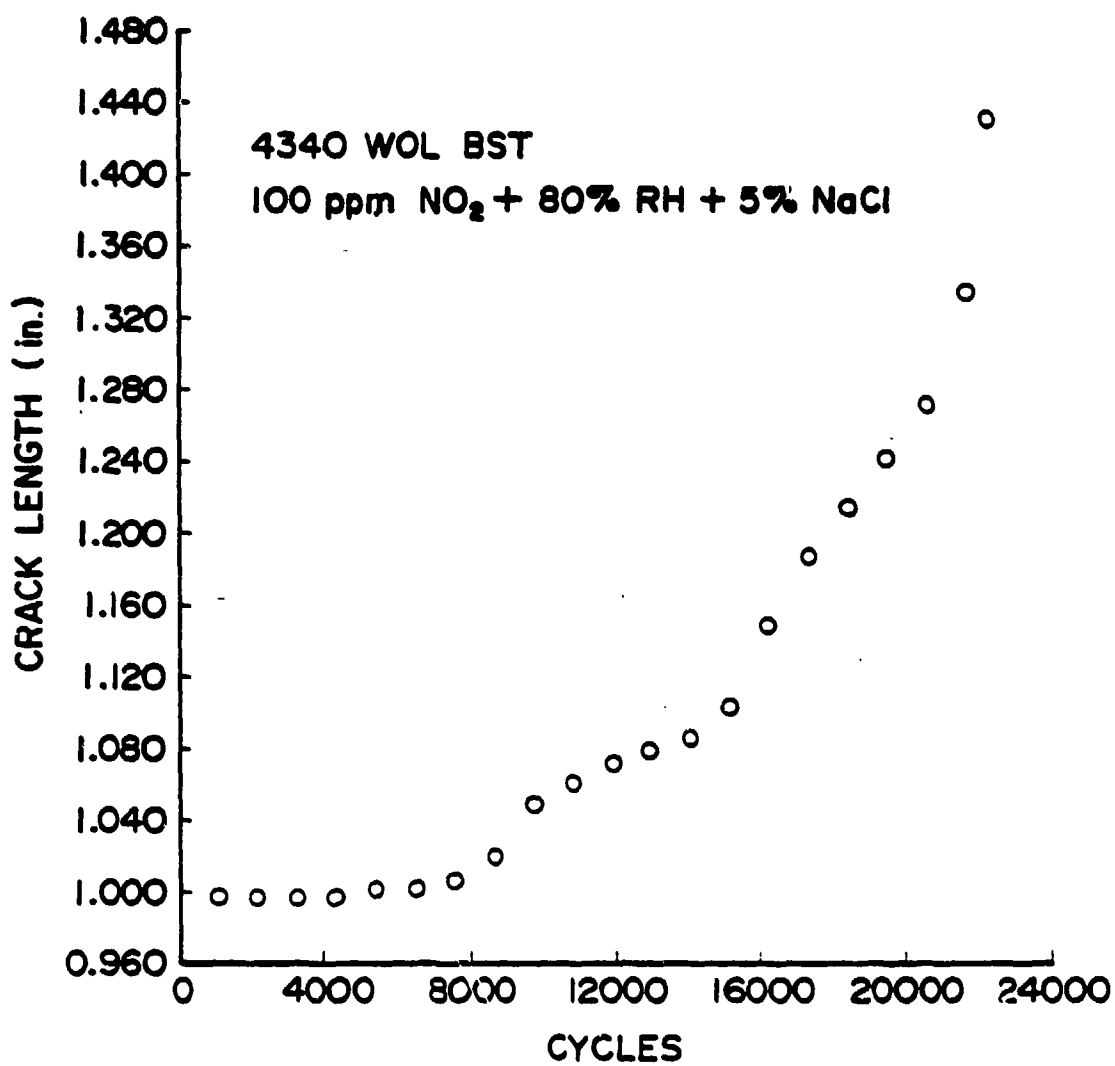


Figure 40. Plot of a -vs- N for 4340 Steel Tested in 100 ppm NO₂ + 80% RH + 5% NaCl.

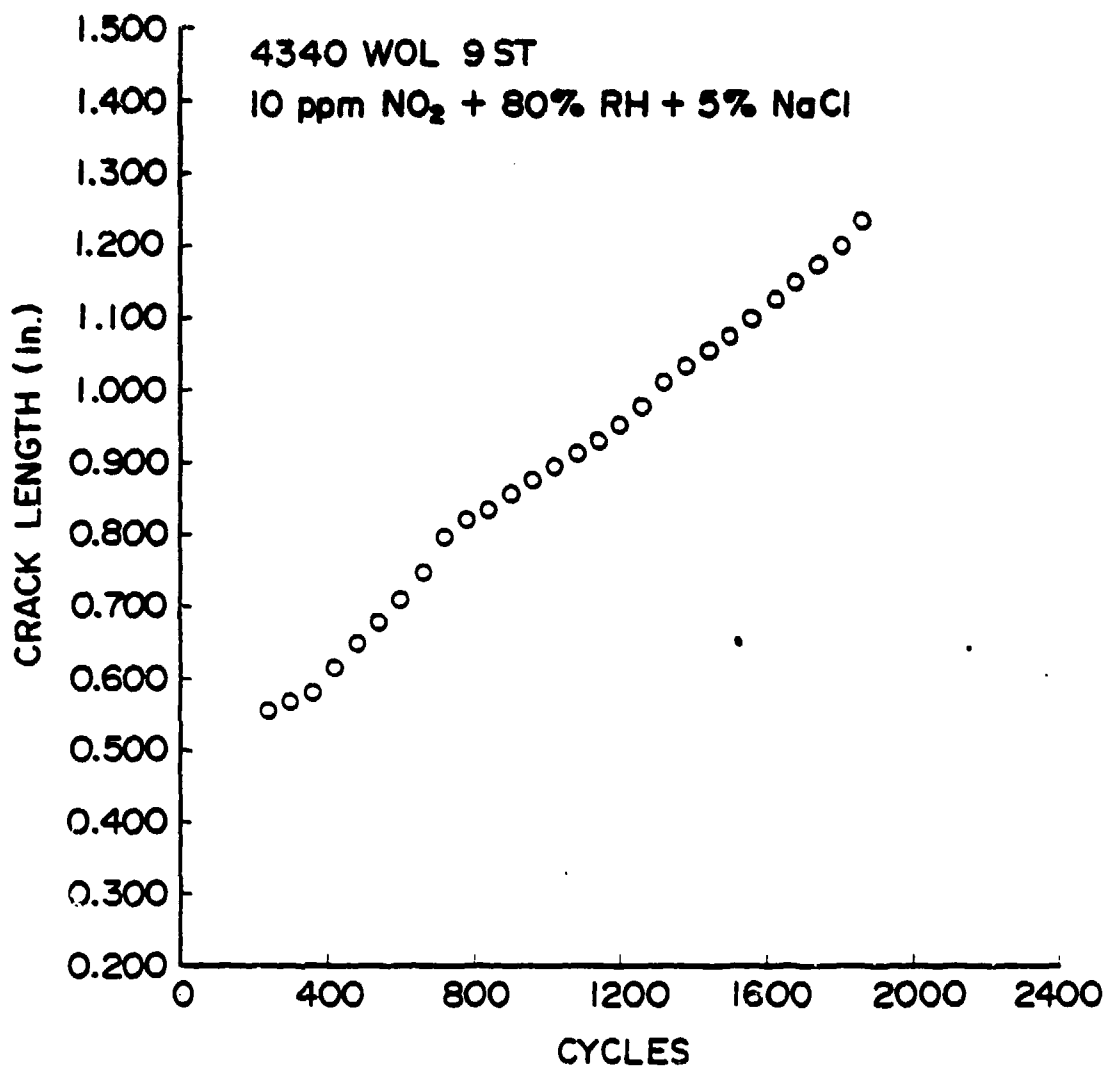


Figure 4i. Plot of a-vs-N for 4340 Steel Tested in 10 ppm NO₂ + 80% RH + 5% NaCl.

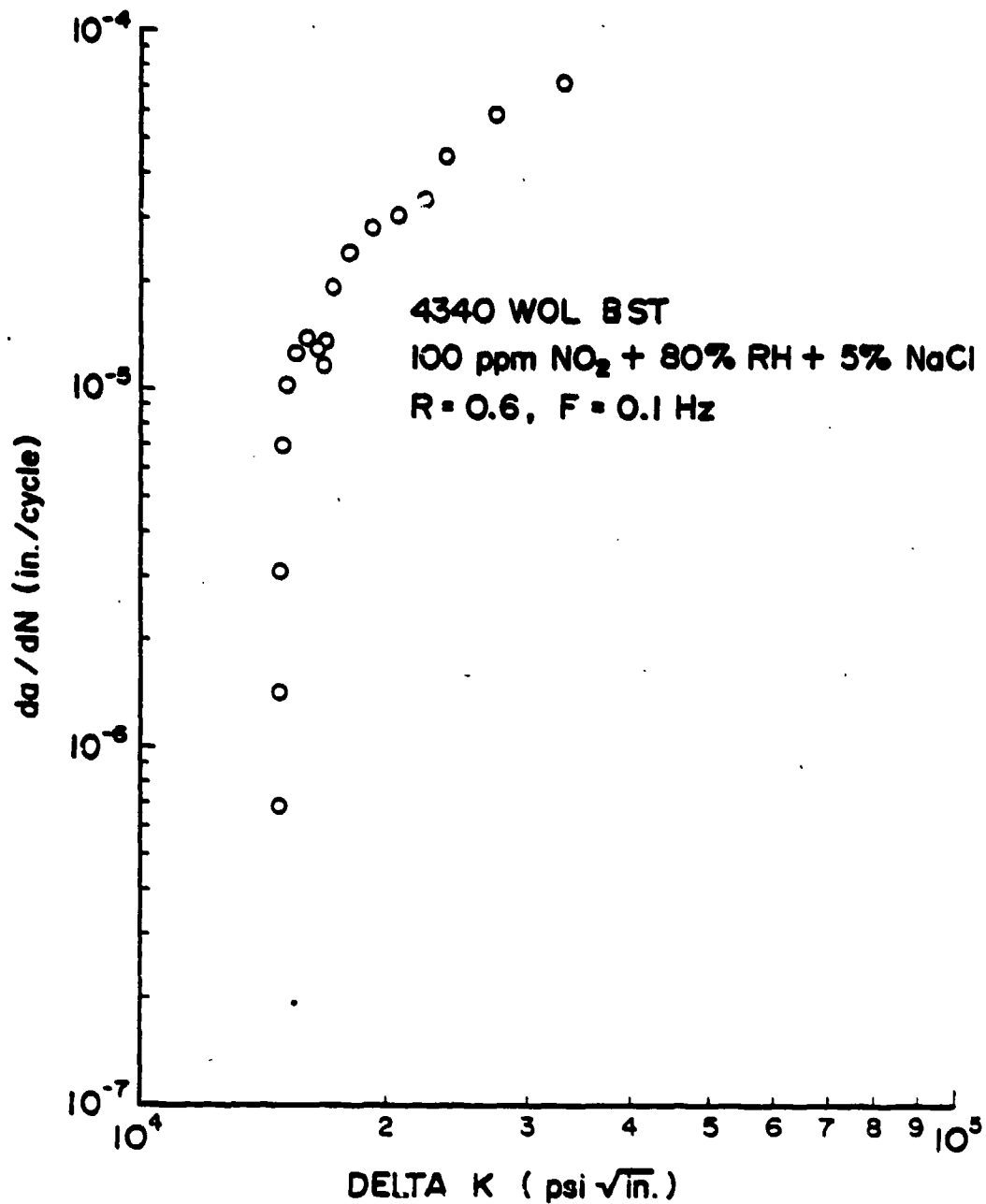


Figure 42. Plot of da/dN -vs- ΔK for 4340 Steel Tested in 100 ppm NO₂ + 80% RH + 5% NaCl.

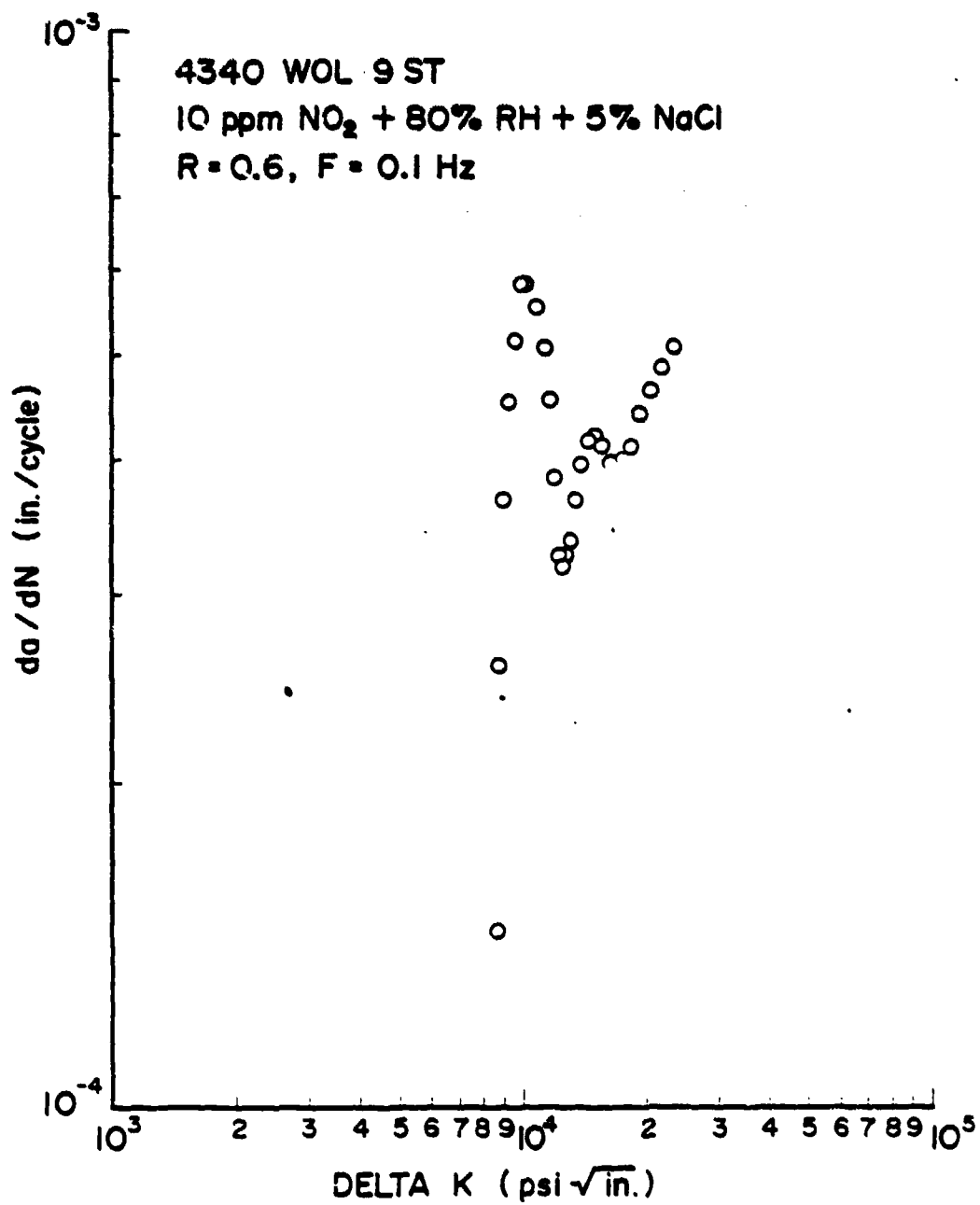


Figure 43. Plot of da/dN-vs-ΔK for 4340 Steel (BST) Tested in 10 ppm NO₂ + 80% RH + 5% NaCl.

Section 4

CONCLUSIONS

The presence of water vapor and small amounts of pollutants such as SO_2 , NO_2 , and surface salt in the atmosphere accelerates the crack-growth rates of high-strength steels and aluminum alloys. Certain combinations of these ingredients are more damaging to the high-strength steels than to the aluminum alloys, and vice versa.

The level of RH in environments of various mixtures of SO_2 + RH and NO_2 + RH was found to play a quite dominant role in crack-growth acceleration.

A mixture of 10 ppm SO_2 + 95% RH and a mixture of higher levels of SO_2 such as 1000 ppm SO_2 and lower amounts of RH such as 80% had a similar effect upon crack-growth behavior. Similar results were obtained for NO_2 .

High-strength 4340 steel was found to be susceptible to SCC in environments made up of different combinations of SO_2 + RH, NO_2 + RH, SO_2 + RH + surface salt, and NO_2 + RH + surface salt. Al 7075-T6, on the other hand, showed significant susceptibility to SCC in environments made up of combinations of NO_2 + RH + surface salt only. Other environments studied in this investigation had very minimal effects.

The value of K_{ISCC} can be extrapolated from the corrosion-fatigue curve, providing the conditions of frequency, R ratio, and the environment-material system are optimized. The results of rising-load tests and extrapolation from corrosion-fatigue data are in excellent agreement for both high-strength steel and aluminum alloys. These values were further verified by quantitative fractography. Thus, a rapid determination of K_{ISCC} is provided for susceptible alloy-environment systems.

Section 5

RECOMMENDATIONS

This investigation has demonstrated clearly that the value of K_{ISCC} can be obtained for high-strength 4340 steel through extrapolation of data obtained from a corrosion-fatigue test conducted under specific conditions. The value of K_{ISCC} for Al 7075-T6 has also been obtained from such test data. More data should be obtained for other metal-environment systems. The question to be answered is why does the uniqueness of certain environments such as $NO_2 + RH + 5\%$ surface salt in the case of Al 7075-T6 exhibit a crack-growth behavior which permits extrapolation of K_{ISCC} from the corrosion-fatigue data. On the other hand, why is it not possible to predict K_{ISCC} values for 4340 steel in a 3.5% salt solution when the environment is known to cause SCC. Solutions to these problems will lead to the development of accelerated-corrosion-testing techniques having wider applicability. Since the investigation deals with stress corrosion and corrosion fatigue, with their mechanisms poorly understood, it is highly advisable to study the mechanisms also in light of these new interesting results. The next step in this direction is to modify and adapt these testing techniques for field application.

The slow-strain-rate test has great potential. This work should be extended to notched and precracked specimens. There is a good possibility that K_{ISCC} can be calculated from data obtained during slow-strain-rate tests conducted on precracked compact-tension specimens.

The main limitation of the rising-load test is the incubation period. This could be minimized or eliminated by programmed loading (a small, high cyclic load combined with the rising load), which would provide an avenue for the development of an accelerated corrosion test.

The general-corrosion study should be pursued to obtain a good correlation between field-exposure and laboratory test data.

REFERENCES

1. L. H. Bennett, J. Kruger, R. L. Parker, E. Passaglia, C. Reimann, A. W. Ruff, and H. Yakovitz, Economic Effects of Metallic Corrosion in the United States, Parts I and II NBS Special Publication 511-1,2. (U. S. Department of Commerce, National Bureau of Standards, Washington, D. C. May 1978).
2. M. Hoch and J. Gwinn (eds.), Proceedings of the AFOSR/AFML Corrosion Workshop, AFML-TR-77-175 (Air Force Materials Laboratory, Wright-Patterson Air Force Base, OH, 1977).
3. E. D. Verink, Jr. (ed.), AFOSR/AFML Workshop on Corrosion of Aircraft, (St. Augustine, FL, September 13-15, 1977) (The University of Florida, Gainesville, FL 1977).
4. G. M. Ugiansky and J. H. Payer (eds.), Stress Corrosion Cracking: The Slow Strain Rate Technique (American Society for Testing and Materials, ASTM STP 665 Philadelphia, PA, 1979).
5. B. Bavarian, A. Moccary, and D. D. Macdonald, Corrosion, 38, 104 (1982).
6. H. F. deJong, Corrosion, 34 (1), 32 (1978).
7. M. J. Povich, Corrosion 34 (5) 162-169 (1978).
8. M. J. Humphries and R. N. Parkins, Corrosion Sci. 7, 747 (1967).
9. R. N. Parkins, F. Mazza, J. J. Royuela, and J. C. Scully, "Stress Corrosion Test Methods," Br. Corrosion J. 7, 138 (1972).
10. F. A. Champion, in Corrosion Testing Procedures (Chapman and Hall, London, 1952), p. 137.

10. F. A. Champion, in Corrosion Testing Procedures (Chapman and Hall, London, 1952), p. 137.
11. H. L. Logan, in The Stress Corrosion of Metals (Wiley, New York, 1966), p. 273.
12. Stress Corrosion Testing, ASTM STP 425 (American Society for Testing and Materials, Philadelphia, PA, 1967), p. 3.
13. R. N. Parkins, in The Theory of Stress Corrosion Cracking in Alloys (J. C. Scully, Ed.) (North Atlantic Treaty Organization, Brussels, 1971), p. 449.
14. D. O. Sprowls, T. J. Summerson, G. M. Ugianski, S. G. Epstein, and H. L. Craig, Jr., in Stress Corrosion - New Approaches, ASTM STP 610 (American Society for Testing and Materials, Philadelphia, PA, 1976), p. 3.
15. M. Khobaib and C. T. Lynch, Presented at ASTM - NBS Symposium on Environment-Sensitive Fracture: Evaluation and Comparison of Test Methods, Gaithersburg, MD, April 26-28, 1982.
16. P. McIntyre and A. H. Priest, Accelerated Test Technique for the Determination of K_{ISCC} in Steels, British Steel Corporation Report MG (31) 72 (Great Britain, 1972).
17. W. G. Clark and J. D. Landes, Stress Corrosion - New Approaches, ASTM-STP-610 (American Society for Testing and Materials, Philadelphia, PA, 1976), p. 108.
18. R. O. Ritchie, S. Suresh, and J. Toplosky, M.I.T. Fatigue and Plasticity Lab Report No. FPL/R/80/1030 (Massachusetts Institute of Technology, Cambridge, MA, January 1980) (Contract DE-AC02-79ER10389, A000).

19. J. P. Gallagher and R. P. Wei, "Corrosion Fatigue Crack Propagation Behavior in Steels," in Corrosion Fatigue, NACE-2 (National Association of Corrosion Engineers, Houston, TX, 1972).
20. M. O. Speidel, M. J. Blackburn, T. R. Beck and J. A. Feeney, Corrosion Fatigue, NACE-2 (National Association of Corrosion Engineers, Houston, TX, 1972).
21. W. W. Gerberith, J. P. Birat, and V. F. Zackay, "On the Superposition Model for Environmentally-Assisted Fatigue Crack Propagation," in Corrosion Fatigue, NACE-2 (National Association of Corrosion Engineers Houston, TX, 1972).
22. H. L. Craig, Jr. (ed.), Stress Corrosion-New Approaches, ASTM-STP-610 (American Society for Testing and Materials, Philadelphia, PA, 1976).
23. D. J. Duquette, in AFOSR/AFML Workshop on Corrosion of Aircraft (Conference held in St. Augustine, FL, September 13-15, 1977) (University of Florida, Gainesville, FL, 1977).
24. A. J. McEvily and R. P. Wei, in Corrosion Fatigue NACE-2, National Association of Corrosion Engineers, Houston, TX, 1972), p. 381.
25. M. J. Blackburn, J. A. Feeney, and T. R. Beck, "Stress Corrosion Cracking of Titanium Alloys," in Advances in Corrosion Science and Technology, Vol. 2 (M. G. Fontana and R. W. Staehle, Eds.) (Plenum Press, N.Y., 1971).
26. M. O. Speidel and M. V. Hyatt, "Stress Corrosion Cracking of High Strength Aluminum Alloys," in Advances in Corrosion Science and Technology, (M. G. Fontana and R. W. Staehle, eds.) (Plenum Press, N. Y., 1971).

27. M. O. Speidel "Current Understanding of Stress Corrosion Crack Growth in Aluminum Alloys".in Proceedings of Conference on the Theory of Stress Corrosion Cracking in Alloys (Enceria, Portugal, 1971).
28. C. Laird, Fatigue Crack Propagation, ASTM STP 415 (American Society for Testing and Materials, Philadelphia, PA, 1967).
29. K. Walker, S. Pendleberry, and R. McElwoe, Effects of Environment and Complex Load History on Fatigue Life, ASTM STP 462 (American Society of Materials, Philadelphia, PA, 1970), p. 234.
30. H. H. Johnson and P. C. Paris, Eng. Fract. Mech. 1, 3 (1968).
31. R. P. Wei, J. Eng. Fract. Mech. 1, 633 (1970).
32. W. A. Spitziz, P. M. Talda, and R. P. Wei, J. Eng. Fract. Mech. 1, 155 (1968).
33. Che-Yu Li, P. M. Talda, and R. P. Wei, Int. J. Fract. Mech. 3, 29 (1967).
34. H. W. Liu, Appl. Mat. Res. 3, 229 (1964).
35. J. P. Gallagher, J. Metals 6, 941. (1971).
36. G. A. Miller, S. J. Hudak, and R. P. Wei, J. Testing and Evaluation 1, 524, (1973).
37. R. P. M. Proctor and K. Moss Presented at the 6th International Congress on Metallic Corrosion, Sydney, Australia, 1975.

38. D. B. Dawson and R. M. Pellonix, *Met. Trans.* 5, 723 (1974).
39. H. W. Liu, *Trans. ASME, Ser. D*, 85, 116 (1963).
40. P. S. Kensley, N. E. Ryan, and G. S. Jost, 8th ICAF Symposium on Problems with Fatigue in Aircraft (J. Branger and F. Berger), ICAF Document 801, (1975), p. 23.
41. I. M. Austen and E. F. Walker, in Conferences on the Influence of Environment on Fatigue, (Inst. Mech. Engr. London, 1977).
42. J. A. Feeney, J. C. McMillan, and R. P. Wei, *Met. Trans.* 1, 1741 (1970).
43. F. J. Bradshaw and C. Wheeler, *Int. J. Fract. Mech.* 5, 255 (1969).
44. R. Bucci, Environment Enhanced Fatigue and Stress Corrosion Cracking of a Titanium Alloy Plus a Simple Model for Assessment of Environmental Influence of Fatigue Behavior, Ph.D. Dissertation, Lehigh University, Bethlehem, PA, 1970.
45. J. M. Barsam, Investigation of Subcritical Crack Propagation, Ph.D. Dissertation, University of Pittsburgh, Pittsburgh, PA, 1969.
46. C. T. Lynch, K. J. Bhansali, and P. A. Parrish, Inhibition of Crack Propagation of High Strength Steels through Single and Multifunctional Inhibitors, Technical Report AFML-TR-76-120 (Air Force Materials Laboratory, Wright-Patterson Air Force Base, 1976).
47. C. T. Lynch, F. W. Vahldiek, K. J. Bhansali, and R. Summit, "Inhibition of Environmentally Crack Enhanced Crack Growth Rates in High Strength Steels," Presented at the Symposium on Environmental Effects on Metals, AIME Fall Meeting, Chicago, IL, 1977.

48. F. W. Vahldiek, F. Thornton, and C. T. Lynch, "Effects of Temperature and Humidity on Corrosion Fatigue of 4340 Steel," Presented at AIME Spring Meeting, Denver, CO 1978.
49. M. Khobaib and C. T. Lynch, "Corrosion and Corrosion Fatigue Inhibition of Al-7075-T6," Presented at the AIME Spring Meeting, Denver, CO, 1978.
50. V. I. Lobaiko, N. N. Zhagalyak, I. J. Vasilenko, V. E. Litvinov, and V. G. Stepanov, Otkrytiya, Izobret, Prom, Obraztsy, Tovarnyeznaki 55 (10), 138 (1978).
51. T. Shoji, T. Oise, J. Takahashi, and M. Suzuki, Corrosion 34, (10) 366 (1978).
52. R. N. Parkins and B. S. Greenwall, Met. Sci. 11 (18-9), 405 (1977).
53. R. P. Wei and J. D. Landes, Mater. Res. Stand., ASTM 9, 25 (July 1969).
54. R. N. Parkins, (University of Newcastle-Upon-Tyne, Newcastle-Upon-Tyne, England), Private communication.
55. K.-H. Schwalbe, "Mechanik and Mechanismen des Stabilen Ribwachstums in Metallischen Werkstoffen," To be published in Fortschr.-Ber. VDI-Z., Reihe 18.
56. K.-H. Schwalbe, Eng. Fract. Mech. 9, 547 (1977).
57. K.-H. Schwalbe, "Bruchflächenuntersuchungen bei der Ausbreitung von Ermüdungsrissen in AlZnMgCu 0,5 F46," Z. Metallkde. 66, 408 (1975).

58. R. N. Parkins, "Stress Corrosion Test Methods," Presented at the European Federation of Corrosion Contribution Specialist Meeting on Stress Corrosion Testing Methods, AGARD Conference Proceedings, No. 98; Paper also presented at the Structure and Materials Panel 33rd Meeting, Brussels, Belgium, October 5-6, 1971, (Distributed by NTIS) AD 740, January 1972, pp. 62-66.
59. M. J. Humphries and R. N. Parkins, Corrosion Sci. 7, 747 (1967).
60. R. N. Parkins, Fifth Symposium on Line Pipe Research (American Gas Association, Inc., Houston, TX, November 1974), Paper V, p. 1-40.
61. H. Buhl, (Abt. Korros., Dtsch Forsch-Versuchsanst. Luft-Raumfahrt, Cologne, Germany), DLRL-FB-76-69 (Avail NTIS), 1976.
62. M. Hishida and H. Nakada, Corrosion 33 (11) 403 (1977).
63. D. C. Deegan and B. E. Wilde, Corrosion 34 (6), 19 (1978).
64. S. Orman, Corrosion Sci. 9, 849 (1969).
65. D. T. Powell and J. C. Scully, Corrosion 24, 151 (1968).
66. H. Bull, "The Validity of the Constant Straining Test Method in SCC Research Compared with Conventional Testing Techniques," for European Federation of Corrosion, Working Party on Stress Corrosion Test Methods- - Minutes of the Sixth Meeting (Enschede, The Netherlands, May 11, 1976).
67. B. F. Brown, Mat. Res. and Stand. 6 (3), 129 (1966).
68. S. R. Novak and S. T. Rolfe, J. Mater. 4 (3), 701 (1969).

69. Standard Test for Plane-Strain Fracture Toughness of Metallic Materials, ASTM Standard E-399-72 (American Society for Testing and Materials, Philadelphia, PA., 1972).
70. Corrosion in Natural Environments, ASTM-STP-558 (American Society for Testing and Materials, Philadelphia, PA, 1974).
71. J. C. Hudson, Trans. Faraday Soc. 25, 177 (1929).
72. C. P. Larrabee and S. K. Coburn, First International Congress on Metallic Corrosion (Butterworth, London, 1962) p. 276.
73. J. A. Capp, Proc. ASTM 14, 474 (1914).
74. W. H. J. Vernon, Trans. Faraday Soc. 23, 113 (1927).
75. W. H. J. Vernon, Trans. Faraday Soc. 27, 255 (1931).
76. W. H. J. Vernon, Trans. Faraday Soc. 31, 1668 (1935).
77. W. H. J. Vernon, Trans. Electrochem. Soc. 64, 31 (1933).
78. V. M. Dorsey, Ind. and Eng. Chem. 30, 1147 (1938).
79. T. Swinden and W. W. Stevenson, J. Iron and Steel 142, 165 (1940).
80. H. Pray and J. Gregg, Proc. ASTM 41, 758 (1941).
81. K. G. Compton, Trans. Electrochem. Soc. 91, 705 (1947).
82. C. D. Cooke and C. Merritt, Mat. and Meth. 25, 77 (1947).

83. F. Todd, Ind. and Eng. Chem. (Analytical Ed.) 16, 394 (1944).
84. H. R. Baker, Ind. and Eng. Chem. 41, 137 (1949).
85. C. R. L. Test, J. Iron Steel Inst. 171, 255 (1952).
86. W. Kesternich, Stahl U. Eisen 71, 587 (1951).
87. W. Kesternich, Werkstoff U. Korrosion 16, 193 (1965).
88. J. Edwards, Trans. Inst. Met. Finishing 35, 55 (1958).
89. R. St. J. Preston and V. E. G. Stroud, J. Inst. Petroleum 36, 457 (1950).
90. R. A. LeGault, S. Mori, and H. P. Leckie, Corrosion 29 (5), 169 (1973).
91. R. A. Legault, and V. P. Pearson, Corrosion 34 (10), 344 (1978).
92. R. A. Legault and V. P. Pearson, Corrosion 34 (12), 433 (1978).
93. M. Pourbaix, Ceelcor Report No. 2087 (Belgium, 1967).
94. H. Guttman and P. J. Sereda, Metal Corrosion in the Atmosphere, ASTM-STP-435 (American Society for Testing and Materials, Philadelphia, PA, 1968), p. 326.
95. H. Guttman, Metal Corrosion in the Atmosphere, ASTM-STP-435 (American Society for Testing and Materials, Philadelphia, PA, 1968), p. 223.
96. P. J. Sereda, Ind. and Eng. Chem. 52 (2), 157 (1960).

97. G. Schikorr and I. Schikorr, *Zeitschrift fur Metallkunde* 35 (9), 175 (1943).
98. J. C. Hudson and J. F. Stanners, *J. Appl. Chem.* 3, 86 (1953).
99. K. Banton, E. Beranek, and G. V. Akimov, *Werkstoffe Und Korrosion* 10 (6), 377 (1959).
100. J. Sydberger and N. G. Vannerberg, *Corrosion Sci.* 12, 775 (1972).
101. F. Mansfeld, Study of the Effects of Airborne Sulfur Pollutants on Materials, AMC 7010.T0112AR (Rockwell International Science Centers, Thousand Oaks, CA, 1977).
102. F. H. Haynie and J. B. Upham, Corrosion in Natural Environments, ASTM-STP-558 (American Society for Testing and Materials, Philadelphia, PA, 1974), p. 33.
103. W. J. Spence and F. H. Haynie, Corrosion in Natural Environments, ASTM-STP-558 (American Society for Testing and Materials, Philadelphia, PA, 1974), p. 279.
104. F. H. Haynie, Stress Corrosion - New Approaches, ASTM-STP-610 (American Society for Testing and Materials, Philadelphia, PA, 1976).
105. F. H. Haynie, J. W. Spence, and J. B. Upham, EPA-60013-76-015 (U. S. Environmental Protection Agency, Triangle Research Park, NC, 1976).
106. F. H. Haynie and J. B. Upham, *Corrosion* 9 (8), 35 (1970).
107. M. Pourbaix, Private communication.

108. ASTM Handbook of Standards, Part 9 (American Society for Testing and Materials, Philadelphia, PA, 1974).
109. G. E. K. O. Schmidt, Z. Metallkunde, 22, 328 (1930).
110. F. A. Champion, Corrosion Testing Procedures (John Wiley, New York, 1965).
111. W. O. Kroenig, Korrosion U. Metallschutz 6, 25 (1930).
112. A. Portevin and E. Herzog, Korrosion U. Metallschutz 14, 205 (1938).
113. J. Cournot and M. Chaussein, Compt. Rend. 199, 1410 (1934).
114. J. Cournot, Compt. Rend 193, 1335 (1931).
115. G. O. Taylor, Metallurgia 25, 63 (1942).
116. W. Patterson, Korrosion U. Metallschutz 20 (3), 125 (1944).
117. A. D. Mercer and F. Womwell, J. Appl. Chem. 9, 577 (1959).
118. F. A. Champion, Corrosion Testing Procedures, 2nd Ed. (Barnes and Noble, New York, 1965), p. 73.
119. J. A. Chess, M. R. Hastings, A. Paolini, Jr., J. Coal Technol. 49 (633), 55 (1977).
120. Biestek, Tadeusz, Powloki Ochr 5 (1), 18 (1977).
121. Miyagi, Yoshimitsu, Keikinzoku 26 (12) 611 (1976)
122. Standard Method of Acetic Acid-Salt Spray (Fog) Testing, ASTM Designation B287-61 (American Society for Testing and Materials, Philadelphia, PA, Adapted 1961).

123. B. A. Whittaker, Unclassified S and T Memo 26/60 (Technical Information and Library Services, Ministry of Aviation, England, September 1960).
124. M. K. Budd and F. F. Booth, Corrosion 18 (May 1962).
125. R. L. Horst, Jr. and B. W. Lifka, Corrosion SBIIA 26, 3 (1970).
126. D. K. Compton and N. W. Mitchell, "Alternate-Immersion and Waterline Tests," in Proceedings of the Symposium on Corrosion Testing Procedures, (Chicago Meeting of ASTM) (American Society for Testing and Materials, Philadelphia, PA, 1937) p. 74.
127. R. B. Mears, C. J. Walton, and G. G. Eldredge, Proc. ASTM 44, 639 (1944).
128. J. D. Hanawalt, C. E. Nelson, and J. A. Peloubet, Trans. AIME 147, 273 (1942).
129. Alternate Immersion Corrosion Test of Non-ferrous Metals ASTM Standard I-B (B192-44T), (American Society for Testing and Materials, Philadelphia PA, 1946), p. 780.
130. H. S. Rawdon, Trans. AIME, Inst. Met. Div. 220 (1929).
131. A. J. Jacobs and H. L. Marcus, Corrosion 30 (9), 305 (1974).
132. W. Pistulka and G. Lang, Aluminum (Duesseldorf) 53 (6), 366 (1977).
133. K. Lage and J. Lars, Korros. Korrosionsschutz Alum. Vernast, Eur. Foed. Korros. Vont. 88, 203 (1976).
134. I. L. Rozenfeld, I. B. Krasnorutskaya, M. V. Konrad, and V. V. Zashch Met. 14 (2), 131 (1978) (Russian).

135. J. L. Pagniez, J. C. Charbonnier, Mater. Tech. 65 (5), 253 (1977).
136. V. Popa, Rev. Chim (Bucharest) 29 (6), 569 (1978).
137. V. Sanchez and P. Patnicio, Acabados Ind., Recubrimientos Org. 15 (16), 125 (1974).
138. J. W. Spence and F. H. Haynie, "Design of a Laboratory Experiment to identify the Effects of Environmental Pollutants on Materials," in Corrosion in Natural Environments, ASTM-STP-558 (American Society for Testing and Materials, Philadelphia, PA, 1974).
139. "Accelerated Corrosion Testing" Interim Report for period June 1979-March 1981 prepared under Contract F33615-79-C-5109 (Systems Research Laboratories, Inc., Dayton, OH, June 1981).
140. M. Khobaib, F. C. Chang, E. Keppler, and C. T. Lynch, ASTM STP 767 "Atmospheric Corrosion of Metals" (American Society for Testing and Materials, Philadelphia, PA, August 11, 1982).

APPENDIX A

SLOW-STRAIN-RATE TESTING IN CONTROLLED ATMOSPHERES

SLOW-STRAIN-RATE TESTING IN CONTROLLED ATMOSPHERES

**M. Khobaib
Systems Research Laboratories, Inc.
2800 Indian Ripple Road
Dayton, Ohio 45440**

**C. T. Lynch
Office of Naval Research
Arlington, VA 22217**

ABSTRACT: The stress-corrosion-cracking susceptibility of Al 7075-T6 alloys has been studied in a controlled-atmosphere chamber utilizing the slow-strain-rate technique. The effects of realistic atmospheres such as high-humidity air with small additions of sulfur dioxide, nitrogen dioxide, and surface salts in different combinations have been investigated. The slow-strain-rate technique has been used to optimize the simulated environments which result in accelerated crack growth and failure by stress-corrosion cracking in high-strength aerospace structural materials. These controlled environmental tests are necessary to provide initial data on environmental susceptibility needed for the development of realistic accelerated-corrosion testing methods. The design of the slow-strain-rate apparatus and the environmental chamber for providing controlled atmospheres will be discussed and initial experimental results presented. Most tests were conducted at 80 - 90% relative humidity. The sulfur-dioxide concentration was varied from 10 to 1000 ppm, while NO₂ was used in the range 10 to 100 ppm. Small amounts of surface salts were obtained by rapid immersion in aqueous salt solutions. The susceptibility of the alloys shows significant differences which are dependent upon the specific environmental contaminants. These differences can be quantified and related to the observed service behavior of the materials. Synergistic effects in several environments were found to maximize the environmental effects upon crack growth in stress corrosion. These effects were subsequently demonstrated in corrosion-fatigue experiments under similar conditions. The qualitative estimates of embrittlement in the fracture surfaces were consistent with slow-strain-rate results. The data provide the basis for the development of accelerated corrosion tests in realistic atmospheres.

Research supported in part by USAF Contract F33615-79-C-5109.

KEY WORDS:

**Slow-Strain-Rate Testing; Controlled Atmospheres; Stress-Corrosion Cracking;
Quasi-Cleavage; Intergranular Separation; Embrittlement.**

INTRODUCTION

Several methods have been used to determine the susceptibility of materials to stress-corrosion cracking (SCC) [1-5]. Over the past five years, the slow-strain-rate technique has found wide-spread application due to the reproducibility of the data and relatively short period of testing time involved. Mainly, the technique has been used to reveal the SCC tendencies of metallic materials in specific environments and is readily being accepted as an accelerated "sorting test." In the present investigation this method has been used to optimize the simulated environments which result in accelerated crack growth and failure by SCC in high-strength aerospace structural materials.

The influence of a combination of environments--consisting of 80 to 95% relative humidity (RH), 10 to 1000 ppm SO_2 , 10 to 100 ppm NO_2 , and nearly 5% surface salt--in producing the SCC for Al 7075-T6 was studied. The main objective of the present research was to determine the most aggressive combinations of environmental constituents which would result in maximum susceptibility of Al 7075-T6 to SCC.

EXPERIMENTAL PROCEDURES

The slow-strain-rate tests for Al 7075-T6 were conducted with simple tensile specimens. The specimen geometry and dimensions are shown in Fig. 1. The high-strength Al 7075-T6 alloy having a yield strength of 440 MPa was obtained from Rockwell International. The specimens were prepared from a 76.2-mm-thick plate with loading axis in the

short transverse (ST) direction. Research-grade SO_2 , NO_2 , and breathing air were employed in the tests.

A slow-strain-rate machine having a capacity of 20,000 lb. (88964 N) was designed and built in our laboratory. Figure 2 is a front view of the machine with the environmental chamber in place. The strain-rate capability of the machine ranges from 10^{-4} to 10^{-9} /s.

The tests were conducted in controlled atmospheres, obtained within an environmental chamber. The chamber and gas-train assembly are shown in Fig. 3. The chamber is made from a 8-in.-diam., 3/8-in.-thick acrylic pipe, having a special water-resistant clear coating on the inside.

The test atmospheres are supplied through the gas train which consists of a gas-mixing and delivery system. High-purity bottled gases (SO_2 , NO_2 , and dry air) are metered by Matheson flow meters and then mixed in the mixing tube. The concentration of SO_2 and NO_2 gases in the chamber is routinely measured by calibrated Gastec analyzer tubes. Special gas-sampling outlets are provided in the chamber. The RH inside the chamber is controlled by means of a BMA dry- and wet-bulb hygrometer. The water vapor is added in the form of steam by boiling distilled water in a flask maintained at a constant temperature. The steam flow is controlled by the output voltage of the BMA controller which monitors the opening and closing of the solenoid valve on the steam line. The steam is injected into the gas mixture prior to entry into the chamber in order to obtain the required mixture of SO_2 , NO_2 , and RH air.

Gas pressures used in all tests have been slightly above atmospheric to provide positive flow through the environmental chamber. The gas inlet and outlet are positioned specifically to minimize the channeling effect. The gas is circulated inside the chamber by means of a circulating fan (placed inside the chamber) to maintain a uniform environment throughout the chamber. Negligible condensation occurred during these tests, except in the case of 100% RH.

Initially, several tests were conducted in air, different levels of RH, and a mixture of surface salts and RH. These tests were followed by experiments in aggressive gaseous environments. Several combinations of SO₂ (ranging from 10 to 1000 ppm), NO₂ (10 to 100 ppm), RH (80 to 95%), and 5% surface salt were studied. The surface salt deposit was obtained by dipping the sample in or squirting it uniformly with 5% NaCl solution, followed by drying. Strain rates used varied from 10⁻⁴ to 10⁻⁹/s and were obtained by manipulating the gear ratios.

RESULTS AND DISCUSSION

The aggressiveness of a combination of environments composed of a mixture of SO₂, NO₂, RH, and surface salt in producing SCC in high-strength Al 7075-T6 was determined by conducting slow-strain-rate tests on tensile specimens. The specimens were tested at various rates in several combinations of the environments described earlier. The results of these tests are given in Table 1. Figure 4 shows the percent elongation versus strain

rate plots of specimens tested in ambient air, 5% surface salt, 1000 ppm SO_2 + 80% RH, 1000 ppm SO_2 + 90% RH, and a mixture of 1000 ppm SO_2 + 5% surface salt + 80% RH. The air run and 5% surface salt plot appear to be very similar. The percent elongation does not change appreciably with strain rate. The fracture surfaces also appear to be very similar. This suggests that the 5% surface salt has very little effect. A minimum in percent elongation can be noted for a mixture of 1000 ppm SO_2 + 80% RH. This minimum occurs at a strain rate of $2.27 \times 10^{-7}/\text{s}$. More noticeable is the minimum in percent elongation occurring for other environments around the same strain rate of $2 \times 10^{-7}/\text{s}$. This may be due to the fact that this material is susceptible to SCC near this rate. On the other hand, more tests must be conducted in order to define the discrete minimum levels for each environment. Since the difference in percent elongation is very small and the situation becomes more complicated in the case of results obtained for 1000 ppm SO_2 + 90% RH mixture, additional support is required to determine (or differentiate) the degree of SCC susceptibility in these environments.

Figure 5 is a fractograph taken from samples tested in 1000 ppm SO_2 + 80% RH at $2.27 \times 10^{-7}/\text{s}$. This fractograph supports the occurrence of SCC at this rate in 1000 ppm SO_2 + 80% RH.

The loss of ductility is more apparent for the specimen tested in a mixture of 1000 ppm SO_2 + 5% surface salt + 80% RH. The percent elongation at all strain rates tested was under 2%, and a minimum in elongation occurred at a strain rate of $1.41 \times 10^{-7}/\text{s}$, indicating the occurrence of SCC.

Figure 6 shows the fracture morphology of the specimen tested in 1000 ppm SO_2 + 80% RH + 5% surface salt. The surface features are very flat. There is evidence of extensive cleaving as well as cracking. The cracking could not be well documented because the specimen was covered with corrosion products.

Figure 7 is another plot of percent elongation versus strain rate. The objective in this case was to study the effect of the difference in humidity level and of surface-salt addition. The plots are similar to those in Fig. 4. The maximum loss in ductility could be noted here also when 5% surface salt was added to 100 ppm SO_2 + 90% RH. A distinct minimum occurs at $3.8 \times 10^{-7}/\text{s}$ for a humidity level of 95%, while the minimum in percent elongation is observed at a lower humidity level of 80% RH in Fig. 4. However, when 5% surface salt is added to the mixture of 100 ppm SO_2 + 90% RH, the loss in ductility is quite significant at this composition also. Again, Fig. 7 shows a minimum at a strain rate of $1.8 \times 10^{-7}/\text{s}$. Figure 8 (a) is the fractograph taken from a specimen tested in 100 ppm SO_2 + 90% RH at a strain rate of $8.9 \times 10^{-7}/\text{s}$. The surface features show more ductility than in Fig. 8 (b) and 8 (c). There is little cracking, and the amount of quasi-cleavage is also minimum. Figures 8 (b) and 8 (c) show the surface features from the specimen tested in 100 ppm SO_2 + 90% RH and 5% surface salt at strain rates of $6.8 \times 10^{-7}/\text{s}$ and $2.3 \times 10^{-7}/\text{s}$. The failure modes are also very similar. Figure 8 (b) shows more quasi-cleavage and less cracking as compared to Fig 8 (c). It is very difficult to quantify the differences since the difference in the percent elongation could be within the error band. However, the surface features show compatibility with the strain-rate results and support the presence of SCC.

Figure 9 is a plot of percent elongation versus strain rate when the SO_2 levels used are nearer the realistic values obtained in industrial environments. Figure 9 includes data from tests conducted at two SO_2 levels (100 ppm and 10 ppm) and two humidity levels (90% and 80% RH). The results show that a combination of higher humidity level (90% RH) and lower SO_2 level (10 ppm) induces more embrittlement than a mixture of higher SO_2 level (100 ppm) and a lower RH level (80%). The more damaging effect in terms of the loss of ductility is produced by the introduction of a small amount of surface salt. No minimum in percent elongation occurs when a mixture of 10 ppm SO_2 + 90% RH + 5% surface salt is used. From the results of the tests conducted in an environment consisting of a mixture of SO_2 , RH, and a small amount of surface salt, it appears that the presence of a small amount of surface salt produces synergism. However, it should be remembered that the presence of 5% surface salt alone is not sufficient to create SCC in this alloy, as shown in Fig. 4. Hence, a high humidity level of 90 - 100% RH in combination with a small amount of SO_2 (as low as 10 ppm), and a trace amount of surface salt (\approx 5%), can render Al 7075-T6 susceptible to SCC.

The effect of NO_2 gas as compared to SO_2 was also studied. The results are shown in Fig. 10. The percent elongation versus strain rate plots are very similar. The maximum loss in ductility in this case also occurs when a small amount of surface salt is added to the mixture of 100 ppm NO_2 + 90% RH. A minimum occurs at a strain rate of $2.8 \times 10^{-7}/\text{s}$, as shown in Fig. 9. The fractograph taken from this specimen is shown in Fig. 11. The fracture surface is severely corroded; the intergranular separation and cracking are apparent, and the fractograph shows less

ductility than that of Fig. 8 (a). It is not possible to differentiate the level of cracking from the fractographs obtained from specimens tested in 100 ppm SO_2 + 90% RH + 5% surface salt and 100 ppm NO_2 + 90% RH + 5% surface salt.

In general it was very difficult to differentiate the level of SCC susceptibility caused by NO_2 from that caused by SO_2 using this test. The visual surface observations, however, along with the results of slow-strain-rate tests, showed that a mixture of 100 ppm NO_2 + 90% RH + 5% surface salt was more aggressive than an environment of 100 ppm SO_2 + 90% RH + 5% surface salt. Limited testing in the rising-load mode was conducted as part of a larger effort to develop an accelerated-corrosion test method. Although preliminary, these rising-load test results show a significant decrease in the K_{ISCC} value when 5% surface salt is added to a mixture of SO_2 + RH or NO_2 + RH, which lends support to the slow-strain-rate results. These results also demonstrate that the effect of NO_2 is more pronounced than that of SO_2 , giving rise to a lower value of K_{ISCC} when a mixture of NO_2 + RH + 5% surface salt was used, as compared to SO_2 + RH + 5% surface salt at the same concentration level.

CONCLUSION

1. SO_2 and NO_2 gases in small concentrations attack the surface of A1 7075-T6.
2. A Small amount of surface salt also has a damaging effect upon A1 7075-T6.

3. When small levels of SO_2 and NO_2 are present with high levels of RH, the surface attack on Al 7075-T6 is quite severe and may cause some SCC.
4. An environment consisting of a mixture of either 10 ppm NO_2 + 90% RH + 5% surface salt or 100 ppm SO_2 + 90% RH + 5% surface salt creates SCC in Al 7075-T6, the NO_2 being the more aggressive of the two.
5. It appears that the slow-strain-rate test with some modifications could be used to optimize a selected combination of environments.

References

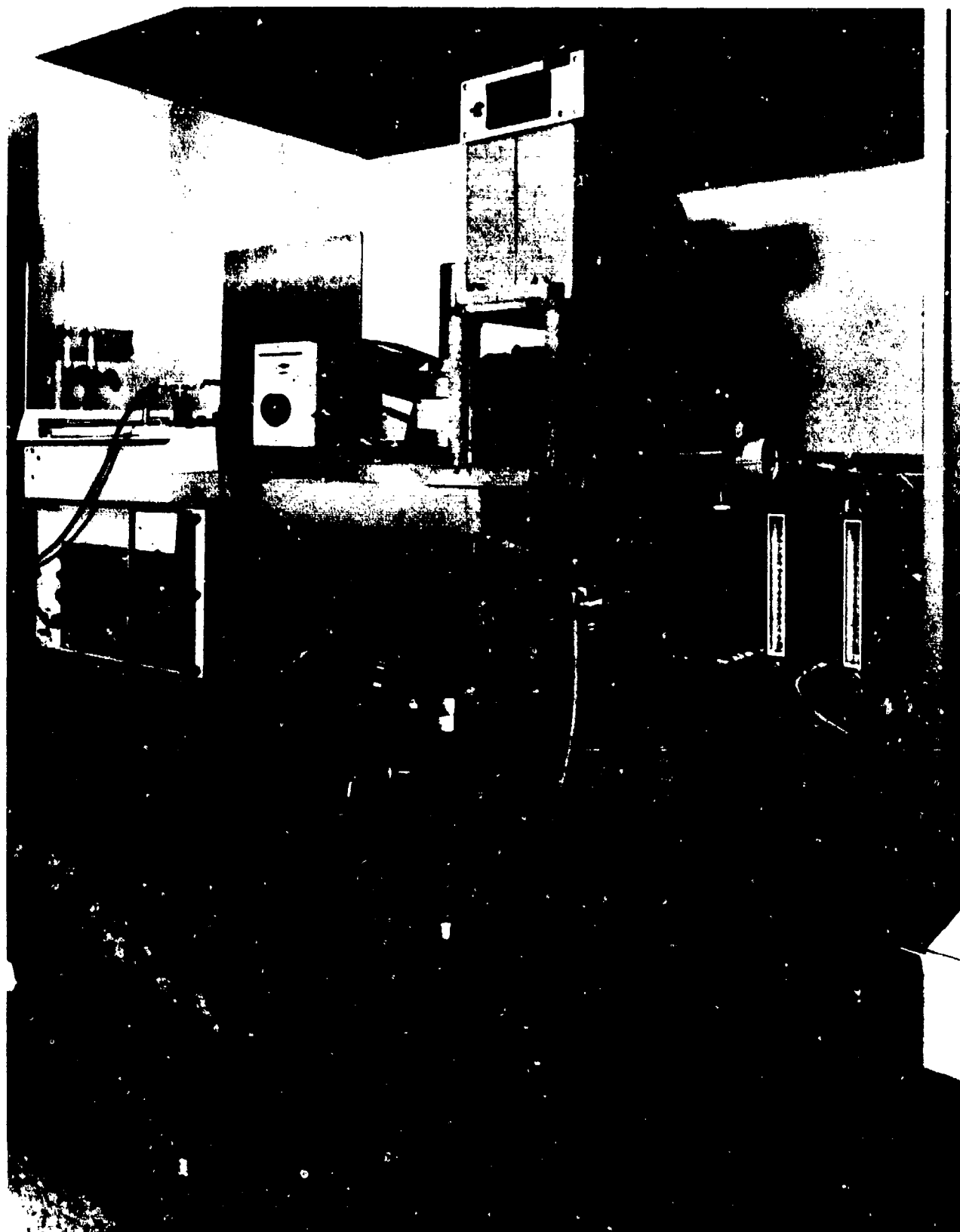
1. F. A. Champion, in Corrosion Testing Procedures (Chapman and Hall, London, 1952), p. 137.
2. H. L. Logan, in The Stress Corrosion of Metals (Wiley, New York, 1966), p. 273.
3. Stress Corrosion Testing, ASTM STP 425 (American Society for Testing and Materials, Philadelphia, PA, 1967), p. 3.
4. R. N. Parkins, in The Theory of Stress Corrosion Cracking in Alloys (J. C. Scully, Ed.) (North Atlantic Treaty Organization, Brussels, 1971), p. 449.
5. D. O. Sprowls, T. J. Summerson, G. M. Ugianski, S. G. Epstein, and H. L. Craig, Jr., in Stress Corrosion - New Approaches, ASTM STP 610 (American Society for Testing and Materials, Philadelphia, PA, 1976), p. 3.

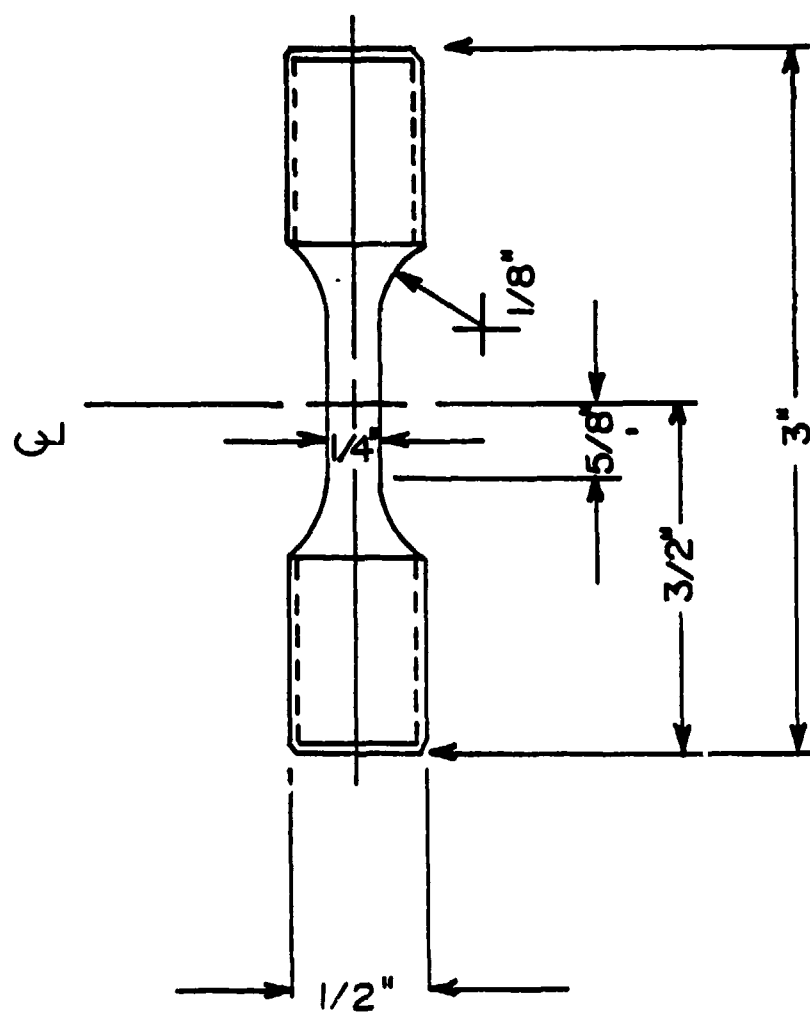
TABLE 1
SLOW-STRAIN-RATE TEST RESULTS

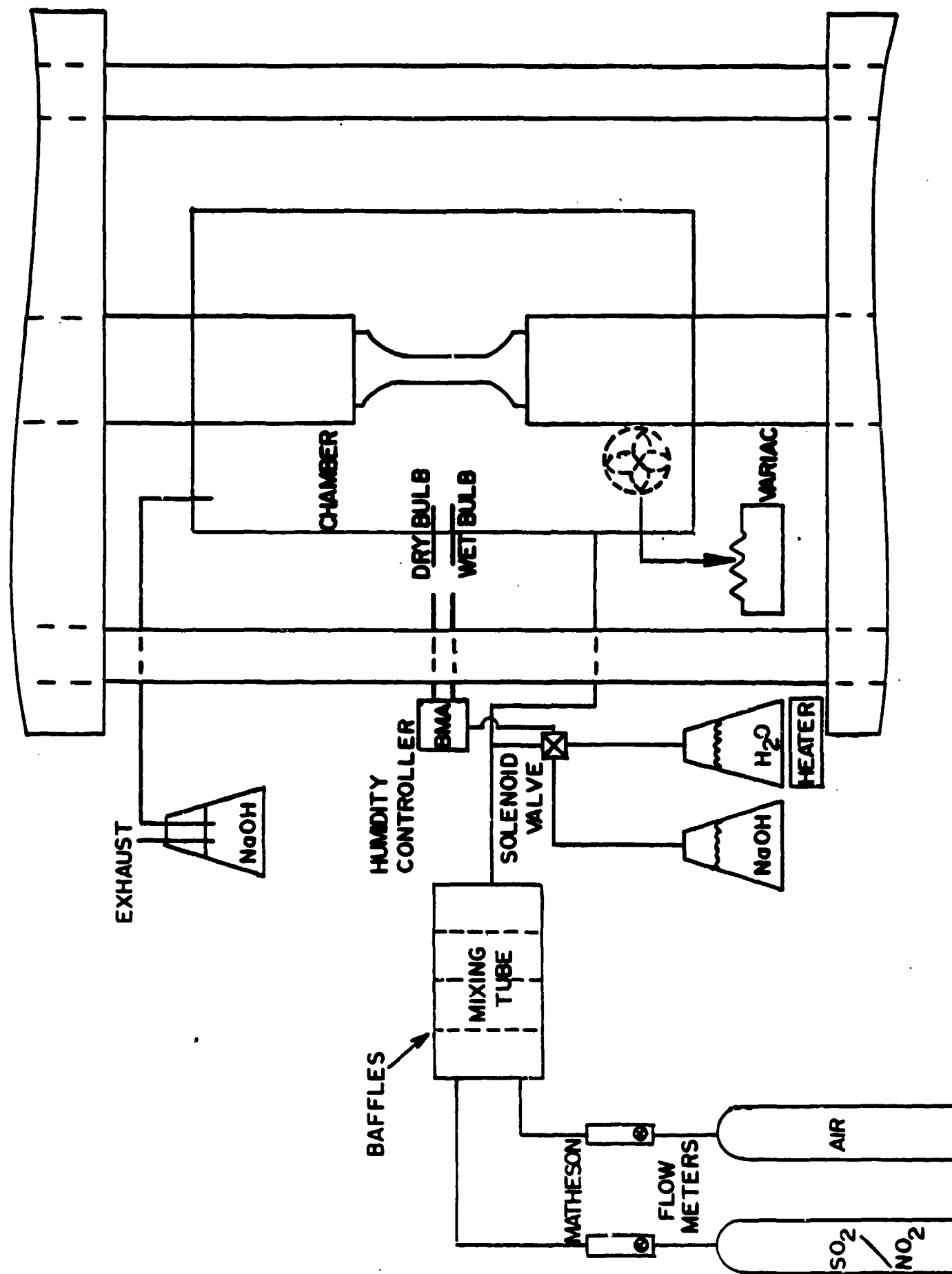
SPECIMEN	TEST DIRECTION	STRAIN RATE 1/s	TEST ENVIRONMENT	% ELONGATION
A1 7075-T6	Short Transverse	5.0×10^{-5}	Ambient Air	4.8
"	"	3.8×10^{-7}	"	4.7
"	"	4.5×10^{-7}	"	4.3
"	"	2.7×10^{-7}	"	5.1
"	"	8.8×10^{-8}	"	5.2
"	"	7.3×10^{-5}	5% Surface Salt	5.5
"	"	4.6×10^{-5}	"	4.3
"	"	4.5×10^{-5}	"	4.5
"	"	2.6×10^{-5}	"	4.1
"	"	3.1×10^{-7}	"	3.6
"	"	8.9×10^{-8}	"	4.6
"	"	4.45×10^{-5}	1000 ppm SO ₂ + 80% RH	5.4
"	"	4.30×10^{-5}	"	5.1
"	"	2.5×10^{-5}	"	5.4
"	"	2.27×10^{-7}	"	1.6
"	"	8.8×10^{-7}	"	4.7
"	"	6.25×10^{-7}	1000 ppm SO ₂ + 90% RH	2.4
"	"	2.7×10^{-7}	"	2.2
"	"	5.5×10^{-8}	"	2.1
"	"	3.1×10^{-6}	1000 ppm SO ₂ + 80% RH + 5% Surface Salt	1.9
"	"	2.8×10^{-6}	"	1.7
"	"	2.5×10^{-7}	"	0.86
"	"	1.8×10^{-7}	"	0.72
"	"	5.1×10^{-6}	"	1.82
"	"	4.7×10^{-6}	"	2.02
"	"	7.7×10^{-7}	100 ppm SO ₂ + 95% RH	5.3
"	"	3.8×10^{-7}	"	4.1
"	"	1.07×10^{-7}	"	5.6
"	"	8.9×10^{-7}	100 ppm SO ₂ + 90% RH	5.1
"	"	8.85×10^{-7}	"	4.9
"	"	3.7×10^{-7}	"	3.9
"	"	9.8×10^{-8}	"	3.1

TABLE 1 (Continued)

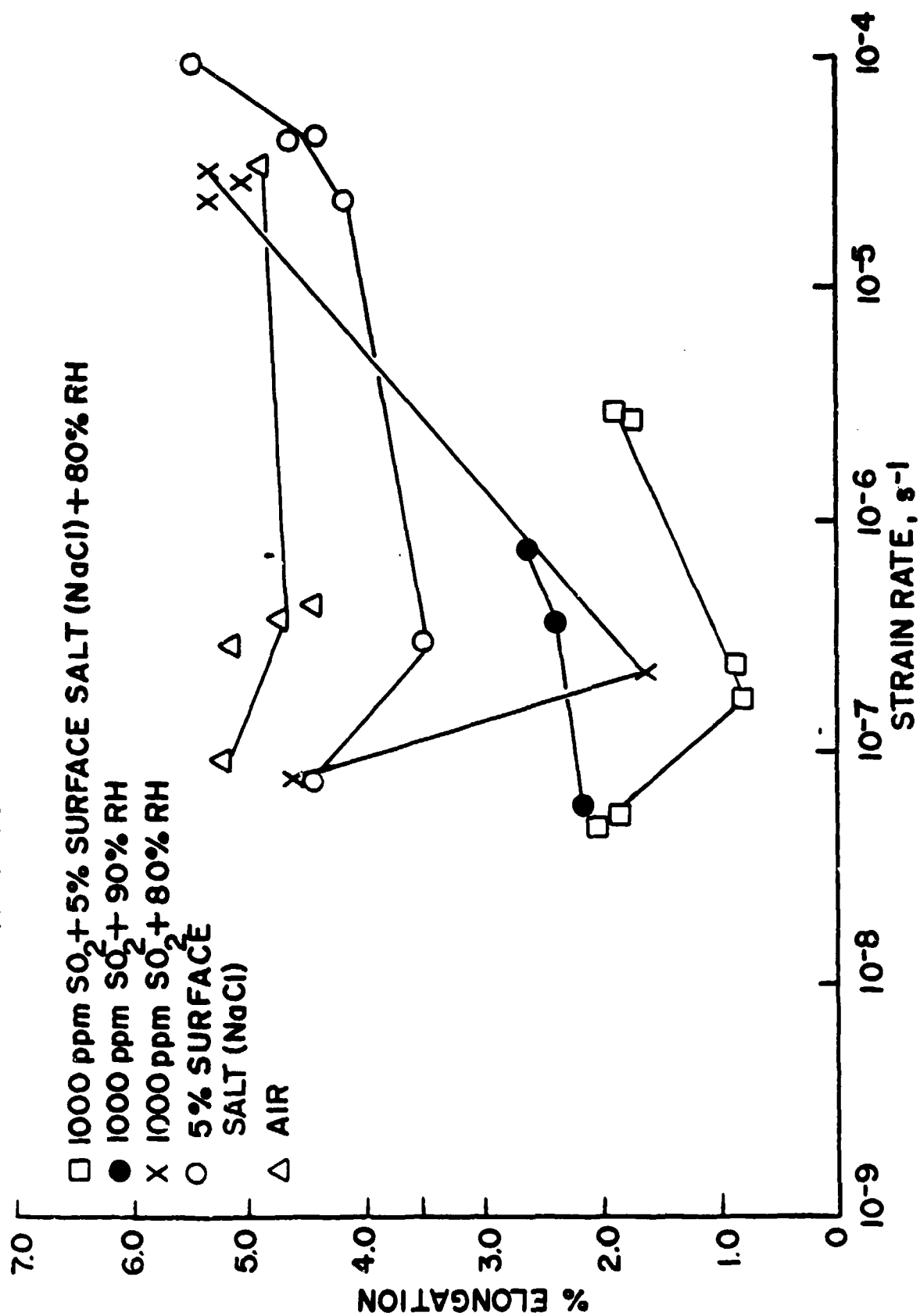
SPECIMEN	TEST DIRECTION	STRAIN RATE 1/s	TEST ENVIRONMENT	% ELONGATION
A1 7075-T6	Short Transverse	5.4×10^{-7}	100 ppm SO ₂ +90% RH + 5% Surface Salt	1.55
"	"	1.8×10^{-7}	"	0.8
"	"	5.9×10^{-8}	"	1.05
"	"	8.8×10^{-7}	100 ppm SO ₂ +80% RH	6.15
"	"	3.6×10^{-7}	"	6.1
"	"	5.1×10^{-7}	"	5.8
"	"	1.19×10^{-7}	"	6.1
"	"	7.5×10^{-7}	10 ppm SO ₂ +90% RH	6.0
"	"	4.2×10^{-7}	"	2.5
"	"	9.1×10^{-6}	"	0.7
"	"	4.8×10^{-5}	10 ppm SO ₂ +90% RH + 5% Surface Salt	6.0
"	"	6.8×10^{-7}	"	3.1
"	"	4.0×10^{-7}	"	1.55
"	"	3.5×10^{-7}	"	1.4
"	"	3.7×10^{-8}	"	0.6
"	"	6.2×10^{-7}	100 ppm NO ₂ +80% RH	5.2
"	"	3.3×10^{-7}	"	4.4
"	"	8.5×10^{-8}	"	4.45
"	"	6.0×10^{-7}	100 ppm NO ₂ +95% RH	4.5
"	"	5.2×10^{-7}	"	5.9
"	"	1.2×10^{-7}	"	1.05
"	"	5.9×10^{-7}	100 ppm NO ₂ +90% RH + 5% Surface Salt	1.33
"	"	2.8×10^{-7}	"	1.09
"	"	6.6×10^{-8}	"	1.30

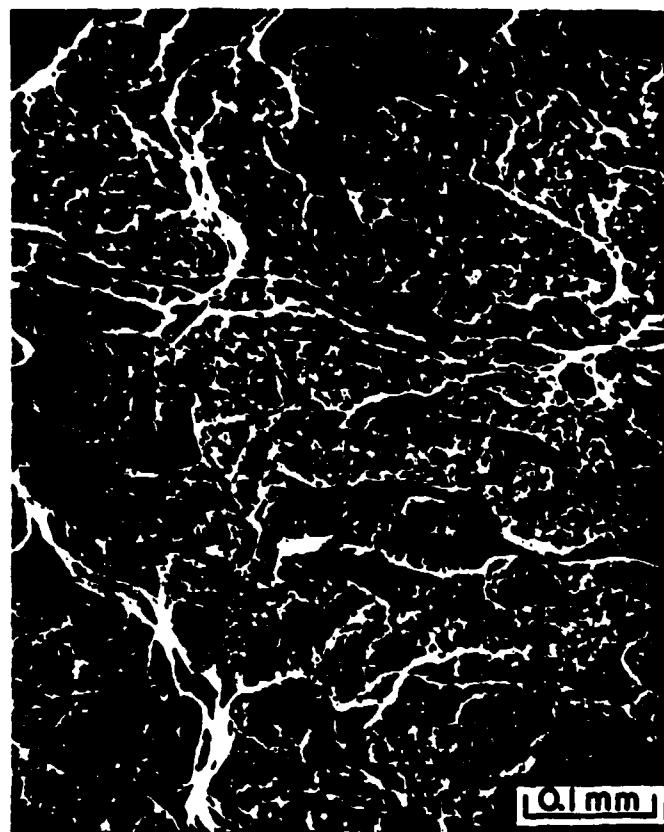




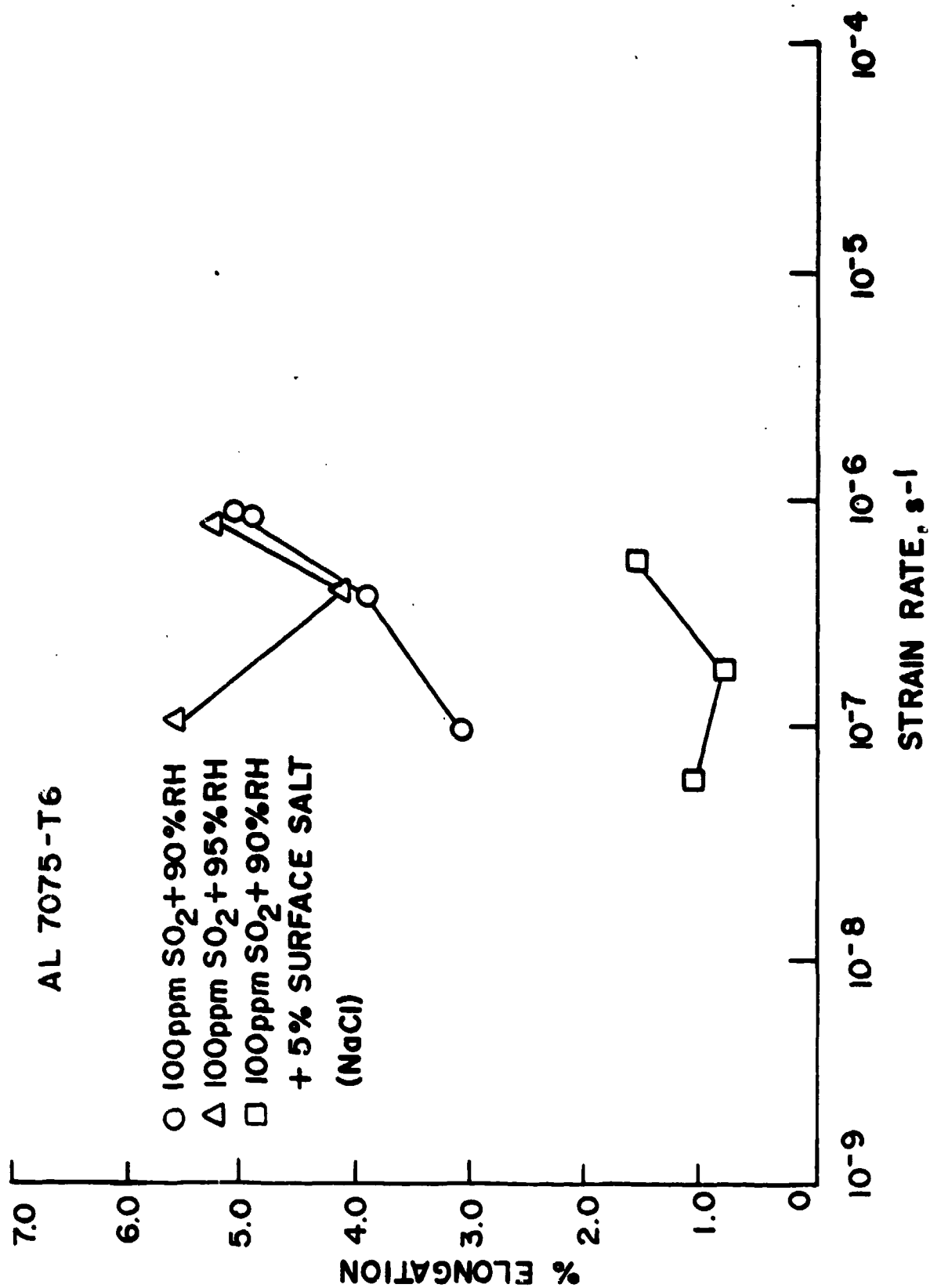


AL 7075-T6

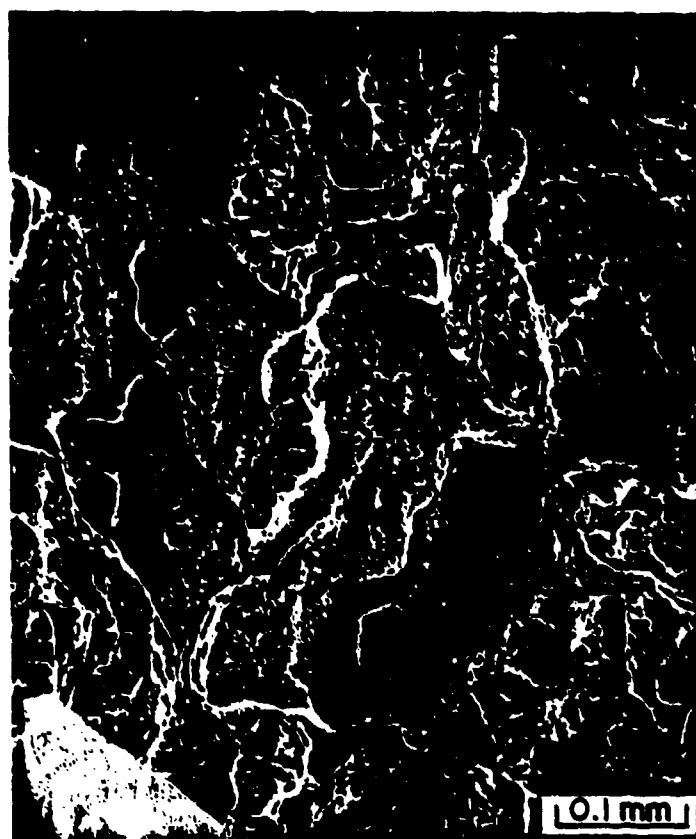




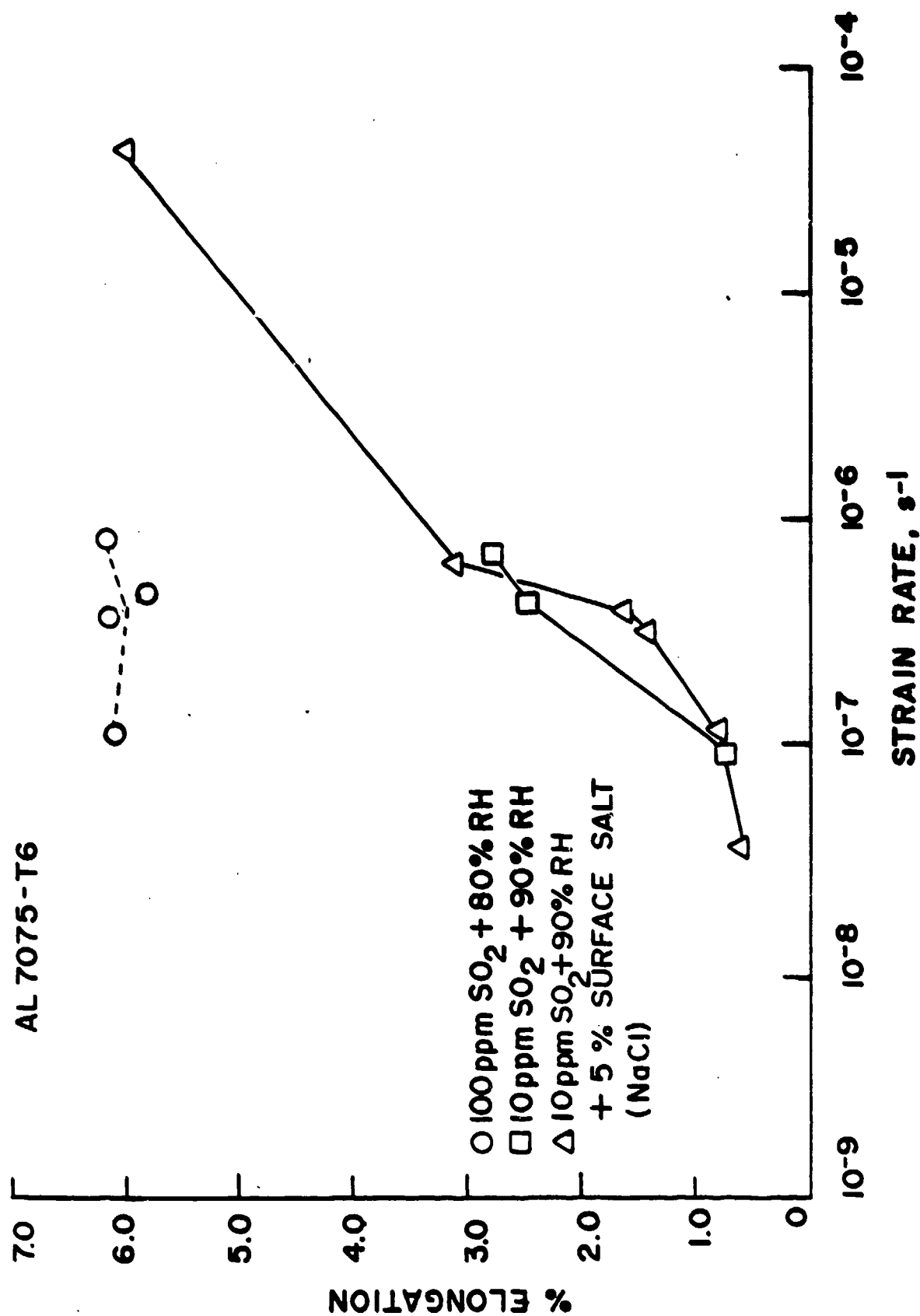




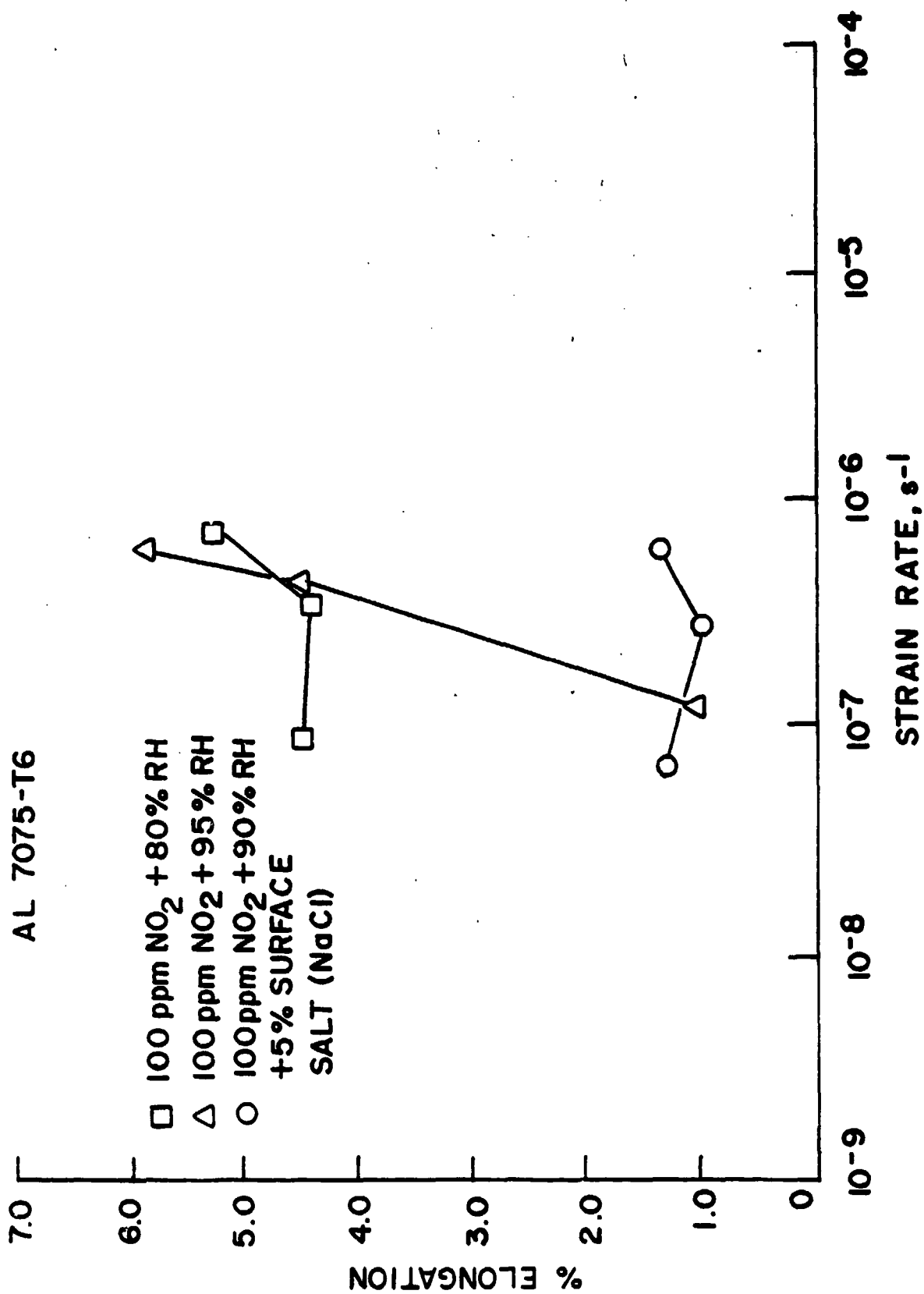












LIST OF FIGURE CAPTIONS

Figure

- 1 Slow-Strain-Rate Testing Machine.
- 2 Slow-Strain-Rate Specimen.
- 3 Gas Train and Environmental Chamber.
- 4 Slow-Strain-Rate Results for Al 7075-T6 in Air, 5% Surface Salt, 1000 ppm SO₂ + 80% RH, 1000 ppm SO₂ + 90% RH, and 1000 ppm SO₂ + 80% RH + 5% Surface Salt.
- 5 Fracture Surface of Al 7075-T6 Tested at $2.27 \times 10^{-7} \text{ s}^{-1}$ in 1000 ppm SO₂ + 80% RH.
- 6 Fracture Surface of Al 7075-T6 Tested in 1000 ppm SO₂ + 80% RH + 5% Surface Salt.
- 7 Slow-Strain-Rate Results for Al 7075-T6 in 100 ppm SO₂ + 90% RH, 100 ppm SO₂ + 95% RH, and 100 ppm SO₂ + 90% RH + 5% Surface salt.
- 8(a) Fracture Surface of Al 7075-T6 Tested at $8.9 \times 10^{-7} \text{ s}^{-1}$ in 100 ppm SO₂ + 90% RH.
- 8(b) Fracture Surface of Al 7075-T6 Tested at $6.8 \times 10^{-7} \text{ s}^{-1}$ in 100 ppm SO₂ + 90% RH.
- 8(c) Fracture Surface of Al 7075-T6 Tested at $2.3 \times 10^{-7} \text{ s}^{-1}$ in 100 ppm SO₂ + 90% RH.
- 9 Slow-Strain-Rate Results for Al 7075-T6 in 100 ppm SO₂ + 80% RH, 10 ppm SO₂ + 90% RH, and 10 ppm SO₂ + 90% RH + 5% Surface Salt.
- 10 Slow-Strain-Rate Results for Al 7075-T6 in 100 ppm NO₂ + 80% RH, 100 ppm NO₂ + 95% RH, and 100 ppm NO₂ + 90% RH + 5% Surface Salt.
- 11 Fracture Surface of Al 7075-T6 Tested at $2.8 \times 10^{-7} \text{ s}^{-1}$ in 100 ppm NO₂ + 90% RH + 5% Surface Salt.

APPENDIX B

ACCELERATED ATMOSPHERIC-CORROSION TESTING

maintenance in the field and at the depot level has been estimated to be \$750 million, and the total corrosion cost including facilities is estimated to be in excess of one billion dollars. During the 1975 and 1977 Air Force Office of Scientific Research-Air Force Materials Laboratory (AFOSR-AFML) Corrosion Workshops, improved accelerated tests were cited as being a major area of need requiring further research [2,3]. One of the major problems in effectively reducing aircraft-corrosion maintenance costs has been the inability of the research community to develop realistic corrosion tests which give meaningful results in a reasonable length of time. There are no accurate methods for accelerated testing for corrosion which yield reliable results for predicting the service life of aircraft components and materials which degrade or fail due to environmental attack. Current alternatives involve the use of gross tests such as saltwater immersion which yield relative corrosivity values that have no quantitative relation to service life or outdoor atmospheric exposure tests which require experiments of three to five years or longer and are specific to one local environment.

A program has been initiated to provide the basis for the development of realistic accelerated tests which can be used to predict the long-range corrosion behavior of materials under actual service conditions. Test environments are based upon reasonable variations in the concentration of accelerating pollutants, humidity, and temperature, using primary and secondary air-quality standards to establish concentration base levels for accelerating pollutants such as sulfur dioxide. Controlled atmospheric experiments are being conducted for general corrosion and for localized environmental enhancement of crack-growth rates. Crack-growth studies include low-cycle corrosion-fatigue, rising-load, and constant-slow-strain-rate tests. Initial results are reported in this paper for 4340 steel and 7075-T651 aluminum alloys under rising-load and low-cycle fatigue. Results of several corrosion studies in a controlled atmosphere will be compared later to results for general corrosion of test panels at outdoor sites located in corrosive and relatively benign atmospheres.

The state of the art in accelerated-corrosion testing methods as described in the ASTM Book of Standards and approved by the National Association of Corrosion Engineers (NACE) involves the aforementioned use of gross tests such as salt fog and alternate salt-immersion tests with their lack of quantitative values for corrosivity or relative corrosivity with respect to service experience. Atmospheric outdoor tests where panels are exposed to various environments require a time scale which precludes rapid materials-selection decisions or paint-protection-measures evaluations. These tests are specific to limited environments and seldom take into account stress factors which may accelerate the localized corrosion and enhance crack growth, leading to premature failure. Cyclic loading is, of course, also precluded. Establishing realistic test environments requires, at a minimum, a reasonable selection of atmospheric environmental variables coupled with stress factors

M. Khobab,¹ F. C. Chang,¹ E. E. Keppler,¹ and C. T. Lynch²

Accelerated Atmospheric-Corrosion Testing

REFERENCE: Khobab, M., Chang, F. C., Keppler, E. E., and Lynch, C. T., "Accelerated Atmospheric-Corrosion Testing," *Atmospheric Corrosion of Metals*, ASTM STP 707, S. W. Dean, Jr., and L. C. Rhee, Eds., American Society for Testing and Materials, 1982, pp. 374-394.

ABSTRACT: No accurate methods are known for accelerated testing of corrosion which yield reliable results for predicting the service life of aircraft components and materials which degrade or fail due to environmental attack. In an effort to provide the basis for development of realistic accelerated corrosion tests, research is being conducted in controlled atmospheres on the localized environmental enhancement of crack-growth rates of aerospace alloys. Corrosion-fatigue and rising-load experiments have been conducted using accelerating pollutants such as sulfur dioxide (SO_2) and ambient air to 100 percent relative humidity air in a specially designed atmospheric chamber. Initial results indicate that realistic environmental enhancement of crack-growth rates can be employed to develop accelerated tests which can be related to actual in-service degradation. For materials with high stress-corrosion susceptibility, the threshold for crack growth (K_{ISCC}) was estimated to be 45 to 46 MPa \sqrt{m} for 4340 steel at a 1440-MPa yield strength level, as compared to 49 to 52 MPa \sqrt{m} as determined by means of rising-load test and 44 to 46 MPa \sqrt{m} by fracture analysis in 1000-ppm SO_2 at 40 percent relative humidity. Thus, a rapid and reproducible method for K_{ISCC} determination appears feasible.

KEY WORDS: accelerated corrosion testing, realistic environments, crack growth, localized environmental enhancement, rising-load testing, low-cycle corrosion fatigue

Over the past four years a considerable number of studies have been conducted within the Air Force and at the National Bureau of Standards (NBS) regarding the total cost of corrosion prevention and control for aircraft. The measurable conclusion is that total corrosion costs in terms of life-cycle management and maintenance of aircraft represent an intolerable burden to the Air Force in maintaining force effectiveness at a reasonable cost to the taxpayer. In a 1978 NBS report [1] the total corrosion cost was calculated to be \$70 billion nationally. For the Air Force the direct cost of corrosion

¹Systems Research Laboratories, Inc., 2600 Indian Ripple Road, Dayton, Ohio 45440. Co-author Chang is now with the Army Materials and Mechanics Research Center, Watertown, Mass.

²An Office Wright Aeronautical Laboratories, Wright-Patterson Air Force Base, Ohio 45433.

The italic numbers in brackets refer to the list of references appended to this paper.

TABLE 1—Apparent K_{ISCC} values obtained by ring load tests.

Specimen No.	Environment	Loading Rate, N/min	Apparent K_{ISCC} , MPa \sqrt{m}	Yield Strength, MPa
2B	1000-ppm SO ₂ + 80% RH	22	55	1440
3B	1000-ppm SO ₂ + 80% RH	88	49	1440
10A	1000-ppm SO ₂ + 80% RH	22	72	1240
23A	1000-ppm SO ₂ + 100% RH	22	70	1240
29A	80% RH	22	78	1240
15A	50% RH	22	78	1240

* These values are approximate

[ASTM Test for Plane-Strain Fracture Toughness of Metallic Materials (E 399-72)], except that a slower rate of loading was employed and the specimen was exposed to the environment while being loaded. These tests were conducted with standard 19.05-mm-thick compact-tension specimens. The specimens were precracked to crack lengths of 2.54 mm at stress intensities below 15 MPa \sqrt{m} ($R = 0.1$ and $f = 0.1$ Hz). A special environmental chamber (to be described in detail later) was used to maintain and control the constituents of the specific environments required for the tests. The specimens were loaded in air, in 80 percent relative humidity, in 1000-ppm SO₂, at RH = 80 percent, and in 1000-ppm SO₂ at RH = 100 percent, at fixed loading rates corresponding to 22 and 88 N/min. K_{ISCC} values were estimated from the load-displacement record, using the 5 percent secant offset procedure similar to that used for the K_{Ic} testing. The results are given in Table 1.

The Environmental Chamber

The environmental chamber and the gas-train assembly are shown in Fig. 2. The chamber is made of 316 stainless steel while the grips, pull rods, and pins are made of 17-4 PH steel, which exhibits good resistance to wet SO₂ and wet NO₂ environments. It is a leak-proof system with bellows and other attachments to attain high vacuum. The temperature inside can be controlled from 0 to 538°C. The unit is installed in a closed-loop Materials Testing System (MTS) machine for conducting mechanical tests in realistic environments.

The test atmospheres were supplied through the gas train, which consists of a gas mixing and delivery system. High-purity bottled gases (SO₂ and dry air in this case) were metered by Matheson Flowmeters 601 and 603 and then moved in the mixing tube. The concentration of SO₂ in the chamber is routinely measured by calibrated Gaslec analyzer tubes. Special gas-sampling outlets are provided in the chamber. The relative humidity inside the chamber is controlled by means of a BMA dry and wet bulb hygrometer. The water vapor is added in the form of steam by boiling distilled water in a flask main-

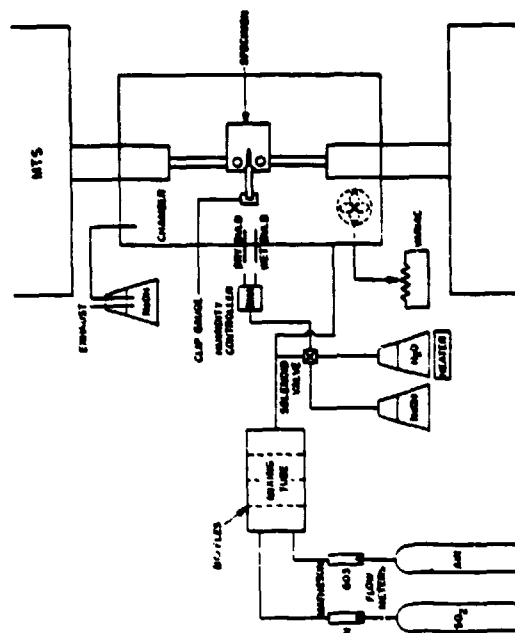


FIG. 2—Gas train and environmental chamber.

tained at a constant temperature. The steam flow is controlled by the output voltage of the BMA controller, which monitors the opening and closing of the solenoid valve on the steam line. The steam is injected into the gas mixture prior to its entry into the chamber in order to obtain the required mixture of SO₂ and relative humidity air.

Gas pressures used in all the tests have been slightly above atmospheric to provide positive flow through the environmental chamber. The gas inlet and outlet are positioned specifically to minimize the channeling effect. The gas is circulated inside the chamber by means of a circulating fan (placed inside the chamber) to maintain a uniform environment throughout the chamber. Negligible condensation occurred during these tests except in the case of RH = 100 percent. The fatigue-crack-propagation data discussed in the next section were obtained using compact-tension plane-strain fracture-toughness specimens (Fig. 1). Tests were conducted in the controlled atmosphere inside the environmental chamber as described. The inert dry nitrogen was used as a control, while the RH = 80 percent air, 1000-ppm SO₂, and RH = 80 percent, and 1000-ppm SO₂ and RH = 100 percent were used as representative aggressive environments for stress corrosion and environmentally accelerated corrosion fatigue.

Corrosion-Fatigue Crack Growth

All tests were conducted at room temperature using a 100-kN Materials Testing System (MTS) machine. The crack length was monitored through crack-opening-displacement (COD) measurements during fatigue testing. To determine the crack length from COD data, compliance measurements were carried out for both high-strength steels and aluminum alloys. Tests were conducted in air, and crack lengths were determined using optical and COD measurements simultaneously on the MTS machine. The COD was measured by a double-cantilever displacement gage prepared in accordance with the ASTM Method E 399-72. The displacement gage was calibrated to measure COD from 0 to 1.25 mm \pm 0.0125 mm using a System Research Laboratories (SRL) developed strain-gage amplifier. The COD was recorded as a function of cycles.

A sinusoidal tension-tension waveform was employed for all fatigue-crack-growth-rate tests. Most of the tests were conducted at an R-ratio (K_{min}/K_{max}) of 0.6 and a frequency of 0.1 Hz. The slow frequency and high R-ratio were utilized to facilitate the observation of environmental effects. Limited tests were conducted at frequencies of 0.25 and 0.5 Hz also. All specimens were initially precracked according to ASTM E 399-72 on the same MTS machine on which the corrosion-fatigue tests were conducted.

No significant differences were found in the COD/load and crack length/load curves. The crack length, a , was calculated from the analytical compliance relationship [5]

$$a/W = 1.001 - 4.6695 U + 18.460 U^2$$

$$- 236.82 U^3 + 1214.94 U^4 - 2143.6 U^5$$

where

$$U = \frac{1}{\sqrt{\frac{EB(COD_{max} - COD_{min})}{P_{max} - P_{min}} + 1}}$$

where E is the Young's modulus and P the stress. W and B are the dimensions indicated in Fig. 1. The stress-intensity values were calculated from [5]

$$K = \frac{P}{BW^{3/2}} \times \frac{(2 + a/W)0.886 + 4.64(a/W) - 13.32(a/w)^2 + 14.72(a/w)^3 - 5.6(a/w)^4}{(1 - a/w)^{3/2}}$$

where B and W are the dimensions indicated in Fig. 1 such that B and $a > 2.5(K_{IC}/YS)^2$, with K_{IC} being the fracture toughness and YS the tensile yield strength. The crack-length-versus-number-of-cycles data were converted to fatigue-crack-growth rates (da/dN) using a computer program [5].

Seven to eleven data points were fitted to a second-order polynomial, and the derivative (da/dN) was then obtained for the middle data point. This process was then repeated over the range of data.

All fractured surfaces were examined visually and then by light microscopy. The specimens were then ultrasonically cleaned in acetone, deionized water, and methyl alcohol. The light-microscopic observation was followed by scanning electron microscopy (SEM) for detailed examination of the fractured surfaces.

Results and Discussion

Crack Propagation

The fatigue-crack-propagation behavior of many ferrous and nonferrous alloys can be schematically represented as in Fig. 3 [6]. The rate of crack growth depends strongly upon K at K -levels approaching K_{IC} or K_{IS} at the high end and at levels approaching an apparent threshold at the low end, with an intermediate region that depends upon some power of K or ΔK . The upper end corresponds to the onset of unstable fracture, while the lower end corresponds to the fatigue "threshold" ΔK_{th} [7,8] which appears to be related to the metallurgical structure [9].

The environment-enhanced fatigue-crack-growth response of high-strength metals may be broadly characterized in terms of three general patterns of behavior [10], as illustrated schematically in Fig. 4. The first type of behavior represents those material-environment systems where fatigue-crack-growth rates are enhanced by the presence of an aggressive environment through

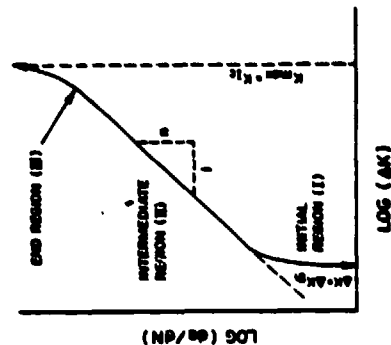


FIG. 3—Schematic diagram of fatigue-crack-growth rate behavior.

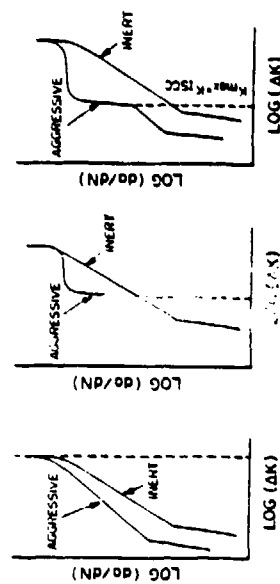


FIG. 4—Types of fatigue-crack growth behavior: (a) True corrosion; (b) stress corrosion fatigue (SCF); (c) SCF on TCF.

synergistic action of corrosion and cyclic loading. This is "below K_{Isc} " behavior [17-18] and applies to materials which are not susceptible to stress corrosion where $K_{Isc} > K_{Ic}$. This behavior is classified as true corrosion fatigue. The second type of behavior is representative of those systems where there is a substantial environment-enhanced sustained-load crack-growth component [14,15], which occurs whenever the stress intensity in the cycle is above K_{Isc} . This behavior is classified as stress-corrosion fatigue. The most common type of behavior pertains to material/environment systems which exhibit stress-corrosion fatigue above K_{Isc} and also true corrosion fatigue at all stress-intensity levels. Such behavior lies between the two extremes and is shown in Fig. 4c.

Crack-Growth Behavior of Al 7075-T651

The accelerated atmospheric effects resulting from the variation of the relative humidity upon observed crack-growth rates were investigated. The low-cycle corrosion-fatigue data are expressed in terms of crack-growth rate da/dN as a function of the stress-intensity-factor range ΔK . The dependence of crack-growth rate upon the humidity level in air for Al 7075-T651 is shown in Fig. 5. At high levels of humidity such as RH = 80 percent, the crack-growth rates were substantially increased as compared to those in dry air (\approx RH = 5 percent). The immersion results for crack growth in aqueous solutions are shown for the sake of comparison. While increasing relative humidity also increases the crack-growth rates, the change in crack-growth rate from gaseous environment to total-immersion aqueous environment is much more significant. This rate is also less realistic for estimating corrosion reactions except where standing water is present. Similar results on several aluminum alloys have been obtained by other workers [16-21]. The com-

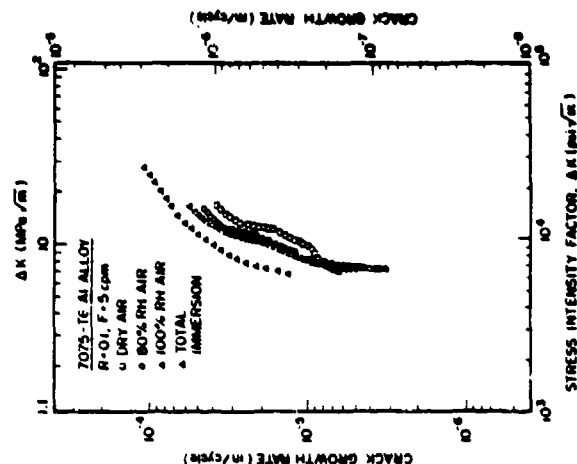


FIG. 5—Crack-growth-rate data obtained for Al 7075-T651, tested at various relative humidity levels.

monly accepted explanation of crack-growth accelerations due to a high level of humidity is the pressure mechanism of hydrogen embrittlement suggested by Broom and Nicholson [19] which requires a water-metal surface reaction and proposes that the increase in the rate of fatigue-crack growth results from the synergistic action of a mechanical process—fatigue, which creates a sufficient amount of fresh surface—and the chemical reaction of water vapor with the resulting fresh surface.

Crack-Growth Behavior of 4340 Steel

Figure 6 represents the crack-growth-rate data on 4340 steel with a yield strength of 1345 MPa obtained at three levels of humidity. In all these tests a frequency of 0.1 Hz and a load ratio R of 0.1 were used. While the shapes of the three curves are similar, noticeable differences exist in the crack-growth rates at high K -levels. Note that although the differences in crack-growth rates (at different humidity levels) are small, very definite differences are present. The differences found are reproducible within an experimental error

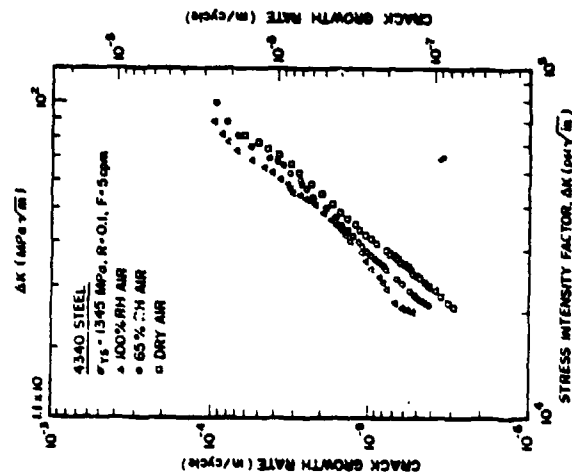


FIG. 11. a—Crack growth rate data obtained for 4340 steel (1545 MPa), tested at various relative humidity levels.

of da/dN less than the $\Delta K/dN$ values. Similar differences in crack-growth rates were observed for 7075-T651 aluminum. These differences became more pronounced when one considers data on cycles to failure. These data are shown in Table 2 for both Al 7075-T651 and 4340 steel. Similar increases in crack-growth rates of high-strength 4340 steel due to water vapor were observed under both sustained and cyclic loading by Lynch and other workers [24–30]. Dahlberg [31] has demonstrated more distinct differences in the crack-growth rates of 4340 steel tested at different humidity levels when an R-ratio of 0.8 was used. However, the differences in crack-growth rates with increasing humidity levels were similar to those obtained in the present investigation where smaller R ratios were used.

Although several mechanisms have been suggested for hydrogen embrittlement [32–35] (such as the decohesion model [34] and the pressure model [35]), no single theory gives a complete description of the problem. For high-strength steels, however, in "hydrogen-producing" atmospheres [for example, hydrogen (H_2), water (H_2O), hydrogen sulfide (H_2S)], decohesion theories are widely accepted [15,35–38] (for monotonic and cyclic loading). Also, the general consensus is that the presence of water vapor in the atmosphere enhances crack-growth rates for both high-strength aluminum and steel alloys.

Crack Propagation of 4340 Steel in Humid SO_2

High-strength 4340 steel at yield strengths of 1240 and 1440 MPa were tested at a load ratio of 0.6 and a frequency of 0.1 Hz. The atmospheres were ambient air, dry nitrogen, air with RH = 80 percent, and 1000-ppm SO_2 in air with RH = 80 percent air. The crack-growth results for 1240-MPa steel are shown in Fig. 7, while Fig. 8 shows the da/dN -versus- ΔK plot for 1440-MPa steel. A comparison of these two figures shows that there is a greater enhancement in the crack-growth rates for 1440-MPa steel compared with 1240-MPa steel due to the SO_2 environment. These data indicate a "bump" (abrupt change in the slope in the intermediate region) of the da/dN -versus- ΔK plot obtained for 1440-MPa steel tested in the 1000-ppm SO_2 and RH = 80 percent environment. A similar "bump" is obtained for 1240-MPa in this same environment. The ambient air and RH = 80 percent plots, however, follow the normal trend [6]. This difference in the nature of the plot (or appearance of the "bump") is expected when the K-level exceeds the K_{th} -value for the metal-environment system. In general, this follows the trend of Fig. 4c, which is most significant because the extrapolation from this slope change to the abscissa of the plot produces the K_{th} -value as shown in Fig. 4c. Accordingly, the K_{th} values have been obtained from Figs. 7 and 8 and are 55 and 46 MPa \sqrt{m} for 1240- and 1440-MPa steels, respectively. The accuracy of this estimate has been further verified by the rising-load method and fractographic observations. The K_{th} -value obtained for 1440-MPa steel by such extrapolation is in very close agreement with the K_{th} -values obtained

TABLE 2—Specimen life in cycles.

4340 Steel			1335 MPa		
Specimen No.	RH	N_f (cycles)	Specimen No.	RH	N_f (cycles)
1	dry air 55%	60 174	1	dry air 55%	40 347
2	65%	40 993	2	80%	26 950
3	100%	33 064	3	100%	41 005

Al 7075-T651		
Specimen No.	RH	N_f (cycles)
1	dry air 55%	40 347
2	80%	26 950
3	100%	41 005

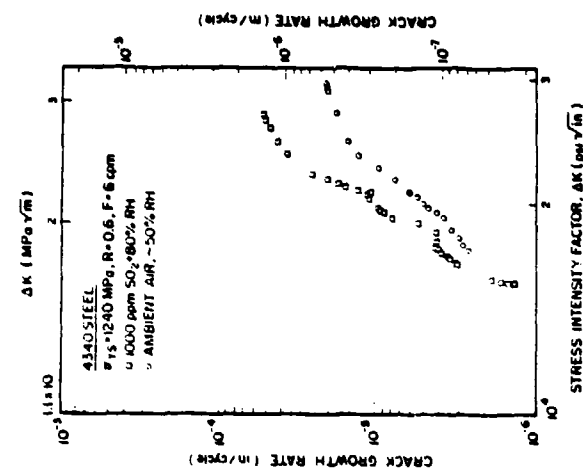


FIG. 7—Crack-growth-rate data obtained for 4340 steel (1240 MPa), tested in 1000-ppm SO_2 , at RH = 80 percent environment.

from the other observations. The high value of K_{Isc} obtained for 1240-MPa steel could not be supported by either rising-load or fractographic observations. Such high values of K_{Isc} obtained by extrapolation of da/dN -versus- ΔK curves have been reported previously [39]. However, the K_{Isc} value obtained by such extrapolation for 1440-MPa steel is quite consistent and accurate. The validity of this extrapolation is supported by the results of Austen and Walter [40] on high-strength 835M30 steel in a 3.5NaCl environment and the results we have obtained on 4340 steel in 3.5NaCl solution. However, the high value of K_{Isc} obtained for 1240-MPa steel requires further studies in several environments. A more detailed investigation of the nature of the da/dN -versus- ΔK plot is required when there is a very small difference in K_{Isc} and K_{Isc} values for the metal-environment system. In this case 1240-MPa steel is not so susceptible as 1440-MPa steel to hydrogen-assisted stress-corrosion cracking in the environment/conditions of the test, and the results apparently are intermediate between the first two cases of the schematic presentation of Fig. 4. In such a case, further detailed study of frequency/

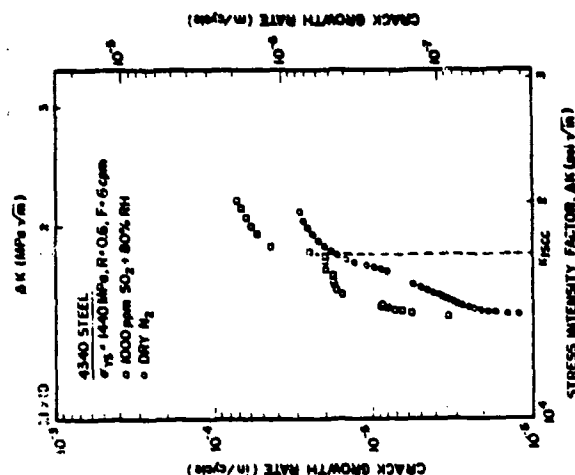


FIG. 8—Crack-growth-rate data obtained for 4340 steel (1440 MPa), tested in 1000-ppm SO_2 , at RH = 80 percent environment.

load/R-ratio effects may be necessary to improve the determination of K_{Isc} by extrapolation.

Rising-Load K_{Isc} Tests

The approximate values of K_{Isc} obtained for 1240- and 1440-MPa steels in various environments are given in Table I. Only two loading rates of 22 and 88 N/min were used. The values quoted in Table I must be taken as the higher-limit estimates because of the rapid A-rates utilized and the limited nature of the test procedure. More experiments at slower rates should improve the approximation of K_{Isc} -values.

Fractographic Analyses

Fractographic analyses of the fracture surfaces of the specimens were conducted to provide further information concerning the crack-tip mechanism in corrosion fatigue of 4340 steels at different K-levels in humid SO_2 envi-

ronments. Figure 9 shows fractographs taken from the surface of a 1240-MPa steel specimen tested in 1000-ppm SO_2 + RH = 80 percent. These fractographs indicate that at low values of K , 40.5 MPa $\sqrt{\text{m}}$, the surface features are very ductile (Fig. 9a). At higher values of K , there is little evidence of intergranular fracture. The fracture is mainly transgranular and ductile in nature. No substantial component of intergranular fracture could be found, even in the fracture zone corresponding to high values of K , ~57.5 MPa $\sqrt{\text{m}}$ (near the fast fracture) (Fig. 9b). Different fracture-surface characteristics were obtained for 1440-MPa steel corrosion fatigued in 1000-ppm SO_2 + RH = 80 percent. Figure 10a shows the ductile nature of failure at low K -values of 35 to 36 MPa $\sqrt{\text{m}}$, while Fig. 10b shows the mixed mode of failure, corresponding to a K value of ~40 MPa $\sqrt{\text{m}}$.

Figure 10c is a typical fractograph obtained in the fracture zone corresponding to a K -value of ~46 MPa $\sqrt{\text{m}}$. The entire fractured surface was scanned several times, and a definite intergranular failure mechanism was observed over the entire cross section when the K -value exceeded 45 to 46 MPa $\sqrt{\text{m}}$. The value of K_{int} was approximated by careful measurement of the crack length and found to be ~46 MPa $\sqrt{\text{m}}$, which is in agreement with the K_{int} -value obtained from the da/dN -versus- ΔK plot; this value falls within good approximation of the value obtained by the rising-load method.

Figure 11 shows the fractographs obtained from the fractured surface of 1240-MPa steel tested in dry N_2 . The fractured surfaces (Fig. 11a) are characteristic of ductile failure, containing dimple rupture. In Fig. 11b the dimples can be more clearly seen at higher magnification.

Conclusions

The presence of water vapor in the atmosphere accelerates the crack-growth rates of high-strength steel and aluminum alloys. Crack-growth rates increase with increasing relative humidity, with the effect being more pronounced in steel at a yield strength of 1440 MPa as compared to 1240 MPa.

There is a significant increase in crack-growth rates (and corresponding decrease in cycles to failure) for high-strength alloys in full immersion in aqueous solutions as compared to an air atmosphere of 100 percent relative humidity.

Corrosion-fatigue crack-growth rates increase from ambient air to air with RH = 80 percent to RH = 80 percent + 1000-ppm SO_2 . This is true for all alloys with the effects being more pronounced in the 1440-MPa steel than in the 1240-MPa steel.

The value of K_{int} can be extrapolated from the corrosion-fatigue curve, provided the conditions of load, frequency, and R-ratio are optimized. The results of rising-load corrosion-fatigue extrapolation and fractography experiments are in excellent agreement for the 1440-MPa steel. Thus, a rapid determination of K_{int} is provided for susceptible alloys.

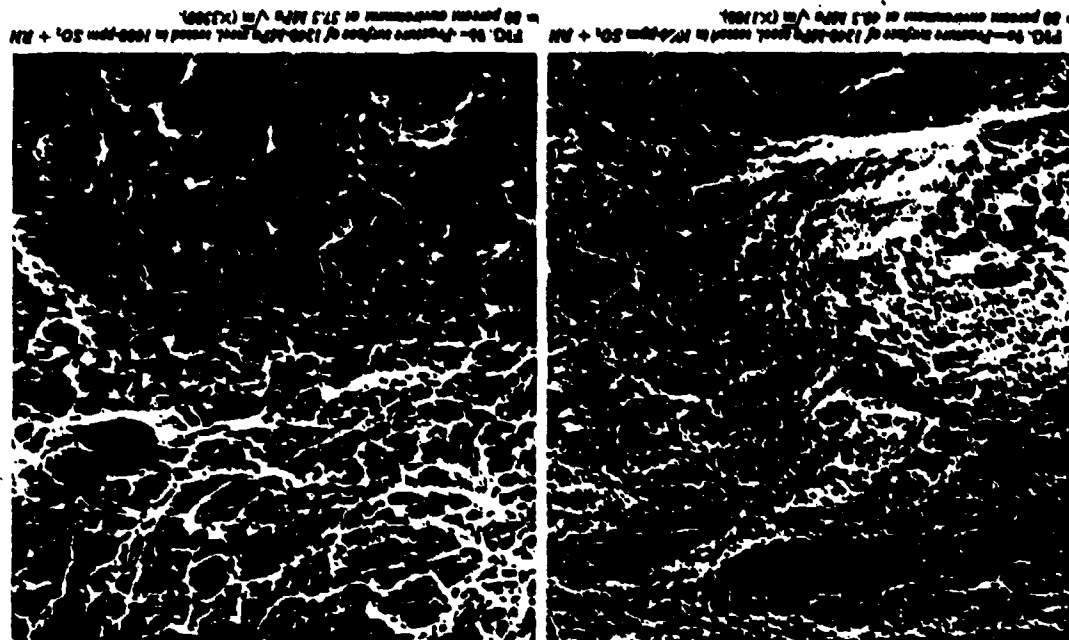


FIG. 9a—Fracture surface of 1240-MPa steel tested in 1000-ppm SO_2 + RH = 80 percent environment at 40.5 MPa $\sqrt{\text{m}}$ (X1500).
FIG. 9b—Fracture surface of 1240-MPa steel tested in 1000-ppm SO_2 + RH = 80 percent environment at 57.5 MPa $\sqrt{\text{m}}$ (X1500).



FIG. 10a—Ductile morphology obtained for 1440-MPa steel, resulting from test in 1000-ppm SO_2 + RH = 80 percent environment in the range 33 to 36 MPa \sqrt{m} ($\times 600$).



FIG. 10b—Mixed-mode fracture obtained for 1440-MPa steel, resulting from testing in 1000-ppm SO_2 + RH = 80 percent environment at 40 MPa \sqrt{m} ($\times 1100$).



FIG. 10c—Intergranular and brittle fracture obtained for 1440-MPa steel, resulting from test in 1000-ppm SO_2 + RH = 80 percent environment in the range 45 to 46 MPa \sqrt{m} ($\times 1100$).

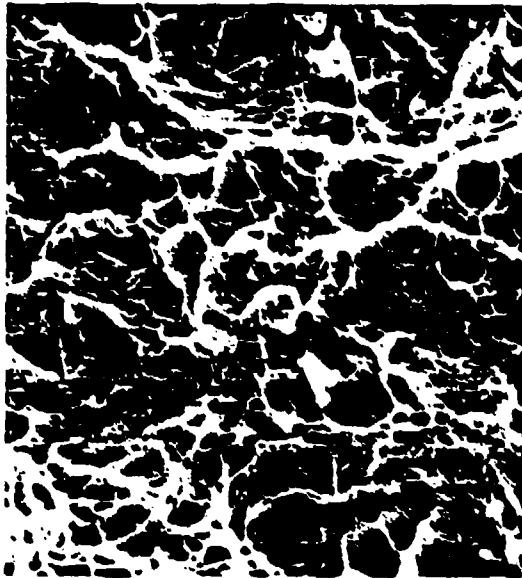


FIG. 11a—Surface morphology resulting from test conducted in dry nitrogen (X2500).



FIG. 11b—Surface morphology resulting from test conducted in dry nitrogen (X2500).

Acknowledgments

The authors express their thanks to F. M. Thomson for reducing the experimental data and to M. B. Stroppe for assisting in the fractographic analysis.

References

- [1] Bennett, L. H., Kruger, J., Parker, B. L., Pennington, E., Brinson, C., Buff, A. W., and Yabumizu, H., *Zinc-Aluminum Corrosion in the United States*, Parts I and II, NBS Special Publication 511-1,2, U.S. Department of Commerce, National Bureau of Standards, Washington, D.C., May 1976.
- [2] Proceedings, AFOSR/AFM Corrosion Workshop, AFM-78-173, M. Mach and J. G. Gilman, Eds., Air Force Materials Laboratory, Wright-Patterson Air Force Base, Ohio, 1978.
- [3] Proceedings, AFOSR/AFM Workshop on Corrosion of Alloys, E. O. Veldick, Jr., Ed., St. Augustine, Fla. 13-15 Sept. 1977, The University of Florida, Gainesville, 1977.
- [4] Clark, W. G., and Landon, J. D., in *Stress Corrosion—New Approaches*, ASTM STP 488, American Society for Testing and Materials, 1976, p. 105.
- [5] Ashbaugh, N. E., Technical Report AFM-78-4037, Air Force Materials Laboratory, Wright-Patterson Air Force Base, Ohio, Sept. 1979.
- [6] *Stress Corrosion Cracking in High Strength Steels and in Titanium and Aluminum Alloys*, B. F. Brown, Ed., U.S. Government Printing Office, Washington, D.C., 1972.
- [7] Pao, P. C., *MTS Crack Loop Magnifier*, Vol. 3, No. 3, 1978.
- [8] Ruck, R. J., Clark, W. G., Jr., and Pao, P. C., in *Stress Analysis and Growth of Cracks*, ASTM STP 512, American Society for Testing and Materials, 1972, p. 177.
- [9] McMillan, J. A., and Wei, R. P., *Metallurgical Transactions*, Vol. 1, 1970, p. 1740.
- [10] McElroy, A. J., and Wei, R. P., in *Proceedings, International Conference on Corrosion—Chemistry, Mechanics and Microstructure*, St. Louis, Mo., 1972, National Association of Corrosion Engineers, 1972, p. 301.
- [11] Bartram, J. M., *Engineering Fracture Mechanics*, Vol. 3, 1971, p. 15.
- [12] Gahleitner, J. P., *Journal of Materials*, Vol. 6, 1971, p. 941.
- [13] Gahleitner, J. P., and Wei, R. P., in *Proceedings, International Conference on Corrosion—Chemistry, Mechanics and Microstructure*, St. Louis, Mo., 1972, National Association of Corrosion Engineers, 1972, p. 489.
- [14] Wei, R. P., *Journal of Engineering Fracture Mechanics*, Vol. 1, 1970, p. 453.
- [15] Wei, R. P., and Landon, J. D., in *Advances in Research and Standards, American Society for Testing and Materials*, Vol. 9, July 1969, p. 25.
- [16] Washburn, N. J., Nicholson, A., and Haddad, J., *Philosophical Magazine*, Vol. 3, 1970, p. 1154.
- [17] Brown, T., and Washburn, A., *Journal of the Institute of Metals*, Vol. 50, 1960/1961, p. 103.
- [18] Washburn, T. J., and Washburn, C., *Applied Materials Research*, Vol. 3, 1964, p. 112.
- [19] Morosini, A., *International Journal of Fracture Mechanics*, Vol. 4, 1968, p. 107.
- [20] Wei, R. P., *International Journal of Fracture Mechanics*, Vol. 4, 1968, p. 120.
- [21] Wei, R. P., and Landon, J. D., *International Journal of Fracture Mechanics*, Vol. 3, 1969, p. 69.
- [22] Horvath, A., and Schipke, J., *Engineering Fracture Mechanics*, Vol. 1, 1970, p. 615.
- [23] Wei, R. P., et al., "Fracture Mechanisms and Surface Studies of Fatigue Crack Growth in Al Alloys," Report No. 9, 1978-79-80, Lehigh University, Bethlehem, Pa.; Contract No. H00014-75-C-0543, April 1979.
- [24] Lynch, C. T., Veldick, F. W., and Thomson, F. W., in *Proceedings, 1978 Test Service Conference on Corrosion*, New Orleans, 4-5 Oct. 1978.
- [25] Che, T. L., P. M., Taha, P. M., and Wei, R. P., *International Journal of Fracture Mechanics*, Vol. 3, 1967, p. 28.
- [26] Johnson, H. H., and Wilmer, A. M., *Applied Materials Research*, Vol. 4, 1965, p. 34.
- [27] Hines, G. G., and Johnson, H. H., *Transactions, Metallurgical Society of the American Institute of Mining, Metallurgical and Petroleum Engineers*, April 1964.

394 ATMOSPHERIC CORROSION OF METALS

- [28] Hanna, G. L., Triano, A. R., and Stieglitz, E. A. *Transactions, American Society for Metals*, Vol. 57, 1968, p. 658.
- [29] van der Sloep, W. A. *Transactions, American Society of Mechanical Engineers*, Vol. 89D, 1967, p. 28.
- [30] Gallagher, J. P. "Environmentally Assisted Fatigue Crack Growth Rates in SAE 4340 Steel." Ph.D. Dissertation, Department of Theoretical and Applied Mechanics, University of Illinois, Urbana, Ill., 1968.
- [31] Dahlberg, E. P. *Transactions, American Society for Metals*, Vol. 56, 1965, p. 46.
- [32] Johnson, H. H. and Paris, P. C. *Engineering Fracture Mechanics*, Vol. 1, 1968, p. 3.
- [33] Johnson, H. H. in *Proceedings, Conference on the Fundamental Aspects of Stress Corrosion Cracking*, Ohio State University, Columbus, Ohio, 1967.
- [34] Oriani, R. A. and Joseph, P. H. *Acta Metallurgica*, Vol. 22, 1974, p. 1043.
- [35] Zappale, C. and Sims, C. *Transactions, American Institute of Mining, Metallurgical and Petroleum Engineers*, Vol. 145, 1941, p. 225.
- [36] Thompson, A. W. and Bernstein, I. M. in *Advances in Corrosion Science and Technology*, R. W. Staehle and M. G. Fontana, Eds., Plenum Press, New York, Vol. 7, 1971.
- [37] Austen, I. M. and McIntyre, P. *Metall Science*, Vol. 13, 1979, p. 420.
- [38] Ritchie, R. O., Castiglione, M. H., Zachary, V. F., and Parker, E. R. *Metallurgical Transactions*, A, Vol. 9A, 1978, p. 35.
- [39] Ritchie, R. O., Suresh, S., and Topolnicky, J. *Fatigue and Plasticity Lab Report No. EPL/R/80/1030*, Contract No. DE-AC02-79E81030, ABB, Massachusetts Institute of Technology, Cambridge, Mass., Jan. 1980.
- [40] Austen, I. M. and Walter, E. F. in *Proceedings, International Conference on the Effect of Environment on Fatigue*, Institute of Mechanical Engineers, London, 1977, pp. 1-10.